



Source: CARM Technical Reference - Models, 2016

MSc Thesis (WSE-FRM.17-21)

Data Assimilation in Hydrodynamic- Hydrological Forecast Systems: A Case Study of the Murrumbidgee Catchment, Australia

Michael Getachew Tadesse
1038428

August 2017



Univerza v Ljubljani



Data Assimilation in Hydrodynamic-Hydrological Forecast Systems: A Case Study of the Murrumbidgee Catchment, Australia



Master of Science Thesis
by
Michael Getachew Tadesse

Supervisors
Dr. Henrik Madsen (DHI)
Peter Nygaard Godiksen (DHI)
Professor Christian Bernhofer (TU Dresden)

Examination committee
Dr. Henrik Madsen (DHI)
Professor Christian Bernhofer (TU Dresden)
Dr. Shalk Jan van Andel (IHE Delft)

This research is done for the partial fulfilment of requirements for the Master of Science degree at the UNESCO-IHE Institute for Water Education, Delft, the Netherlands

Dresden
August 2017

The findings, interpretations and conclusions expressed in this study do neither necessarily reflect the views of the UNESCO-IHE Institute for Water Education, nor of the individual members of the MSc committee, nor of their respective employers.

Dedicated to the fatalities of the August 2006 flash flooding in **Dire Dawa, Ethiopia**

Declaration

I hereby confirm that this thesis is the presentation of my original work and the contribution of others with respect to literature and collaborative research as well as discussions was indicated in this document.

Michael Getachew Tadesse

August 30, 2017

Dresden, Germany



Topic of Masters Thesis

Subject area: Hydro Science & Engineering (EM Flood Risk Master)

Name: Michael Getachew Tadesse

Date of birth: 28.09.1980

***Theme:* DATA ASSIMILATION IN HYDRODYNAMIC-HYDROLOGICAL
FORECAST SYSTEMS**

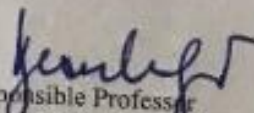
More often than not, operational hydrological forecasts' performance is compromised due to the inherent uncertainty involved with the model parameters, model forcings as well as model structure. As a result operational forecasts are carried out with the wrong catchment/river initial states which in turn leads to unreliable and inaccurate forecasts. Hydrological data assimilation is the state-of-the-art method that is being implemented with several hydrological-hydrodynamic models in order to quantify and reduce uncertainties in addition to capturing the true catchment/river states so that reliable and more accurate forecasts can be issued. In this study the effects of hydrodynamic-hydrological model states update will be investigated by assimilating available observations (river discharges). One of the most important research questions is; "What is the benefit of updating both hydrodynamic as well as hydrological model states as opposed to updating only one of them?" A sensitivity analysis will be carried out in order to calibrate/tune the data assimilation filter parameters as well as to find the optimum ensemble size. And finally the benefit of using remotely sensed precipitation data (radar data or satellite data) will be investigated for potential improvement of forecast quality. urements as well as for climate model output data for future GHG concentrations and therefore climate scenarios. The modeled data of the recent climate are used to validate the model and to assess the associated uncertainty. This is therefore depending on availability of data, both measurement and model output. This data are often missing or are unknown.

Supervisor:

Dr. Hendrik Madsen, IHE, Denmark

Start date: 30.04.2017

Anticipated end date: 30.08.2017


Responsible Professor
Prof. Dr. Christian Bernhofer

Abstract

The main objective of this study is to investigate the benefit of updating both hydrological and hydrodynamic model states for better streamflow forecasting. A data assimilation scheme based on the Ensemble Transform Kalman Filter (ETKF) was implemented in order to assimilate observed discharge. Four precipitation products (rain gauge as well as three satellite rainfall products) were checked for suitability with respect to rainfall-runoff modelling. The hydrological-hydrodynamic model, MIKE 11/NAM was used for rainfall-runoff as well as river modelling. The upper Murrumbidgee catchment in Australia was chosen as a case-study; major peak events were identified at Gundagai, (a downstream gauging station and an interesting location in terms of flood risk management), to validate the performance of the data assimilation. Two major data assimilation methods were implemented; Firstly hydrodynamic states (discharge and water level) were updated along the river and the performance of the data assimilation was tested by issuing a sequence of simulated streamflow forecasts. Secondly, both the hydrodynamic and hydrological model states were updated and the corresponding forecasts were verified. The streamflow simulation from the calibrated model (open loop run) was considered as a reference/benchmark forecast. Sensitivity of the ETKF was also studied with respect to several parameters such as model uncertainty, observation uncertainty as well as half-time constant of the time correlated error. As a result appropriate filter parameters were selected for a specific sub-catchment. Ensemble size sensitivity analysis was also done in order to find the optimal ensemble size that balances the trade-off between forecast accuracy and computational expense.

It was found that the satellite rainfall products with daily temporal resolution can generally represent catchment rainfall-runoff process at large and could be used for large-scale hydrological modelling, however, it was not possible to simulate important peak events and thus the daily satellite rainfall products were rendered as unsuitable for flood forecasting/reservoir management system for the Murrumbidgee catchment. Hence, the rain gauge precipitation data was used for data assimilation and forecast experiments for the rest of the study. Sensitivity analysis results showed that an optimal ensemble size of 20 was appropriate for the analysis. More importantly, this study demonstrated that there is a significant advantage in updating both hydrological and hydrodynamic states. Looking at a 48 hr lead time alone, average RMSE and CRPS skill scores of the forecasts based on the combined update are 23% (RMSES) and 18% (CRPSS) more skilful than the forecasts which are based on hydrodynamic states update alone.

Keywords: Data Assimilation, MIKE 11, Ensemble, Kalman Filter, TRMM, CHIRPS, PERSIANN

Acknowledgements

First of all, I would like to thank God Almighty for giving me the strength and the wisdom to carry out this research work. Second of all, my sincere gratitude goes out to IHE Delft (especially Dr. Biswa Bhattacharya) and DHI for collaborating together in order to provide me this opportunity. Such collaboration between academic/research and development institutes helps a lot of students like me and should be encouraged ever more. I thank the European Commission for providing me the Erasmus Mundus Scholarship for the entire master's program.

I also owe it to several other people without which I could not have come this far. Dr. Henrik Madsen, my main supervisor in DHI, I would like to say thank you for providing me with your guidance and supervision throughout the research period. Thank you Peter Nygaard Godiksen and Dr. Marc-Etienne Ridler for all the technical support you provided me with. Professor Christian Bernhofer, my supervisor from TU Dresden, I appreciate your guidance and advice. Special thanks goes to Dr. Jeanne-Rose René for your unrelenting support, Dr. Michael Brian Butts, Bertrand Richard, Vasana Dharmadasa, Jake Longenecker thank you for your comments and suggestions, they helped me a lot. Eulampius Frederick thank you for your prayers and encouragement.

Most importantly I want to thank my family Getachew Tadesse, Zenebech Disassa, Yared Getachew, Addis Disassa and Wiebke Erchinger for your enormous support, motivation, and prayer. It's what got me here. And finally it goes without saying how grateful I am for the Erasmus Mundus experience I had for the last two years. Thank you floodies for bringing up a diversity of talent, unforgettable memories and everlasting friendships.

Table of Contents

Abstract.....	ii
Acknowledgements	iii
List of symbols and abbreviations	ii
1. Introduction	3
2. Literature Review.....	5
2.1 Uncertainty in hydrological models and forecasts	6
2.2 Data for Data Assimilation	7
2.3 Data Assimilation Algorithms	8
2.3.1 Ensemble Kalman Filter (EnKF).....	10
2.3.2 Ensemble Transform Kalman Filter (ETKF).....	11
2.4 Verification Methods.....	12
2.4.1 Verification Statistic for deterministic simulations	12
2.4.2 Verification Statistic for ensemble simulations.....	13
2.4.3 Skill scores.....	14
3. Case Study.....	15
4. Data and Model Setup.....	18
4.1 Data Used	18
4.1.1 Precipitation.....	18
4.1.2 Discharge	18
4.2 Model Set-up	19
4.2.1 Hydrological model	19
4.2.2 Hydrodynamic model	21
5. Research Methodology.....	22
5.1 Selecting appropriate precipitation data	22
5.1.1 Bias Correction Method.....	26
5.1.2 Rainfall-runoff simulation	26
5.2 Model states to be updated	27
5.3 Data Assimilation Framework.....	27
5.3.1 Perturbation Methods	29
5.3.2 Localization	30
5.4 Implementation of Data assimilation.....	31
5.4.1 Hydrological model states update.....	32
5.4.2 Hydrodynamic model states update.....	33
5.4.3 Combined hydrodynamic - hydrological model states update	33
5.5 Investigating the effect of DA on forecasting	34
5.6 Sensitivity Analysis	34
5.6.1 First phase of sensitivity analysis	35
5.6.2 Second phase of sensitivity analysis.....	35
5.7 Verification Methods.....	36
6. Results and Discussion	37
6.1 Selecting appropriate precipitation product for data assimilation.....	37
6.1.1 Comparison of rainfall estimates.....	37
6.1.2 Bias correction of satellite rainfall estimates.....	40

6.1.3	Rainfall-runoff simulation	40
6.2	Hydrological model states update.....	44
6.3	Forecasting and Verification	54
6.4	Sensitivity Analysis	54
6.4.1	First Phase of Sensitivity Analysis	54
6.4.2	Second Phase of Sensitivity Analysis.....	56
6.5	Hydrodynamic model states update.....	61
6.5.1	Model Area	61
6.5.2	Major Peaks	62
6.5.3	Analysis Parameters	62
6.5.4	Streamflow Forecast	65
6.6	Hydrodynamic-Hydrological model states update	68
6.6.1	Streamflow Forecast	75
7.	Conclusions	77
8.	Limitation of the study and further recommendation.....	80
9.	References	81
10.	Glossary	85
Appendix	86

List of Figures

Figure 1: Different updating (data assimilation) methodologies. Adapted from (Refsgaard, 1997)	9
Figure 2: EnKF Algorithm. Adapted from (Jo et al., 2016)	11
Figure 3: Illustration of CRPS, adopted from (T. Hamill, 2010)	13
Figure 4: Study Area - Murrumbidgee catchment.....	15
Figure 5: Average annual rainfall in the Murrumbidgee catchment. Adopted (NSW Office of Water, 2011).....	16
Figure 6: Structure of MIKE NAM model. Adopted from (Dhi, 2007).....	19
Figure 7: Model domain - selected sub-catchments shown in yellow.....	20
Figure 8: Model discretization for discharge and water level computation. Adapted from (Blasone, 2014).....	21
Figure 9: MIKE 11 setup for the model domain	21
Figure 10: High-level workflow	22
Figure 11: Detailed workflow #1.....	23
Figure 12: Detailed workflow #2.....	24
Figure 13: Detailed workflow #3.....	25
Figure 14: Overview of the modules included in the DA framework. Source (DHI, 2017)	28
Figure 15: Localization (Source: DHI Data Assimilation Framework)	31
Figure 16: Two chosen catchments (purple) for implementation of data assimilation ..	32
Figure 17: Monthly Mean Discharge Comparison for the selected catchments (2012 to 2017).....	32
Figure 18: Model domain, points marked white are used for hydrodynamic update whereas stations marked red are used for both hydrological and hydrodynamic update	33
Figure 19: Data assimilation and forecasting procedure	34
Figure 20: DA and forecasting procedures for sensitivity analysis.....	36
Figure 21: Comparison of the three satellite rainfall estimates with rain gauge rainfall	38
Figure 22: Comparison between daily rainfall from rain gauges and three satellite products TRMM (top left), CHIRPS (top right), PERSIANN (bottom left).....	39
Figure 23: Accumulated mean daily rainfall over Goobarragandra sub-catchment before and after bias correction	41
Figure 24: Re-calibration of rainfall-runoff model using TRMM (top) and CHIRPS (bottom) datasets (red and black lines represent observed and simulated flows)	42
Figure 25: Daily streamflow hydrographs at the Goobarragandra outlet simulated with TRMM (top left) and CHIRPS (top right), in-situ (bottom left) rainfall datasets, also statistic for the three simulations (bottom right)	43
Figure 26: Streamflow hydrographs for the Oct 2016 peak event using TRMM (top left), CHIRPS (top right), and in-situ (bottom left) datasets.....	44
Figure 27: Comparison of observed and simulated discharge (three years) for Jugiong (top left) and Goobarragandra (top right) catchments; selected events for data assimilation for Jugiong catchment (bottom left) and for Goobarragandra catchment (bottom right).....	45
Figure 28: Control Simulation (no data assimilation): Total runoff for Jugiong catchment.....	47
Figure 29: Control Simulation (no data assimilation): Total runoff for Goobarragandra catchment.....	48
Figure 30: Control simulation for the hydrological model states - Jugiong sub-catchment	49

Figure 31: Control simulation for the hydrological model states - Goobarragandra sub-catchment.....	50
Figure 32: Updated total runoff for Jugiong (top left) and Goobarragandra (bottom left) and comparison of statistical analysis for both updates	51
Figure 33: Updated hydrological states for Jugiong sub-catchment	52
Figure 34: Updated hydrological states for Goobarragandra sub-catchment	53
Figure 35: Forecast RMSE (top left), CRPS (top right), RMSES (bottom left), and CRPSS (bottom right) for Goobarragandra catchment.....	55
Figure 36: Forecast error as a function of lead time for different ensemble sizes	57
Figure 37: Average RMSE of forecasts for different ensemble sizes	57
Figure 38: Calibration period for sensitivity analysis	58
Figure 39: Validation period for sensitivity analysis.....	59
Figure 40: Sequence of forecasts made in the validation period.....	59
Figure 41: RMSE (Top left) and CRPS (Top right) of 1 year forecast on validation period, RMSES (lower left) and CRPSS (lower right) skill score of forecast	60
Figure 42: Murrumbidgee catchment and the subdivision into eleven sub catchments. Gauging stations are also shown in white and red circles	61
Figure 43: Implementation of data assimilation on the major peaks.....	64
Figure 44: Improvement of statistical errors for the eight major peaks after DA	65
Figure 45: Verification of forecast based on HD update as a function of lead time	66
Figure 46: Comparison of forecast skills in high-flow (the top-most plots) and low-flow periods (bottom plots) for HD update.....	67
Figure 47: Assimilation results after combined HD+RR update.....	70
Figure 48: Improvement MAE & RMSE after combined HD+RR update	71
Figure 49: Top left and right show the HD update results with missing observations (purple) and bottom left and right show the HD+RR update results with missing observations.....	72
Figure 50: Verification of hindcast results based on HD+RR update as a function of lead time	73
Figure 51: Comparison of forecast skills in high-flow (the top-most plots) and low-flow periods (bottom plots) for HD+RR update	74
Figure 52: Forecast skill Comparison for HD and HD+RR update	76

List of Tables

Table 1: Satellite rainfall dataset used for analysis	18
Table 2: Sub-catchments within the model domain	20
Table 3: Selected model states for data assimilation	27
Table 4: Verification methods used in this study	36
Table 5: Selected Filter parameters for updating.....	46
Table 6: Amount of time (min) it takes to propagate the different ensemble members in forecast mode.....	56
Table 7: Filter parameter ranges for sensitivity analysis	56
Table 8: Best filter combination with low forecast errors (forcing and observation uncertainty are standard deviation values)	58
Table 9: Gauging stations used for assimilation and validation.....	61
Table 10: Major peak events at Gundagai station (2013 - 2016)	62
Table 11: Gauging stations used for assimilation and validation in the combined update	68

List of symbols and abbreviations

AR1:	Auto-regressive (first order)
CDF:	Cumulative Distribution Function
CHIRPS:	Climate Hazards Group InfraRed Precipitation with Station data
CRPS:	Continuous Ranked Probability Score
CRPSS:	Continuous Ranked Probability Skill Score
DA:	Data Assimilation
EnKF:	Ensemble Kalman Filter
ETKF:	Ensemble Transform Kalman Filer
HD:	Hydrodynamic
HD+RR:	Hydrodynamic and Rainfall-Runoff
NAM:	Nedbør-Afstrømnings-Model (Precipitation-Runoff Model)
PERSIANN:	Precipitation Estimation from Remotely Sensed Information using Artificial Neural Networks
RR:	Rainfall-Runoff
TRMM:	Tropical Rainfall Measuring Mission
X_a :	Analysis
X_b :	Priori or background estimate of the true state before the analysis is carried out

1. Introduction

Hydrological-hydrodynamic modelling is crucial for water resources management (e.g., reservoir management, flood control and drought management). However, the accuracy and reliability of hydrological and hydrodynamic models are oftentimes in question owing to the uncertainties inherent to model parameters, model forcing inputs, and model structures. In order to tackle this problem, data assimilation techniques that merge models and observations by jointly considering the uncertainties of each entity have become commonplace in hydrology.

Streamflow forecast quality depends on how good one can estimate the initial state of the catchment as well as the river. Initial states can be estimated with a reasonable accuracy by implementing data assimilation techniques whereby models are merged with observations by appropriately considering the uncertainty in each entity. Hydrologic models are not perfect since they simplify the real world processes; there is usually an error in the mathematical approximations of the governing processes. Besides model predictions will diverge from reality as time progresses; observations are not accurate either due to errors from measuring devices and representation errors (Madsen et al., 2006). Hence, there is a need to use models and observations synergistically to obtain optimum estimation of the model states. Data assimilation corrects forecasts by introducing new information observed from the environment (Guzzi, 2015).

There are several data assimilation techniques, however Kalman Filter and its variants are the most well-known (Chen et al., 2013). The Kalman Filter is oftentimes used to adjust model simulated values toward observed values keeping the system dynamics consistent (Butts et al., 2005). Ensemble Kalman filtering technique, which is implemented in this study uses a member of ensembles to represent the probability distribution of the model state and performs stochastic analysis on the ensemble (refer 2.3.1).

The potential of data assimilation in hydrology has been demonstrated by several studies; (Clark et al., 2008) used the Ensemble Kalman filter (EnKF) to update multiple model states such as soil storage, and surface storage by assimilating streamflow. (Xie et al., 2010) implemented EnKF to the Soil and Water Assessment Tool (SWAT) in order to update several states and parameters such as runoff and groundwater flow. (Madsen et al., 2003) showed that flood forecasting skills improved significantly after assimilating observed water levels and fluxes in the MIKE 11 Flood Forecasting system.

The objectives of this study are the following:

- To investigate the suitability of remotely sensed precipitation products for rainfall-runoff modelling and data assimilation as an alternative to rain gauge precipitation data.
- To carry out sensitivity analysis to find optimal filter parameters and optimal ensemble size that represent modelling and observation uncertainty appropriately such that forecast errors are minimized.

- To investigate the effect of a combined hydrodynamic-hydrological model states update on the improvement of streamflow prediction for the upstream part of Murrumbidgee catchment, Australia.

This study aims to address the following research questions:

- What is the significance of using remotely sensed precipitation products instead of in-situ precipitation products in rainfall-runoff modelling as well as streamflow forecast improvement?
- How sensitive is the data assimilation technique (Ensemble Transform Kalman filter) to the data assimilation configuration parameters? [How does the change in filter configuration impact the forecast?]
- How does ensemble size affect the updating process and what is the optimal ensemble size?
- What are the benefits of updating hydrological and hydrodynamic model states independently and in a combined manner? Is there an improvement in streamflow forecast?

The novelty of this research lies on the implementation of a combined hydrodynamic-hydrological model states updating for the Murrumbidgee catchment. Operational forecasts issued for the Murrumbidgee catchment employ data assimilation techniques to update only the hydrodynamic states (discharge and water level). The internal catchment states that drive the hydrodynamic process are not being updated. However, there is now a need to incorporate the hydrological model states updating in the data assimilation. By doing so it is anticipated that streamflow forecast improvements will be achieved.

Ensemble Transform Kalman filter, a deterministic variant of Kalman filter was used with the MIKE 11 model (both rainfall-runoff and river model). Firstly, several precipitation products were investigated including rain gauge precipitation data for their capability to simulate the rainfall-runoff processes in the catchment. After selecting the most appropriate precipitation product, the hydrological model states of selected sub-catchments were updated by implementing data assimilation. In this analysis, only the catchment states are updated. Following this, a sensitivity analysis was carried out to find the appropriate filter parameters, which also includes finding the optimum ensemble size for the analysis. Using the filter parameters obtained from the sensitivity analysis, a hydrodynamic model states update was done which updated only the model states in the river (discharge and water level). Finally a combined hydrological-hydrodynamic model states update was done in order to update the catchment as well as the river states. Performance of the data assimilation in all the above analysis was tested by simulating a series of forecasts which were verified by the chosen verification methods that will be described in 2.4.

Overall, the study is organized as follows; chapter 2 presents the relevant literature in data assimilation, the case study and data availability including model setup will be discussed in chapter 3 and 4 respectively and the research methodology and major findings follow in chapters 5 and 6.

2. Literature Review

River operation is a complex process that is needed to cater for water demands of households, industry, hydropower, navigation, and environmental requirements. In order to meet these demands, river operators need to take into account geometry and physical characteristics of rivers, inflows and outflows from reservoirs, weather forecasts, and water orders which need to be accounted for in several numerical models so that optimal reservoir releases are issued (Munier et al., 2015). However the models that are used are subject to a lot of errors arising from model structure, model parameters, initial conditions and hydrometeorologic forcings. Data assimilation which is the focus of this study, is one of the solutions among others that reduces the impacts of errors by assimilating information from observations in order to correct model errors (Munier et al., 2015).

Hydrological models even after calibration, could imperfectly predict streamflow evolution. Therefore, before they can be used on forecasting mode, it is recommended to put them in agreement with available observations (Aubert et al., 2003). Data assimilation (DA) is an approach that optimally merges information from model simulations with observations through appropriate uncertainty modelling towards an accurate prediction and quantification of uncertainty (Y.Liu et al., 2012). DA is concerned with three fundamental problems, viz. state updating, parameter estimation and error updating (Y.Liu et al., 2012). State updating is where observed data such as water levels, discharge, snow depth etc. are assimilated into lumped or distributed hydrologic or hydraulic models to update the models' dynamic states. Whereas, parameter estimation is the optimization of model parameters using observed data; and error updating revises the prediction of error models that represent the difference between hydrologic forecasts and observations. For state updating a state-space model approach is usually used which can be solved by techniques like filtering or smoothing. This study is limited to the state updating part of data assimilation; several model states, both catchment and hydraulic, will be updated and the update will be verified by statistical analysis of consecutive forecasts.

Data assimilation takes advantage of both imperfect models and limited observations by considering the uncertainties in both in order to provide a more accurate prediction (Zhang et al., 2016). It improves the accuracy of forecasts by making use of observations up to the time of forecast, in a way providing the best initial conditions and boundary conditions for a forecast (Katrine et al., 1994). The wetness of a catchment prior to a rainfall event is for instance, a vital information that determines the outcome of the event in terms of runoff. Thus, a flood forecasting system based on a rainfall-runoff model entails an accurate estimation of the initial catchment wetness in order to make a reliable flood forecast (Brocca et al., 2012). DA is an important component of an operational forecasting system that improves the initialization of a forecast model at the time of forecast and thereby improves forecast accuracy (Madsen et al., n.d.). Considering the adverse impact of floods on both lives and property, the need to reduce forecast uncertainty is ever growing. According to WMO, data assimilation is identified as an essential requirement for accurate flood forecasting [WMO, 1992].

When hydrological data assimilation is implemented, the usual trend is to update the model simulated streamflow by assimilating the measurements of river discharge and/or water levels. This methodology allows for improvement of forecasts over a period

corresponding to the travel time it takes for the flood wave to propagate through the river. However, the uncertainty in streamflow forecast can be traced back to the meteorological boundary conditions which are believed to be the main sources of uncertainty when it comes to flood forecasting. The uncertainty in the meteorological boundary conditions such as precipitation further generate uncertainties both directly on the simulated runoff and indirectly on the actual catchment wetness prior to precipitation (Katrine et al., 1994).

2.1 Uncertainty in hydrological models and forecasts

Despite the growing development in computational power and distributed hydrological modelling, it's still challenging to adequately quantify and reduce the uncertainty related to hydrological predictions (Yuqiong Liu et al., 2007). Evidently, understanding of the hydrological processes increased with the evolution of hydrologic models from lumped to the complex distributed ones. However, the need to deal with the uncertainty of the models themselves has also been increasing. Thus, it has now become apparent that the proper consideration of uncertainty in hydrologic predictions is very important both for research and operational modelling (Wagener et al., 2003). In order to appropriately address uncertainty in hydrologic modelling and prediction, one has to understand, quantify and reduce uncertainty.

A classical way of quantifying uncertainty, as presented in different literature, is representing the predictions in terms of probabilistic distribution which is obtained by performing a probabilistic modelling instead of a deterministic one (Yuqiong Liu et al., 2007) for instance by producing an ensemble of hydrologic predictions as opposed to a deterministic prediction. An ensemble is a collection of model trajectories (Bröcker, 2012) generated by slightly tweaking the initial conditions as well as by using perturbed model equations. These varied initial conditions and perturbed equations are introduced to represent the uncertainty about the current state of the variable (i.e. catchment). However, the high non-linearity of a hydrologic system and the different interactions between model components make accurate probabilistic distribution of the system a daunting task. Thus, linear assumptions are made in order to simplify the uncertainty representation. Gaussian distributions are commonly used to quantify the different sources of uncertainty (Yuqiong Liu et al., 2007). Background uncertainty comes from the uncertainty in the initial conditions from the previous analysis and from the “model error” that represents the discrepancy between the dynamics of the model and that of the actual system dynamics (Hunt et al., 2007) In addition, in hydrological forecast systems there is uncertainty originating from model forcing forecasts such as precipitation forecasts.

In order to quantify the uncertainty in hydrologic outputs, ensemble methods (sampling methods) have become the state-of-the art in which samples are taken from a prior assumed error probability distribution function and the model will be propagated in time. By taking adequate sample of predictions and applying statistics on the ensemble, the uncertainty in the model outputs can be quantified (Yuqiong Liu et al., 2007). The uncertainty of the initial state estimates is represented by the initial spread of the ensemble members. In the method outlined by Evensen (2003), ensemble members are generated by taking an initial best-guess of the states, and then adding perturbations in the form of random correlated fields to each ensemble member (Turner et al., n.d.).

There are three basic remedies for the inherent uncertainty problem rooted in hydrologic modelling and prediction. The first one is to acquire a higher quality hydrologic data which incorporate advanced measuring techniques; the second is advancing hydrologic models so that the physical system can be represented by the models more accurately and the last one, which is of interest to this study is the application of efficient and effective techniques that can extract and assimilate information from available data via the model identification and prediction processes (Yuqiong Liu et al., 2007).

Data assimilation combines available observations with prior knowledge (which is the representation of the physical system by the model) in order that the true state of the system can be estimated along with its estimation uncertainty (Katzfuss et al., 2016). An important and non-trivial task is reasonably quantifying the uncertainties in the different sources and feeding them to the data assimilation framework in order to reduce uncertainty in hydrologic prediction. The data assimilation algorithm, very often requires the specification of errors of the major sources of uncertainty. (Yuqiong Liu et al., 2007). The assimilation estimates will be close to observations at times and locations for which accurate observations are at hand, whereas at times and locations for which there are no available observations (or of low quality) assimilation estimates will be close to the model solution (Reichle et al., 2008).

2.2 Precipitation data for Data Assimilation

Data assimilation uses model results and observations synergistically in order to provide more accurate state estimation. The two major inputs to the data assimilation algorithm among others, are model forcing and observation. The data assimilation algorithm provides state estimate by considering the uncertainty in each of the above entities. Precipitation is the most important component of model forcing and it drives the rainfall-runoff process determining the uncertainty in streamflow. It is also a major input for data assimilation. Observed discharge is usually used to calibrate a rainfall-runoff/river model and it is also a prognostic variable in data assimilation meaning results of data assimilation are compared to the observed discharge for validation. Hence, the quality of hydrologic data used in hydrological/hydrodynamic models influences the outputs of data assimilation significantly.

Precipitation is one of the most important constituents of hydrological model forcing and its quality plays a major role in the reliability of model simulations (Kneis et al., 2014) (Xing Liu et al., 2015). Accurate precipitation data is required for a rainfall-runoff modelling; since precipitation is the main driver for streamflow, the inherent uncertainty in the precipitation forcing highly influences the efficiency of assimilating the streamflow observations (Maggioni et al., 2017). However, due to its spatial and temporal variability, precipitation remains to be a difficult meteorological component to quantify accurately. Inaccuracy in precipitation estimation has an adverse effect on streamflow estimation and prediction bringing large uncertainty. There are three ways how a precipitation can be estimated; gauge observations, meteorological radar observations and satellite observations (Ashouri et al., 2014). In remote and mountainous regions, it is difficult to obtain reliable rainfall estimates from gauges or radars owing to sparse distribution of gauges and beam blockage effects especially in extreme events. Besides, the precipitation measurements from gauges are subject to device malfunction errors, human errors, and data transmission mishaps (Kneis et al.,

2014). Thus implementing hydrological modelling and prediction with such unreliable rainfall estimate could propagate the inherent meteorological uncertainty giving rise to unreliable streamflow simulation and prediction. Satellite rainfall estimates have a better spatial coverage than gauges, which allows for a reliable streamflow estimation and prediction. In light of this, the use of satellite rainfall estimates comes in handy for streamflow simulation and prediction (Xiaomang Liu et al., 2017). It has become commonplace recently, to use satellite precipitation products such as TRMM, CHIRPS and PERSIANN as an alternative precipitation products instead of in-situ rainfall estimates.

The Tropical Rainfall Measuring Mission (TRMM), is a joint mission of NASA and the Japanese Aerospace Exploration Agency (JAXA) that was launched in 1997 to study rainfall for weather and climate research (NASA, 2015). It became operational on 1998 and covers the tropical zone, between 50° N and 50° S with a spatial resolution of 0.25° (Arias-Hidalgo et al., 2013). TRMM has several variants; 3B40, 3B41, 3B42 etc. This study uses the TRMM 3B42 RT which has the highest spatial resolution ($0.25^{\circ} \times 0.25^{\circ}$).

The Climate Hazards group Infrared Precipitation with Stations (CHIRPS) is a quasi-global, daily, high resolution (0.05°) precipitation dataset with more than 30 years precipitation data covering the 50° S to 50° N latitudes. It was developed by the United States Geological Survey (USGS) Earth Resources Observation and Science Center and the University of California Santa Barbara Climate Hazards Group (Kimani, 2017). It uses the TRMM multi-satellite precipitation analysis version 7 in order to calibrate global Cold Cloud Duration (CCD) rainfall estimates (Funk et al., 2015). It merges remotely sensed precipitation with in-situ station data using a modified inverse distance weighted algorithm.

Precipitation Estimation from Remotely Sensed Information using Artificial Neural Networks – Cloud Classification System (PERSIANN-CCS) is a satellite rainfall estimate of finer spatial resolution ($0.04^{\circ} \times 0.04^{\circ}$) extracted from infrared geostationary satellite imagery (Hong et al., 2007) covering the 50° S to 50° N latitudes available since the year 2003. It uses artificial neural networks to find the relationships between infrared and precipitation estimates from several microwave products (Behrangi et al., 2014).

2.3 Data Assimilation Algorithms

In operational hydrologic forecasting, it is customary to adjust the model forcings, model states and in certain cases, model parameters in order to account for errors in the initial conditions, parameters and structure of hydrologic models based on stream flow observations (Seo et al., 2009). Data assimilation makes use of additional information obtained from satellite or in-situ measurements in order to improve model results. The additional information can be used to modify input variables, state variables or even the parameters that describe the physical properties of the model as depicted in Figure 1. Generally the system is updated at the state and parameter level such that the model is optimized leading to an optimal simulation. Therefore, by optimizing the system at time step t , the system will simulate better outputs at the following time step $t+1$.

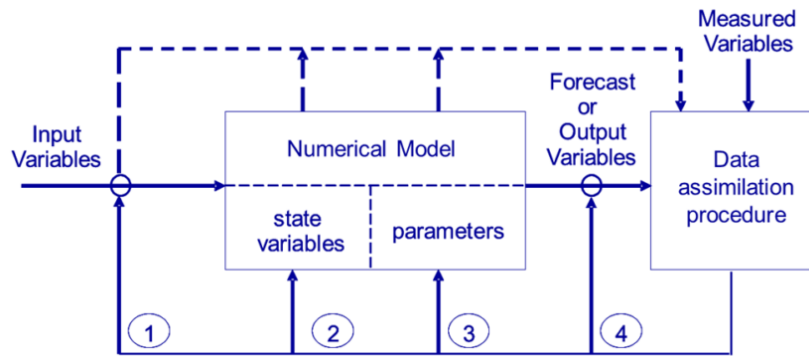


Figure 1: Different updating (data assimilation) methodologies. Adapted from (Refsgaard, 1997)

Several DA techniques are available and can be categorised depending on the variables that are updated in the assimilation process, namely input variables, model states, model parameters, and output variables. In real-time applications, sequential or filtering procedures are implemented for state-updating and the most common technique in this group is the Kalman Filter (KF) (Madsen et al., 2003). Filtering is the process in which the best estimate of a state is computed from noisy data amounts (Kleeman, 1996). Kalman filter is a set of mathematical equations that recursively estimates the state of a process in such a way that the mean of the squared error is minimized (Welch et al., 2006). The main benefit of the KF in comparison to other DA techniques is that during the updating process, it considers model as well as data uncertainties and provides an estimate of the model prediction uncertainty (Madsen et al., 2003).

Kalman filter assumes a linearity of the error growth and normality of error distribution. The background error covariances influence the magnitude of adjustment to the observation. When the background errors, the adjustment draws more to the observation (T. M. Hamill, 2006). The Kalman filter operates in two distinct stages; forecast stage and analysis stage. In the former one, the background state of the system is propagated forward in time by the model until the time of observation. In the latter stage, assimilation of the observation is carried out into the forecast state by apportioning the ration of errors in the background state and in the observation (Petrie, 2008). The equations related to Kalman filter are listed below in this chapter.

Considering a model and describing it in a deterministic discrete-time dynamic system setting (Deliu et al., 2014);

$$X_{k+1} = \Phi(X_k, U_k) \tag{1}$$

$$Z_k = C_k X_k \tag{2}$$

X_k represents the state variables of the system at time step k (for instance, water levels, discharge), U_k – forcing of the system (boundaries) and $\Phi(\cdot)$ denotes the numerical scheme used to solve the equations in order to propagate the model from time step k to $k+1$. The second equation describes the measurement vector (Z_k) which is a function of C_k (a matrix which describes the relation between measurements and state variables). As explained in the previous paragraph, the data assimilation process consists of two steps. The first step is to issue a forecast as shown by equation 3 and then the observed data is merged with the forecast in order to provide an updated state also called analysis state. The updated state is formulated by the linear combination of the observed data and the model.

$$X^f_k = \Phi(X^a_{k-1}, U_k) \quad (3)$$

$$X^a_k = X^f_k + G_k(Z_k - C_k X^f_k) \quad (4)$$

X^f_k denotes the forecast state vector, G_k is a matrix of weighting that considers the relative uncertainties of the model dynamics as well as the observations and it takes into account the correlations between state variables and observations. $Z_k - C_k X^f_k$ represents the innovation vector which includes the differences between the measurements and their respective model forecasted values.

The Kalman filter is founded on the stochastic formulation of the model and the measurement;

$$X_{k+1} = \Phi(X_k, U_k + \varepsilon_k) \quad (5)$$

$$Z_k = C_k X_k + \eta_k \quad (6)$$

ε_k is a stochastic element that denotes the different types of model error, in other words the uncertainty of the modelled system whereas η_k is the random observation error vector with zero mean and covariance matrix R_k . Model forecast uncertainty is designated by the covariance error matrix P^f_k and the Kalman gain which is used in the update is computed as in equation 7. The Kalman gain (G_k) describes the weight assigned to the model forecasts as well as the measurements depending on the uncertainties of each. It also shows the correlation between the diagnostic state variable (the measured state variable for instance discharge) and the model state variables that need to be updated (Madsen et al., 2007). The updated covariance follows in equation 8 (Madsen et al., 2003). This is based on the assumption that the model is linear and measurement errors are white noise processes with known covariance matrices in which case the Kalman filter is the best linear unbiased estimator (Ridler et al., 2014).

$$G_k = P^f_k C_k^T (C_k P^f_k C_k^T + R_k)^{-1} \quad (7)$$

$$P^a_k = P^f_k - G_k C_k P^f_k \quad (8)$$

The computation of the covariance matrix, P^f_k , is computationally expensive and thus makes the filtering process infeasible for real-time applications especially when the model is nonlinear. Therefore, different approximations of the Kalman filter have been developed the most popular of which is the ensemble representation of the error covariance matrix P^f_k (Ridler et al., 2014).

2.3.1 Ensemble Kalman Filter (EnKF)

Though the classical Kalman filter gives a comprehensive solution for state estimation of linear systems based on Gaussian noise, main interest lies in state estimation of nonlinear systems since hydrological systems are nonlinear. Even though rigorous solutions were introduced to tackle nonlinear problems, oftentimes these methods were either narrow in applicability or computationally expensive (Gillijns et al., 2006). Ever since its introduction by Evensen in 1994, the Ensemble Kalman Filter has been tested and applied over several studies and it has become popular due to its simple formulation and ease of implementation (Geir Evensen, 2003).

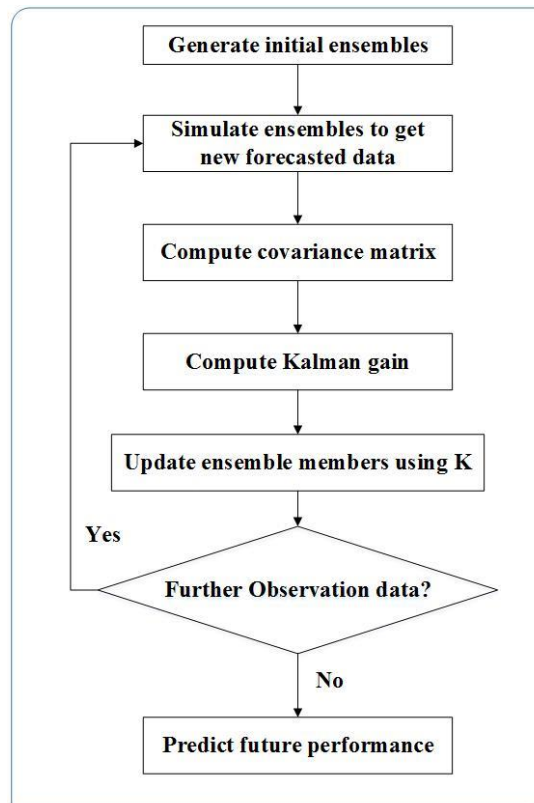


Figure 2: EnKF Algorithm. Adapted from (Jo et al., 2016)

The Ensemble Kalman filter is an approximation of the classical Kalman filter in which the probabilistic distribution of a model state is represented by a sample from a distribution (Stroud, 2015). An ensemble of vectors that approximate the state distribution is stored, propagated and updated by EnKF. This allows for dimension reduction in a way that a small ensemble is propagated instead of the full error covariance matrix. (Katzfuss et al., 2016). Figure 2 outlines the major steps used in EnKF implementation. The assumption here is that the ensemble mean is considered to be the best estimate whereas the ensemble spread around the mean defines the error in the ensemble mean (Geir; Evensen, 2009).

In EnKF, the stochastic model equation shown in equation 5 is represented by an ensemble of state vectors. During model forecast, these states are forced with model errors and propagated in time according to model dynamics. This allows for the estimation of the covariance error P^f . The Kalman gain is also calculated using equation 7. During the update step, each state vector is updated with the equations represented in equation 4.

2.3.2 Ensemble Transform Kalman Filter (ETKF)

ETKF was used for this study and the following description of ETKF is based on the works of (Ridler et al., 2014; Zhang et al., 2016).

ETKF is deterministic and computationally efficient in a way that it does not require the generation of the full error covariance matrix (Rasmussen et al., 2015). The probability density of the model state is approximated by a finite number m of ensemble in such a

way that $\mathbf{X} = [\mathbf{x}^1, \mathbf{x}^2 \dots \mathbf{x}^m]$. These ensemble members are forced with a system noise that is randomly generated and propagated through the model. Accordingly the forecast error covariance can be calculated from the sample covariance of the ensemble members. This quantifies the accuracy of the state estimate.

$$\mathbf{P}^f = (\mathbf{m} - \mathbf{1})^{-1} \mathbf{A}^f (\mathbf{A}^f)^T \quad (9)$$

Where \mathbf{A}^f represents a matrix of ensemble perturbations, or anomalies,

$$\mathbf{A}^f = [\mathbf{x}^{f1} - \overline{\mathbf{X}}^f, \mathbf{x}^{f2} - \overline{\mathbf{X}}^f, \dots, \mathbf{x}^{fm} - \overline{\mathbf{X}}^f] \quad (10)$$

And $\overline{\mathbf{X}}^f$ is the ensemble mean. The analysed state mean and the analysed error covariance are computed as follows just after assimilation:

$$\overline{\mathbf{X}}^a = \overline{\mathbf{X}}^f + \mathbf{K}(\mathbf{Y} - \mathbf{H}\overline{\mathbf{X}}^f) \quad (11)$$

$$\mathbf{P}^a = (\mathbf{I} - \mathbf{K}\mathbf{H})\mathbf{P}^f \quad (12)$$

Where the superscript a stands for ‘‘analysed’’, and \mathbf{K} represents the Kalman gain which is computed as follows:

$$\mathbf{K} = \mathbf{P}^f \mathbf{H}^T (\mathbf{H}\mathbf{P}^f \mathbf{H}^T + \mathbf{R})^{-1} \quad (13)$$

Where \mathbf{R} represents the observation error covariance. The ensemble mean and the ensemble anomalies are updated based on the transform matrix \mathbf{T} :

$$\mathbf{A}^a = \mathbf{A}^f \mathbf{T} \quad (14)$$

$$\mathbf{T} = \mathbf{T}^s \mathbf{U} \quad (15)$$

$$\mathbf{T}^s = \left[\mathbf{I} + \frac{1}{m-1} (\mathbf{H}\mathbf{A}^f)^T \mathbf{R}^{-1} \mathbf{H}\mathbf{A}^f \right]^{-1/2} \quad (16)$$

\mathbf{U} denotes an arbitrary orthonormal matrix and the solution to \mathbf{T}^s is symmetric.

2.4 Verification Methods

Discrepancies between model simulated results and observations can be quantified using several verification tools. Generally there are two categories of verification; verification for deterministic simulations and verification for ensemble simulations. In both categories, the following notations were used. Y_i^{obs} represents the observed value, where as Y_i^{sim} represents the simulated or forecasted value, and Y_i^{mean} is the mean of the observed value.

2.4.1 Verification Statistic for deterministic simulations

I. Nash-Sutcliffe efficiency (NSE):

NSE computes the relative magnitude of the residual variance compared to the variance of the observed data. Its value ranges from $-\infty$ to 1, 1 being the optimal value (Moriassi et al., 2007).

$$NSE = 1 - \frac{\left[\sum_{i=1}^n (Y_i^{obs} - Y_i^{sim})^2 \right]}{\left[\sum_{i=1}^n (Y_i^{obs} - Y_i^{mean})^2 \right]}$$

II. Mean error (ME):

$$ME = \frac{1}{N} \sum_{i=1}^N (Y_i^{sim} - Y_i^{obs})$$

III. Mean Absolute Error (MAE):

$$MAE = \frac{1}{N} \sum_{i=1}^N |(Y_i^{sim} - Y_i^{obs})|$$

IV. Percent Bias (PBIAS):

PBIAS computes the deviation of simulated data/forecast from the observation as a percentage. The optimal PBIAS value is 0 (Moriassi et al., 2007).

$$PBIAS = \left[\frac{\sum_{i=1}^n (Y_i^{obs} - Y_i^{sim}) * 100}{\sum_{i=1}^n Y_i^{obs}} \right]$$

V. Root Mean Square Error (RMSE):

$$RMSE = \sqrt{\frac{\sum_{i=1}^n (Y_i^{obs} - Y_i^{sim})^2}{N}}$$

VI. Pearson Correlation Coefficient (r):

$$r = \frac{\sum_{i=1}^n (Y_i^{sim} - \overline{Y_i^{sim}}) (Y_i^{obs} - \overline{Y_i^{obs}})}{\sqrt{\sum_{i=1}^n (Y_i^{sim} - \overline{Y_i^{sim}})^2 * \sum_{i=1}^n (Y_i^{obs} - \overline{Y_i^{obs}})^2}}$$

2.4.2 Verification Statistic for ensemble simulations

Continuous Ranked Probability Score (CRPS):

In order to interpret the ensemble simulations and forecasts, they need to be converted to probabilities so that they could be evaluated using probabilistic scoring rules. The Continuous Ranked Probability Score (CRPS) is a vital verification tool for probabilistic forecasts of continuous variables (Carney et al., 2006). This method evaluates the probability of forecasts in the form of cumulative distribution functions (Bröcker, 2012) converting the ensembles to a piecewise constant cumulative distribution function.

$$CRPS = CRPS (P, X_a) = \int_{-\infty}^{\infty} [P(x) - P_a(x)]^2 dx$$

Where P and P_a are cumulative distributions:

$$P(x) = \int_{-\infty}^x [\rho(y)] dy$$

$$P_a(x) = H(X - X_a)$$

$$H(x) = \begin{cases} 0, & \text{for } x < 0 \\ 1, & \text{for } x \geq 0 \end{cases}$$

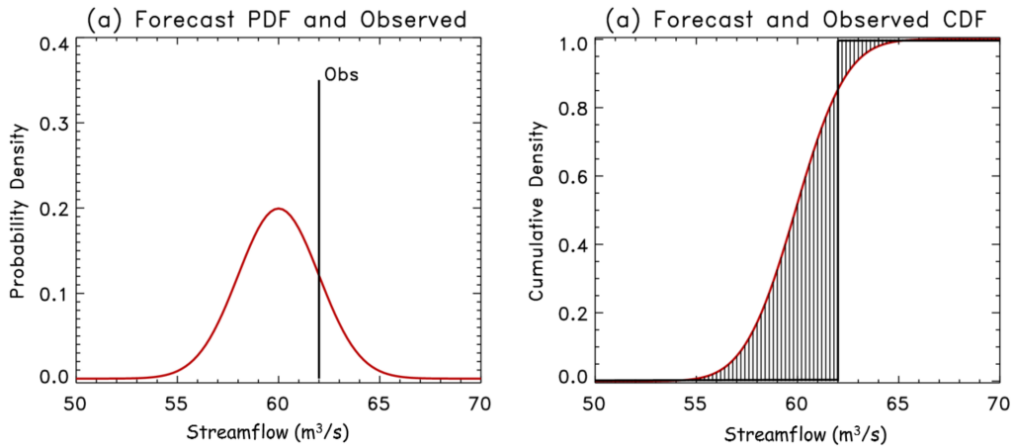


Figure 3: Illustration of CRPS, adopted from (T. Hamill, 2010)

Like RMSE, CRPS statistic has dimensions the same as the observed variable. As illustrated in Figure 3, CRPS compares the cumulative probability distribution (CDF) of the ensemble and the observation. An optimum value of 0 occurs when the CDF of the ensembles matches that of the observation. CRPS computes the square of the difference between the forecast and observed CDFs.

2.4.3 Skill scores

In order to quantify the quality of the ensemble forecasts, it is not enough to have the verification statistics alone. It is customary to define a reference against which a forecast can be judged (Jolliffe, 2003). In other words, the forecasts need to be compared with other reference forecasts or climatology. The general equation used to calculate forecast skills and the two forecast skills used in this study are as follows:

$$Skill = \frac{Score_{ref} - Score_f}{Score_{ref}} \quad CRPS = \frac{CRPS_{ref} - CRPS_f}{CRPS_{ref}} \quad RMSES = \frac{RMSE_{ref} - RMSE_f}{RMSE_{ref}}$$

Where $Score_f$ represents the verification score (calculated using one of the statistics) and $Score_{ref}$ is the verification score of the reference forecast. In this study, open loop simulation (simulation without data assimilation) is considered as the reference forecast. A long term simulation is done with the model (without data assimilation) and the simulation error is quantified with the deterministic verification statistic outlined in 2.4.1 and this error is assumed to be the verification score for the reference forecast.

3. Case Study

The study area is the upper Murrumbidgee catchment (shown in Figure 4), located in the Murray Darling Basin, in southern New South Wales, Australia with a total area of 84,000 km². Elevations reach up to 2,200 meters in the eastern ranges plummeting to 50 meters in the western plains. The climate varies significantly from alpine conditions in upper parts of the catchment to semi-arid conditions in the Riverina plains further downstream. The Murrumbidgee River spanning almost 1,600 kilometres, is Australia's second longest river and a major tributary of the Murray river. The catchment supports a population of 520, 200 people in addition to several irrigation districts and a complex range of natural ecosystems that rely on it (NSW Office of Water, 2011).

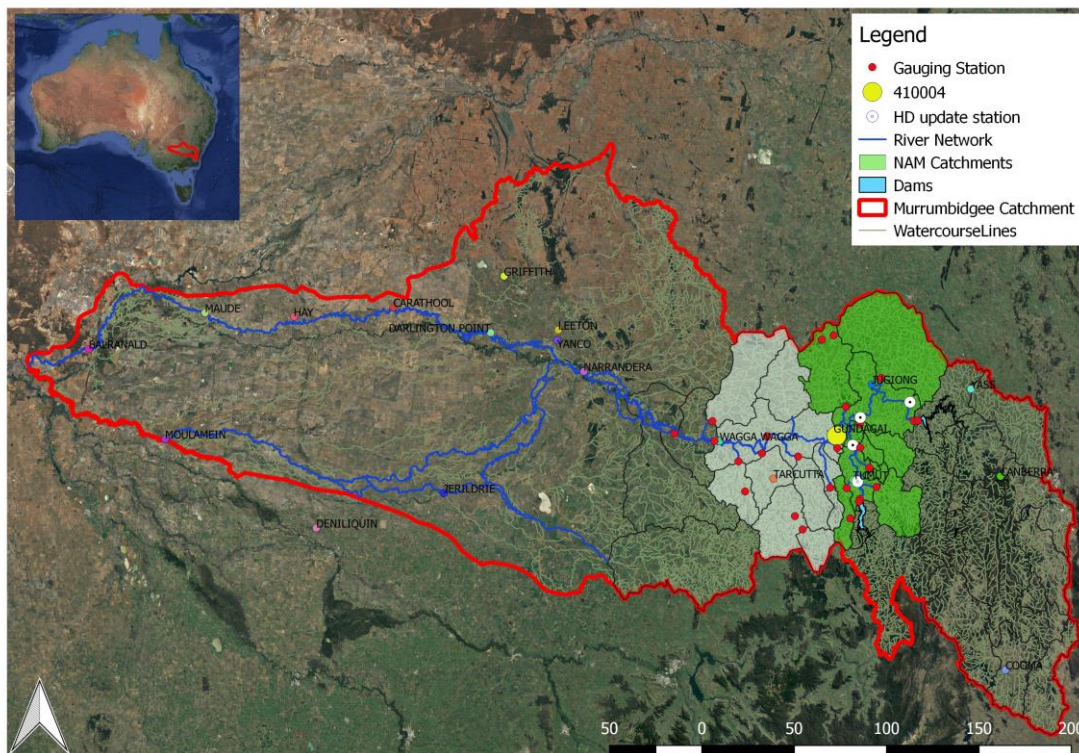


Figure 4: Study Area - Murrumbidgee catchment

Rainfall in the catchment varies a lot but it ranges from 350 millimetres on the western plains to well over 1,700 millimetres in the Snowy Mountains as shown in Figure 5. The land use in the catchment is mainly devoted to extensive agriculture with grazing occupying 64% of the catchment (NSW Office of Water, 2011). However, the upper-Murrumbidgee which is the specific case study area is mainly comprised of conservation areas and forests. Streamflow is monitored with more than 100 river gauges within the catchment that record flows continuously. The Murrumbidgee River at Gundagai (location of interest for data assimilation) has a mean daily flow of about 114 m³/s with a catchment area of 21,100 km². Gundagai was hit by severe floods several times, recent flooding events include the 2012 and the 2016 floods. The 2012 flood had a staggering 4000m³/s discharge at Gundagai. Gundagai was also hit by the “worst flood to ever hit Australia” in 1852 that claimed the lives of 89 people (FloodList, 2013).

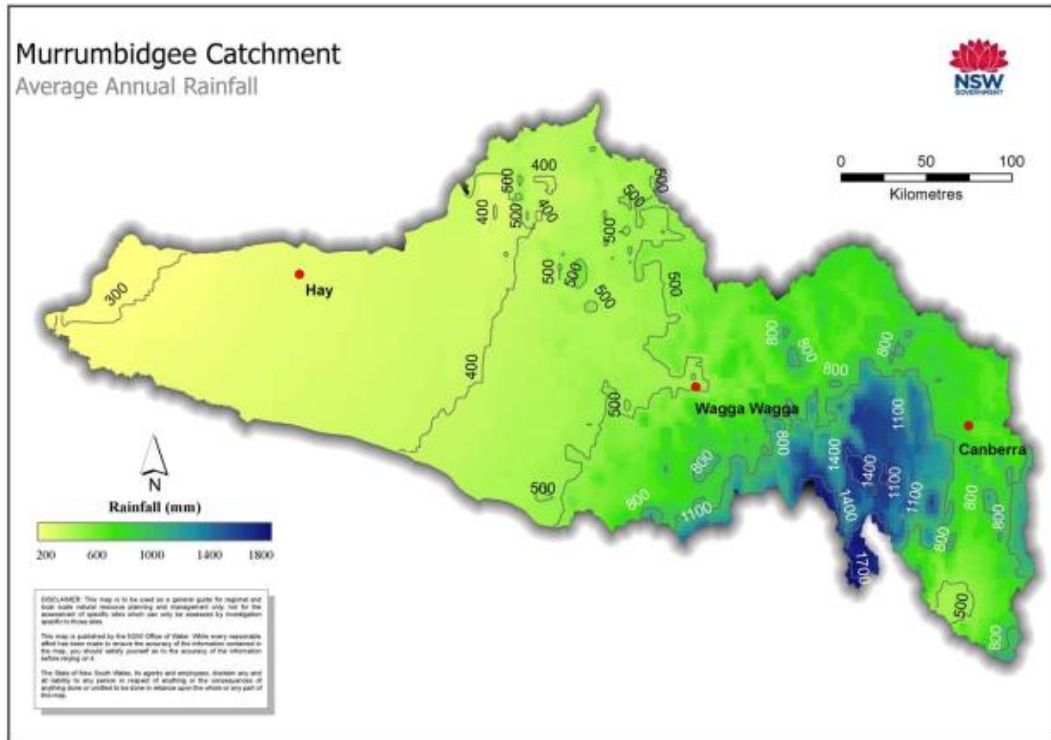


Figure 5: Average annual rainfall in the Murrumbidgee catchment. Adopted (NSW Office of Water, 2011)

The Murrumbidgee River caters for the water demands of towns, irrigation fields, wetlands, and hundreds of other users that extract water along the river by direct pumping. The river flow is regulated by the Burrinjuck and Blowering dams and other weirs and off-stream storages. The required amount of water is delivered by the State Water through a controlled release of water from the two dams.

The daily management of the river to fulfil the above demands is very complex. The different river processes are difficult to quantify and thus the optimal reservoir release is compromised and oftentimes a surplus release is issued. Moreover the river tributaries downstream of the two dams contributing additional flows and the change in water orders further complicate the river operation process. This is evidenced by river operators issuing a conservative reservoir release which is more than required because of the high uncertainty they are dealing with. As a result, the common suboptimal release strategies have been leading to inefficient river management. This inefficient operational practice needed to be redeemed and a new decision support system, the Murrumbidgee Computer Aided River Management (CARM) was introduced. Its overall goal is to enhance the efficiency of operational dam and weir release strategies. It is composed of different MIKE simulation models developed by DHI that capture the key catchment runoff and other relevant river flow processes. The tool makes use of real time measurements and models to provide a comprehensive decision support system. Taking into account forecasts of river inflows and real time water orders, optimization of dam operations is possible. (T. van Kalken et al. 2012).

With the implementation of the CARM decision support system (DSS), it is intended to assimilate measured flows and water levels in the hind-cast period in order to capture accurate description of the state of the river just before the time of forecast. This will enhance the streamflow forecast accuracy greatly. However, the data assimilation

system in the current CARM DSS operates in such a way that only the rainfall-runoff modelling outputs (catchment outflows) are updated and state variables which describe the hydrological state of a catchment [surface storage, overland flow reservoirs, Interflow reservoir, Groundwater storage etc.] are not updated. It is obvious that the hydrological states determine the actual state of the catchment and not considering them in the data assimilation will have some adverse effect on streamflow forecast as the current condition of the catchment is not represented well. This study is expected to bring an added value [by incorporating combined hydrodynamic-hydrological model states updating] to the current data assimilation procedures being implemented within CARM DSS in order that the actual state of the catchment will be represented with greater accuracy which will in turn lead to a more accurate streamflow forecast.

4. Data and Model Setup

This chapter discusses the types of data used for the study as well as the different model setups used for the analysis. The hydrological-hydrodynamic model has already been calibrated and validated thus this study is focused mainly in applying the ready-to-use model together with the Data Assimilation Framework in order to make state updating and forecasting experiments.

4.1 Data Used

4.1.1 Precipitation

Observed rain gauge precipitation data is obtained from the New South Wales, Department of Primary Industries Water main website (DPI, 2017) for the period of 2012 to 2016.

In this study, alternative precipitation products were also used in addition to the rain gauge rainfall data. Three satellite rainfall products namely, TRMM 3B42 RT, CHIRPS, and PERSIANN-CCS were used in comparison with rain gauge data. Sub-catchment level daily rainfall estimate was downloaded for the above satellite products using in-house (DHI) scripts.

Table 1: Satellite rainfall dataset used for analysis

Satellite product	Temporal Resolution	Spatial Resolution ¹	Calibration period	Validation period	Remarks
TRMM 3B42 RT	Daily	0.25 ⁰ x 0.25 ⁰	2005-2012	2013-2016	-
CHIRPS	Daily	0.25 ⁰ x 0.05 ⁰	1990-2012	2013-2016	-
PERSIANN-CCS	Daily	0.04 ⁰ x 0.04 ⁰	-	-	Several missing data

The satellite rainfall estimates were used in a rainfall-runoff model and the model was calibrated and validated for the periods outlined in Table 1. Since the PERSIANN dataset has several missing data, it was not considered for rainfall-runoff simulation.

Considering several factors, the most appropriate precipitation product will be used to run the rainfall-runoff simulations, hydrodynamic modelling as well as data assimilation experiments.

4.1.2 Discharge

Hourly discharge data from 1990 to 2016 was obtained from the same source as that of the rain gauge precipitation. These include discharges measured at catchment outlets and also along the river. The hourly discharge observations are used as diagnostic variables in the assimilation process meaning the observed discharges are considered true values with which the assimilated discharge will be verified against. A time series for the release information from the Burrinjuck and Blowering dams is also obtained which was used as a boundary condition for the hydrodynamic model.

¹ One degree around the equator is approximately 110km

4.2 Model Set-up

The hydrological-hydrodynamic modelling in this study was carried out with MIKE 11 hydrological-hydrodynamic model.

4.2.1 Hydrological model

MIKE NAM, which is the rainfall-runoff module of the MIKE 11 modelling system, simulates rainfall-runoff processes at the catchment scale (Madsen et al., n.d.). It is a lumped, conceptual model that comprises of several mathematical equations describing the simplified version of the land-phase of the hydrological cycle. Different components of the rainfall-runoff process are represented by the model by continuously accounting for the water content in four different storages which are interrelated, viz. snow storage, surface storage, root zone storage, groundwater storage (Dhi, 2007).

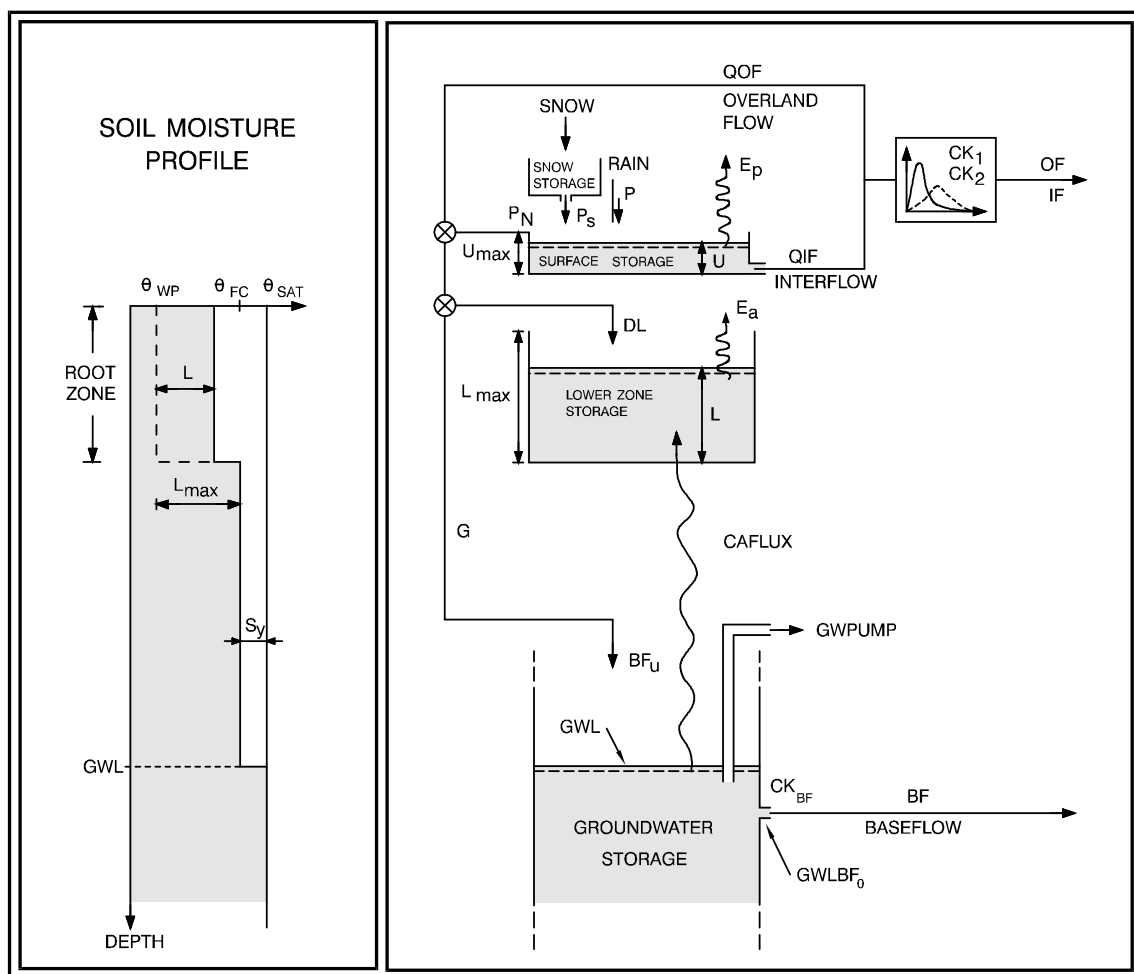


Figure 6: Structure of MIKE NAM model. Adopted from (Dhi, 2007)

Figure 6 illustrates the physical processes that are involved in the simulation of runoff in the NAM model, the catchment runoff computed by NAM split into overland flow, interflow, and baseflow as shown in Figure 6. The inputs to the rainfall-runoff model include catchment average meteorological data such as precipitation, potential evapotranspiration and temperature (when snow module is considered). Taking into account the above inputs, NAM computes the catchment runoff which can in turn be used for hydrodynamic modelling. The rainfall-runoff model includes all the sub-

catchments that are shown in Figure 7, however, this study is concerned with all the eleven catchments upstream of Gundagai which is a small town that has been hit by flooding several times.

The sub-catchments of interest (for the implementation of data assimilation) are marked yellow as shown in Figure 7. Detailed MIKE 11 rainfall-runoff and river hydrodynamic models for the model domain have already been setup and calibrated by DHI in collaboration with State Water Corporation (SWC). Table 2 outlines the sub-catchments within the model domain. Comparison of hydrological model states update was done for the Goobarragandra sub-catchments.

Table 2: Sub-catchments within the model domain

Sub-catchment name	Area (Km ²)	Annual Precipitation (mm)	No. rain gauges
JUGIONG	2133.6	466	7
GOOBARRAGANDRA	668.7	930	5
MUTTAMA	1079.8	846	7
BRUNGLE	119.1	824	4
ADJUNGBILLY	390.1	886	5
GILMORE	276.9	1348	4
RES_BJUCK_GUND	1257.8	828	7
RES_TUMUT_US_BRUNGLE	444	747	7
RES_TUMUT_DS_BRUNGLE	111	965	3
KILLIMCAT	22.6	1327	1
UG_BOMBOWLEE	78.3	1028	3

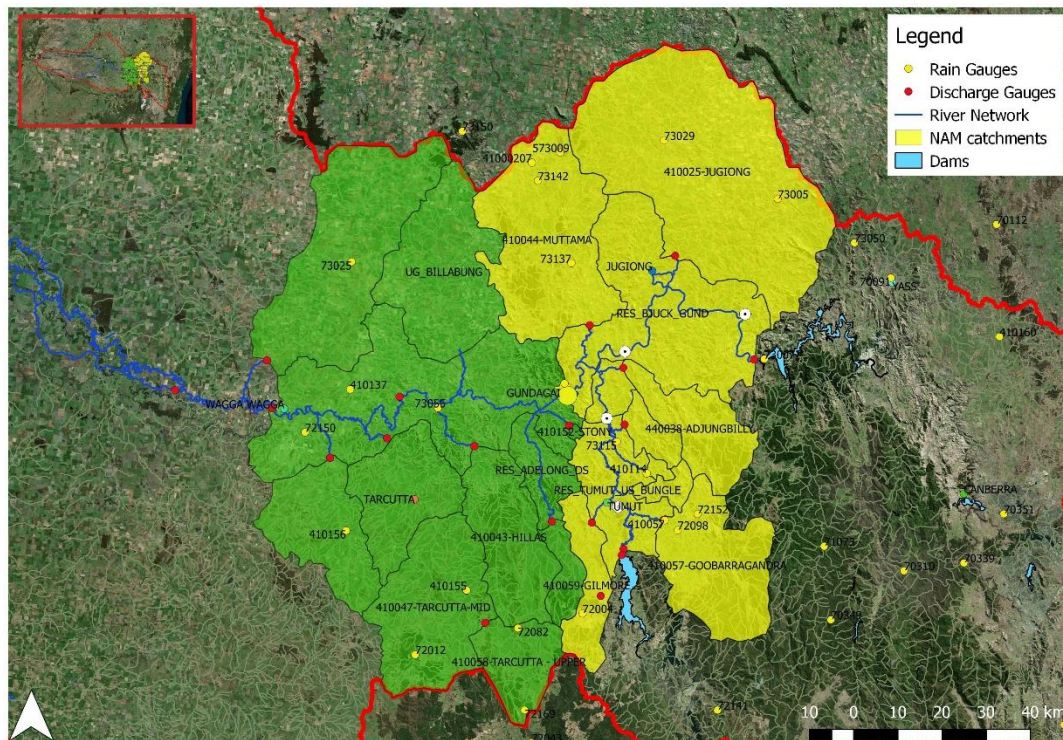


Figure 7: Model domain - selected sub-catchments shown in yellow

4.2.2 Hydrodynamic model

MIKE 11 hydrodynamic module (HD) is a one dimensional flow model that implements an implicit, finite difference scheme in order to compute unsteady flows in rivers and channels (Dhi, 2007). Boundary conditions in the model include, discharge, water level, discharge/water level relation, wind field, dam break and resistance factor. Rivers and floodplains are represented as interconnected branches (Kamel, 2008). Discharge and water levels along the river branches are computed at alternative points with respect to time as illustrated in Figure 8.



Figure 8: Model discretization for discharge and water level computation.
Adapted from (Blasone, 2014)

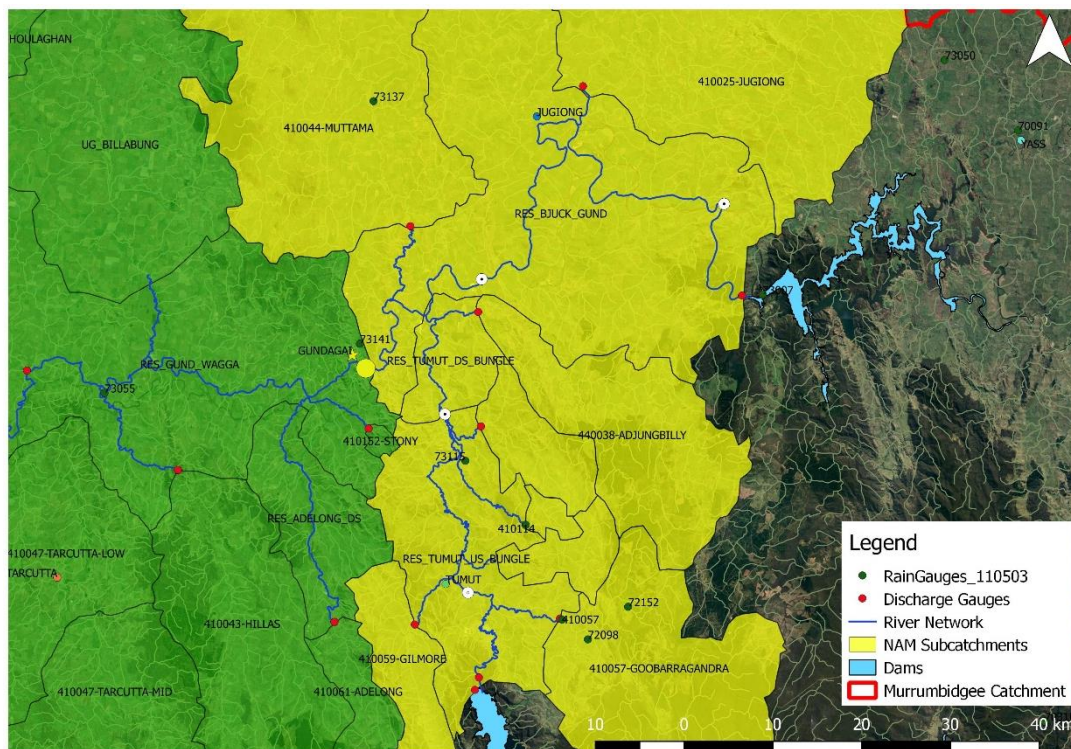


Figure 9: MIKE 11 setup for the model domain

The eleven sub-catchments in the model domain (see Figure 7) generate a lateral inflow in the MIKE 11 river model. The river network and the corresponding sub-catchments with the two dams upstream are shown in Figure 9.

5. Research Methodology

This chapter is devoted to the detailed description of the methodology used in this study. It begins with the outline of the method used to select appropriate precipitation product for further analysis in 5.1. Followed by a brief introduction of the model states (5.2) that will be updated with the data assimilation technique. A through description of the data assimilation framework used for the study is discussed in 5.3. The different categories of data assimilation implemented in the study and the effect of data assimilation on forecasts will be elaborated subsequently. Procedures used to carry out sensitivity analysis of the data assimilation filter follow in 5.6. The high-level workflow of this study is shown in Figure 10 and the corresponding detailed workflows are displayed in Figure 11, Figure 12, and Figure 13 respectively.

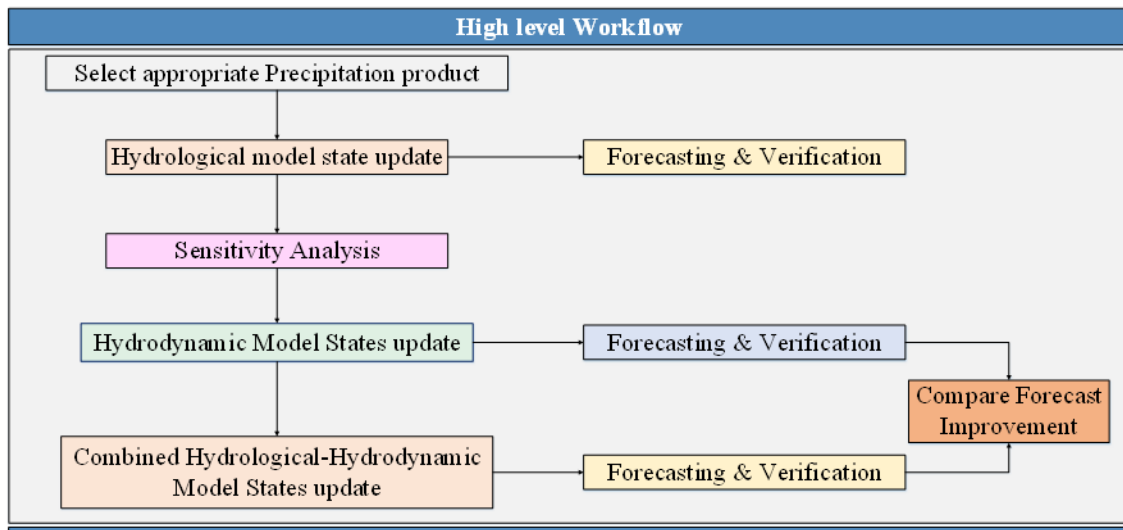


Figure 10: High-level workflow

5.1 Selecting appropriate precipitation data

This section discusses the methodology used to compare and select appropriate precipitation data for data assimilation and forecast experiments. As described in 2.1, one of the methods used to reduce uncertainty in hydrological models and forecasts is to acquire a higher quality hydrologic data. This includes acquiring reliable precipitation data. This guarantees better model calibration, simulation and more reliable forecasts. In pursuit of this, the use of three satellite rainfall products was studied on rainfall-runoff modelling for one of Murrumbidgee sub-catchments. First, the different satellite rainfall products will be compared with rain gauge observations, followed by the application of bias correction on the satellite rainfall products in order to account for errors. The bias corrected satellite precipitation will then be used to re-calibrate the already available model (which is calibrated with rain gauge rainfall data). Finally, the bias corrected satellite precipitation will be used for rainfall-runoff simulation and the corresponding errors in simulation will be analysed and compared with that of the rain gauge. Eventually the rainfall product that can simulate the rainfall-runoff process in a better way will be selected as the appropriate precipitation data.

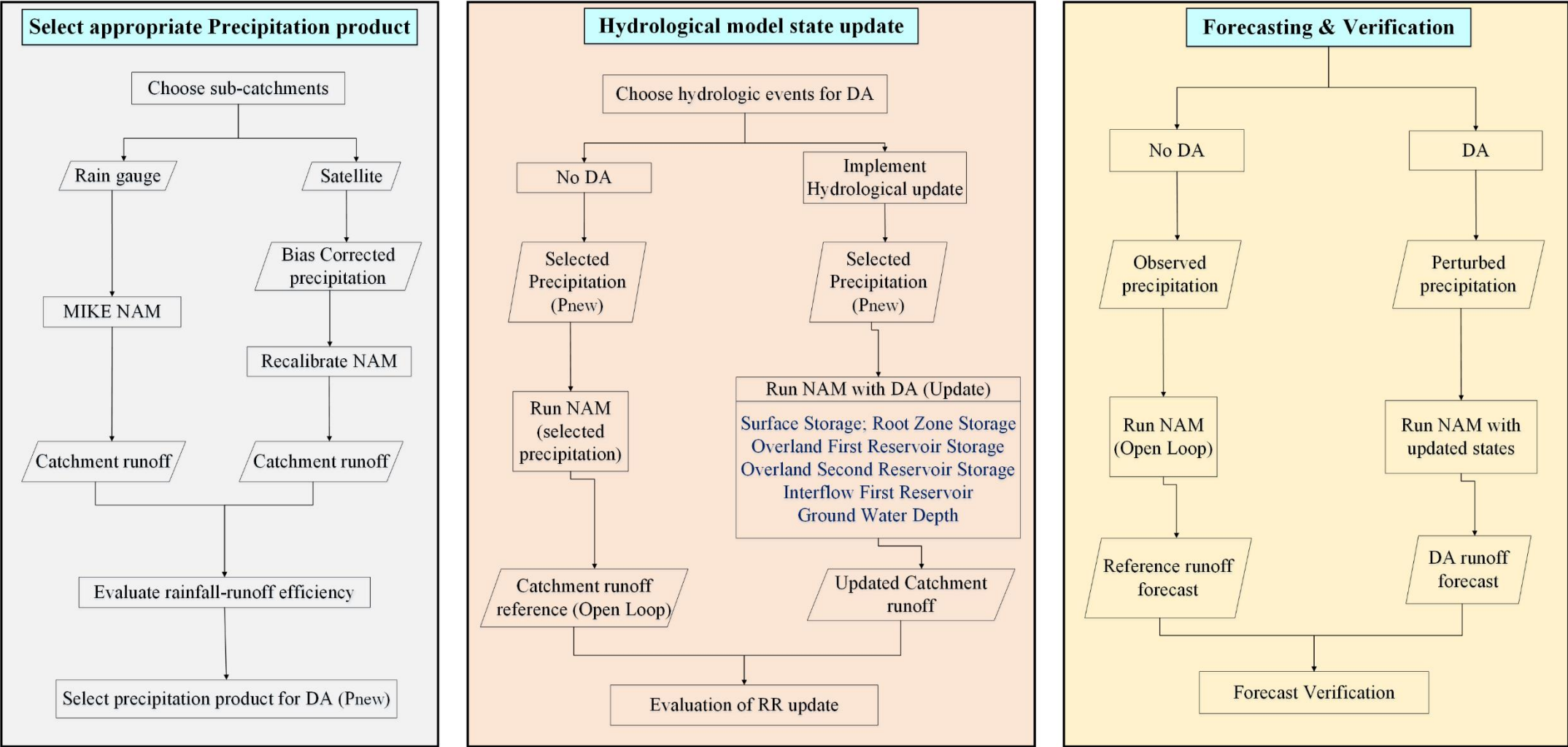


Figure 11: Detailed workflow #1

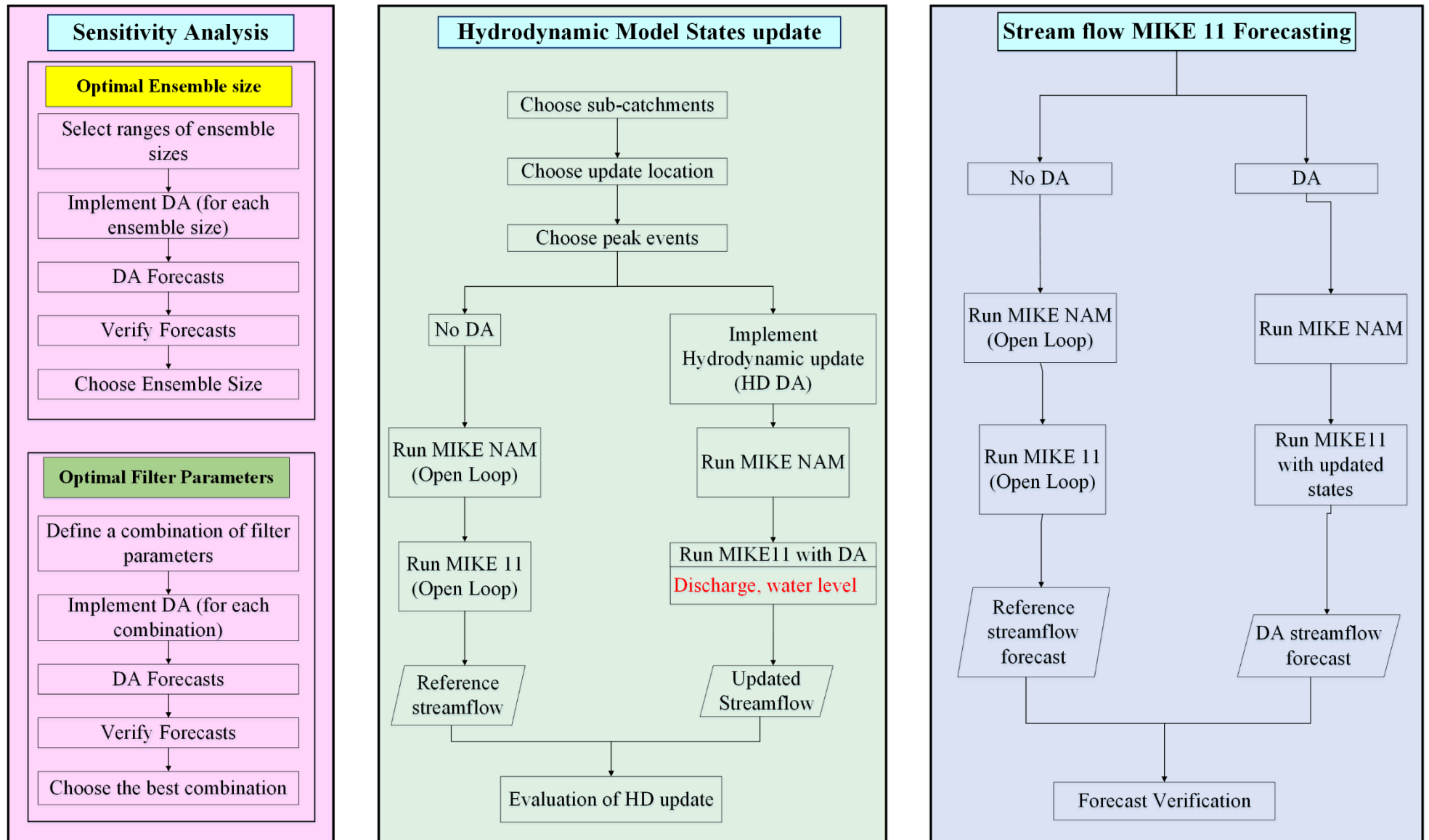


Figure 12: Detailed workflow #2

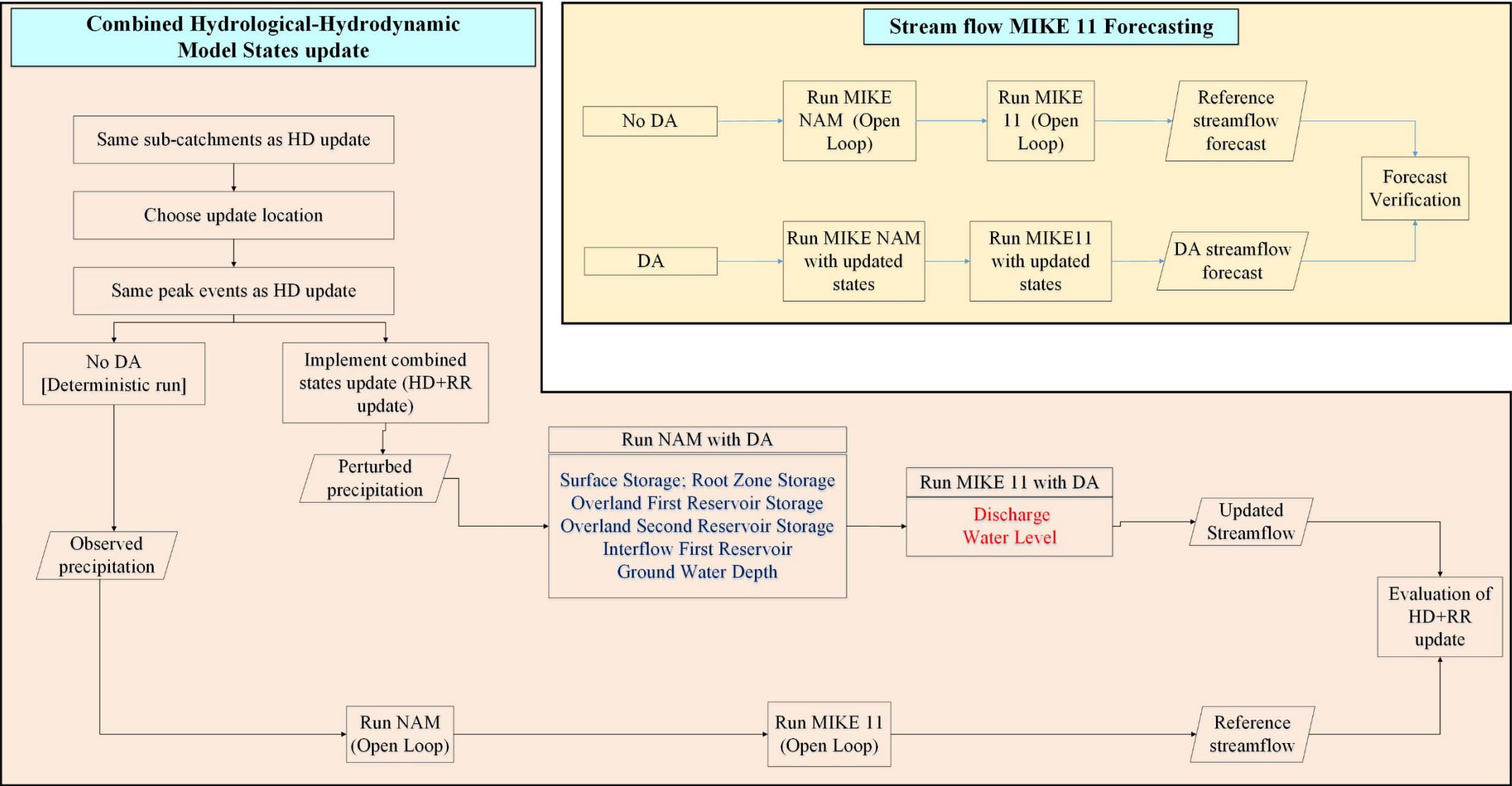


Figure 13: Detailed workflow #3

5.1.1 Bias Correction Method

Satellite rainfall estimates contain large systematic as well as random errors (Habib et al., 2014) and this could be due to gaps in revisit times, discrepancies between remotely sensed signals and rainfall rates or due to atmospheric fields that affect the radiation field (Xing Liu et al., 2015). Thus, it is crucial to investigate and correct the bias in satellite-based precipitation products before they are to be used for rainfall-runoff modelling. Otherwise, if the bias is not taken into account, the rainfall-runoff modelling will exhibit large uncertainty. A multiplicative bias correction factor is used in this study, whereby the satellite rainfall estimate is multiplied by a factor which is the ratio between the satellite and rain gauge rainfall estimates. Better correlation was found in the monthly scale, thus bias correction factors are computed on monthly basis. Daily rainfall estimates from the satellite products as well as instantaneous rain gauge measurements were aggregated to a monthly time scale and the following equation was used to compute the bias correction factor K .

$$RG_m = K_m * SRE_m$$

Where RG_m and SRE_m represent the monthly average rainfall during the month m from the rain gauge and the satellite rainfall products respectively, and K_m is the bias correction factor for the month of m . Since the average monthly rainfall data were used (from 2013 to 2016), all the months of January for instance are corrected with the same bias correction factor (K_m). Thus, monthly corrected satellite rainfall estimates can be computed as follows where $SRE_{corr,m}$ and $SRE_{raw,m}$ are corrected and raw (uncorrected) rainfall estimates for the month m .

$$SRE_{corr,m} = K_m * SRE_{raw,m}$$

In order to simulate the rainfall-runoff process, the monthly corrected satellite rainfall estimates need to be disaggregated to daily time steps. To this end, an empirical factor adopted from (Arias-Hidalgo et al., 2013) was computed using the following equation:

$$f_{d,m} = \frac{P_{d,m}}{RG_m}$$

Where $f_{d,m}$ represents the temporal disaggregation factor, and $P_{d,m}$ is the total rainfall measured on the day d of the month m , and RG_m is the total rainfall (rain gauge) measured during the month m . Thus:

$$SRE_{corr,d} = f_{d,m} * SRE_{corr,m}$$

Where $SRE_{corr,d}$ represents the corrected satellite rainfall on the day d .

5.1.2 Rainfall-runoff simulation

The usefulness of the bias corrected satellite rainfall estimates will be investigated by performing a rainfall-runoff simulation. To this end, a single sub-catchment, Goobarragandra was selected and the hydrological model was re-calibrated for this sub-catchment using the bias corrected satellite rainfall estimates. It is to be recalled that the rain gauge rainfall data is limited to four years (2013 - 2016), however in order to re-calibrate the hydrological model with adequate data, the satellite rainfall estimates dating back to 2005 (TRMM) and 1990 (CHIRPS) were corrected with the same bias correction factor computed using the equations in 5.1.1. After re-calibration, the model will be validated and corresponding errors in simulation of runoff will be analyzed. Eventually the rainfall-runoff simulation (using satellite precipitation) will be compared with that of the rainfall-runoff simulation (using rain gauge precipitation) and depending on how good the process is represented the appropriate precipitation product will be chosen.

5.2 Model states to be updated

This study aims to update hydrological and hydrodynamic model states separately as well as in a combined manner making use of streamflow observations. As explained in 4.2.1, the NAM model states consist of several storages that represent the different components in the catchment process which are illustrated in Figure 6. It's apparent that incorrectly estimated catchment states would lead to discrepancies between observed and simulated streamflow. Thus by assimilating observed streamflow both the hydrological and hydrodynamic states can be updated. Eventually, the updated hydrological-hydrodynamic states help to attain a better prediction of streamflow.

Table 3: Selected model states for data assimilation

No.	Model State	unit	Type	Class ²
1	Surface Storage	%	Hydrological	G
2	Root Zone Storage	%	Hydrological	G
3	Overland First Reservoir Storage	m	Hydrological	G
4	Overland Second Reservoir Storage	m	Hydrological	G
5	Interflow First Reservoir	m ³ /s	Hydrological	G
6	Ground Water Depth	m	Hydrological	G
7	Total Runoff	m ³ /s	Hydrological	O
8	Discharge	m ³ /s	Hydrodynamic	G/O
9	Water Level	m	Hydrodynamic	G

Table 3 outlines the list of model states selected for data assimilation. A hydrological update (RR update) is where the rainfall-runoff model states are updated. These are the model states ranging from 1 to 6. By assimilating observed discharges (total runoff) at the catchment outlets, the six internal model states will be updated. The second category of data assimilation is where only the hydrodynamic model states are updated; these are the eighth and ninth model states shown in Table 3. Using the observed discharges on selected gauging stations, the discharge and water levels will be updated. Note that this category of update does not update the hydrological model states. Finally, all the hydrological model states (1 to 6) as well as the hydrodynamic states (8 & 9) can be updated simultaneously. The above three categories of data assimilation will be explained in detail in 5.4.

Several data assimilation experiments have been done by accessing the DHI Data Assimilation Framework (which will be explained shortly) in order to update the above hydrologic as well as hydrodynamic model states.

5.3 Data Assimilation Framework

The DHI Data Assimilation Framework (DA framework) is a set of generic assimilation filters, noise models, observation mapping methods and result analysis tools (DHI, 2017). Object-oriented best practices were used to design the DA framework in a modular fashion with interfaces that define the boundaries of each module. The DA framework is coded in C# by using the .NET 4.0 Framework. The matrix equations are solved using the system optimized Intel Math Kernel Library (MKL) (Madsen et al.,

² G and O stand for general and observable model states

n.d.). The DA framework can implement different types of assimilation in order to update the state variables or parameters. However, in this study the framework was used to update the state variables (model states); the parameters are assumed to be optimized during calibration. The framework supports different ensemble based KF algorithms such as classical EnKF, ETKF (which is used for this study), as well as Deterministic Ensemble KF. In order to apply these filters, an ensemble of model runs is needed after which the filter recursively computes the Kalman gain based on the uncertainty in the model and the uncertainty in the observations. Procedures for localization (described in detail in 5.3.2 are also included in the framework in addition to the different stochastic error models that describe model and measurement errors.

A discretized MIKE 11 model shown in Figure 8 for instance is comprised of a number of state variables some of which are outlined in Table 3. With the framework, state variables of interest are chosen as in Table 3. A state vector is then defined that includes the selected state variables, thus all the state variables within the state vector will be updated during the assimilation period. The DA framework contains five main modules as illustrated in Figure 14.

- **Core:** communicates and controls all the modules
- **User configuration:** reads a PFS file that contains the details of the assimilation experiment specified by the user such as ensemble size, location of the model on disk, location observation, chosen filter, localization details, noise models, and the selected state variables to be included in the state vector.
- **Filters:** the filter takes abstracted vectors and matrices from the Core and solves the KF equations to calculate the optimal correction to the ensemble of models.
- **Observations:** handles observations and mapping observation points to the model space.
- **Error models:** include generic perturbation algorithms for defining uncertainty in model forcings, initial conditions, model states and observations.

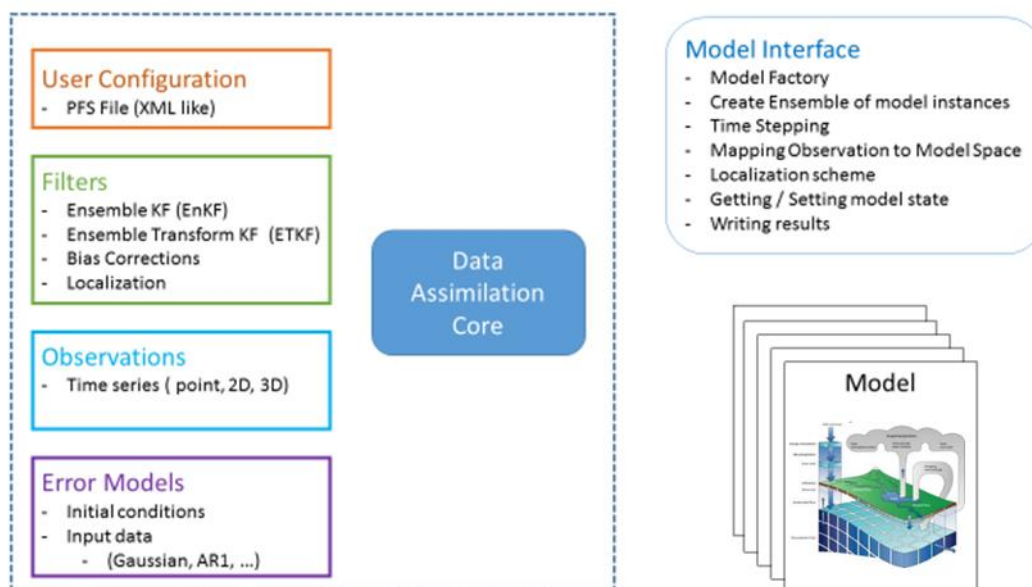


Figure 14: Overview of the modules included in the DA framework. Source (DHI, 2017)

The Model Interface shown in Figure 14 is required in order to connect the MIKE 11 model to the DA framework. These interfaces define how the model is created and

controlled in time. The ensemble of models is created from a single model instance, and each ensemble member is perturbed during simulation within the MIKE 11 model engine. The DA implementation supports the update of discharge and water level states in the hydrodynamic model and the internal model states in the hydrological (rainfall-runoff model) as outlined in Table 3.

The DA framework performs a number of tasks:

1. Reads a configuration (PFS) file to set up the assimilation system
2. Creates an ensemble of model instances and a main model³
3. Reads observation files and collects them in an Observation Collection class.
4. Maps the observations to the model indices to find the “H”⁴ matrix. Also if localization is enabled, it calculates the distances between model grid elements.
5. Time steps all model instances (Ensemble and MainModel) to the time of first observation.
6. The Core reads model values and observation values to create the matrices for assimilation.
7. The Filter is called with access to the matrices. Assimilation step calculates the new updates. Filter results are stored to files.
8. The models are updated.
9. Steps 5-8 are performed until there are no more observations.
10. The models are allowed to run to their end times.

5.3.1 Perturbation Methods

Discrepancies between observations and model predictions stem from three sources of uncertainty, viz., observations, model forcings or model boundaries and model structure. By perturbing the model an ensemble is generated that represents the uncertainty in the model state estimate. Each ensemble member is then propagated forward and the hydrological model states are simulated given the continuously perturbed forcing as well as states (Xie et al., 2010). Model uncertainty inherent to the NAM model states can be addressed by carrying out state or forcing perturbation utilising appropriate perturbation methods in the DA framework. Precipitation is the sole model forcing that is perturbed in this study considering that it is a dominating source of uncertainty. In this study perturbation is applied on model forcing (precipitation).

Forcing Perturbation

Precipitation is considered as the most uncertain model forcing owing to its short temporal and spatial correlation length scales. Thus it is challenging to reduce the uncertainty in precipitation (Y. Liu et al., 2012). In a data assimilation context, the most common way to quantify uncertainty in precipitation is by stochastically perturbing the precipitation inputs. The DA framework has several perturbation methods that can be used for a specific model. It consists of several forcing perturbation types, however, the relative normal perturbation is implemented for this study. The perturbation equation is as follows:

$$u_{perturbed} = u + u * \varepsilon$$

³ Main model: the ensemble mean

⁴ Observation operator: Relates available observations to the model states in the state vector

Where u is forcing (precipitation in this case) and ε represents the relative error drawn from a normal distribution, $\varepsilon \in N(0, \sigma_{frac}^2)$, where σ_{frac}^2 is the standard deviation of the fractional error specified by the user (DHI, 2017).

Time correlation

Errors associated with forcings are time correlated and their dependency between model time steps should be considered. A first order autoregressive (AR1) normal distribution error model is used to model the time correlated error in the perturbation methods (DHI, 2017). The following equation describes the sampling of the error.

$$\varepsilon_t = \varphi \cdot \varepsilon_{t-1} + \gamma_t$$

Where ε_t and ε_{t-1} are the errors sampled on the current and previous time steps, φ the correlation coefficient and γ_t the independent sample added to the error from the previous time step. Rather than defining φ directly it is calculated from an exponential decay equation where the half time constant, $T_{1/2}$, of the time correlated error must be specified:

$$\varphi = \exp\left(-\frac{\Delta t \cdot \ln(2)}{T_{\frac{1}{2}}}\right), \quad T_{\frac{1}{2}} > 0$$

Δt is the time span from $t-1$ to t and $T_{1/2}$ the half time. The AR1 model is applied to the error, ε . γ_t , the independent sample, $\varepsilon \in N(0, (1 - \varphi^2) \cdot \sigma^2)$. σ is specified by the user as the standard deviation of the relative error when relative perturbation is used and otherwise as the standard deviation of the error in real values.

5.3.2 Localization

Localization is an algorithm used to reduce the impact of errors in ensemble Kalman filters (Anderson, n.d.). It reduces the spatial domain of influence of observations during the update. In large systems inadequate sampling due to limited number of ensemble sizes leads to spurious correlations⁵ between distal locations in the background covariance matrix. The purpose of localization is to prevent these spurious correlations from causing observations from one location to affect erroneously the analysis at a distal location. When localization is implemented, ensemble anomalies outside of a local window are set to zero; greater emphasis is given to states closest to the observation (DHI, 2017). A distance-based localization (shown in Figure 15) technique was used in this study in which a spatial window is created around each observation point where non-zero localization weights are used. In other words a localization weight of zero is used for model grid points far away (can be specified by the user) from the observation. The DA framework offers constant, triangular, exponential, linear and Gaussian localization methods. A triangular localization method was used for this study where the model grid closest to the observation point will have the highest localization weight and this weight decreases linearly when going away from the observation point in a triangular fashion.

⁵ A false premise that two variables are correlated when in actuality they are not (Investopedia, n.d.)

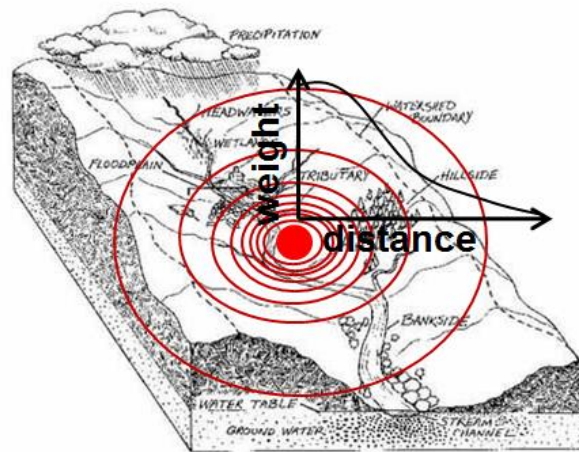


Figure 15: Localization (Source: DHI Data Assimilation Framework)

Spatial correlation

Catchment rainfall is not only temporally correlated; it is spatially correlated too. Thus the spatial correlations can be introduced similarly as for time correlations through the sampling of the errors, ε . If an AR1 model is used the transformation of the error is applied to the independent sample.

Cholesky decomposition is used to transform the uncorrelated errors, ε into correlated errors. The correlation matrix, itself must be generated outside the DA framework and specified as input.

Through Cholesky decomposition the correlation matrix, C is factorized into:

$$C = LL^T$$

Where L is used to generate correlated errors by:

$$\varepsilon_{corr} = L \cdot \varepsilon$$

The correlation matrix, C , was prepared by computing the correlation of monthly accumulated rainfall for the eleven catchments in the model domain. Due to the several missing rainfall data from the rain gauges, the correlation matrix was calculated on a monthly time scale by aggregating the instantaneous precipitation time series.

5.4 Implementation of Data assimilation

Under this section, the three different data assimilation methods applied will be discussed. The three assimilation methods are hydrological model states update, hydrodynamic model states update and combined model states update. The implementation of data assimilation is following the selection of the appropriate precipitation product.

5.4.1 Hydrological model states update

The first step in the process of studying the combined hydrodynamic-hydrological model state updates is to test the data assimilation on individual sub-catchments. The Murrumbidgee catchment is comprised of several sub-catchments and two sub-catchments (marked purple in Figure 16) were chosen based on differences in terrain and rainfall variability. This will allow to investigate the performance of the data assimilation in different types of catchments and it will also help study the optimum values for the filter parameters for different types of sub-catchments.

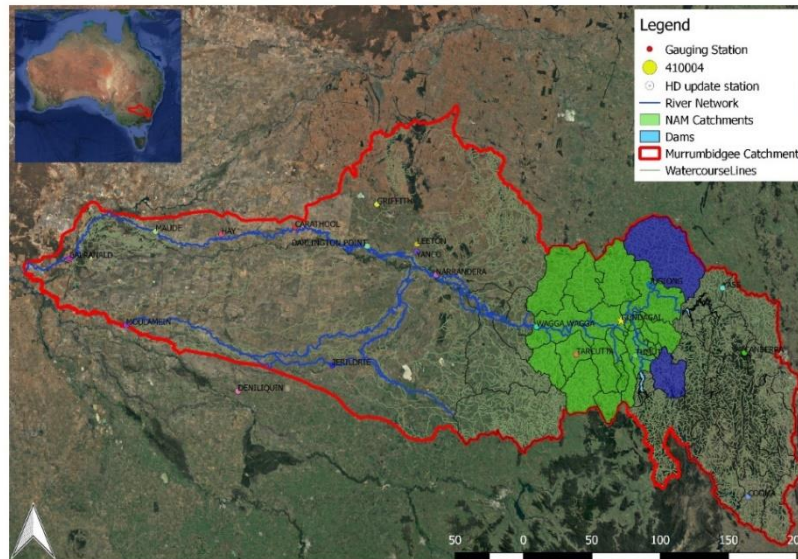


Figure 16: Two chosen catchments (purple) for implementation of data assimilation

To this end two sub-catchments namely, Goobarragandra and Jugiong were chosen for this specific part of the study as shown in Figure 16. The former one is characterised by a mountainous terrain and it is a high yielding sub-catchment (wet sub-catchment) whereas the latter is mostly dry. A comparison of monthly mean discharge (2012 to 2017) for the two catchments is shown in Figure 17.

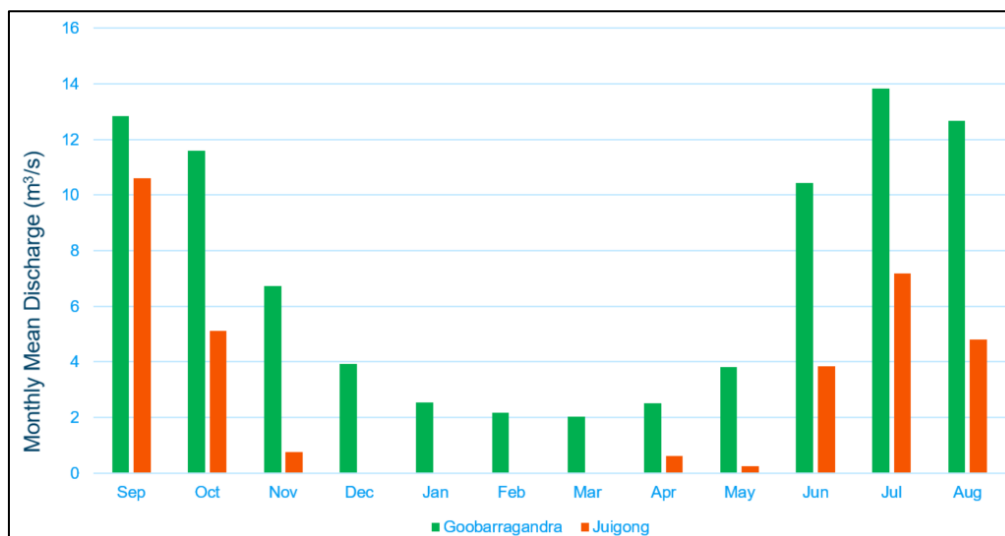


Figure 17: Monthly Mean Discharge Comparison for the selected catchments (2012 to 2017)

5.4.2 Hydrodynamic model states update

Streamflow measurements from four interior gauging stations (marked white in Figure 18) are assimilated and observed discharge at a downstream location (Gundagai) is used for streamflow validation purposes. In this case, the state vector includes only the hydrodynamic states, namely discharge and water level. Similarly the results of the assimilation will be further evaluated by generating consecutive forecast experiments to estimate the discharge at Gundagai. Consecutive forecasts with a lead time of seven days will run for a period of a year. Thus the performance of the forecasts based on the hydrodynamic update will be verified as a function of lead time. Detailed results and discussion of this analysis can be found in 6.5.

5.4.3 Combined hydrodynamic - hydrological model states update

The state vector in this analysis is comprised of two hydrodynamic states (Discharge and Water level) and six hydrological states. There are 11 gauging stations where hourly discharge is made available of which seven are located at the catchment outlets and the other four in the middle of the river network. Thus, assimilating the observed discharges at the catchment outlets, the hydrological states of the catchments are updated and assimilating the river discharges in the middle of the river, the hydrodynamic states of the river are also updated. The results of this analysis are illustrated in in 6.6.

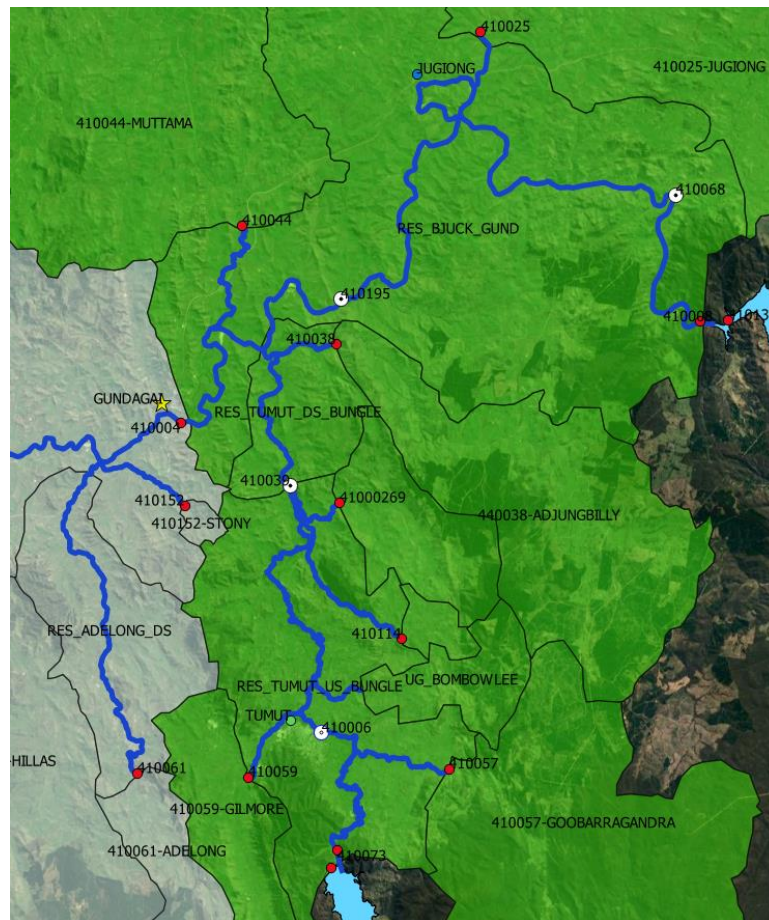


Figure 18: Model domain, points marked white are used for hydrodynamic update whereas stations marked red are used for both hydrological and hydrodynamic update

5.5 Investigating the effect of DA on forecasting

After the model states are updated up until the time of forecast, the effect of data assimilation can be validated by making a series of forecasts. The forecast strategy used in this study is similar for all the three categories of updating explained in 5.4. The forecast strategy used for the Sensitivity Analysis is slightly different and will be explained in 5.6. Data assimilation is employed for a longer time frame, mostly ranging from 6 months to 1 year by assimilating available observations and sequentially updating the model states. At the end of the data assimilation period, a hot-start information is stored to be accessed at the time of forecast. The time of forecast is chosen within the time frame covered by the assimilation period (refer Figure 19) in order to study the benefit of the assimilation on forecast improvement. Every forecast is based on the information stored prior to the time of forecast and this is accessed from the hot-start file. After the series of forecasts is complete, different forecast verification techniques are applied to test the performance of the data assimilation and the forecast error is quantified as a function of lead time.

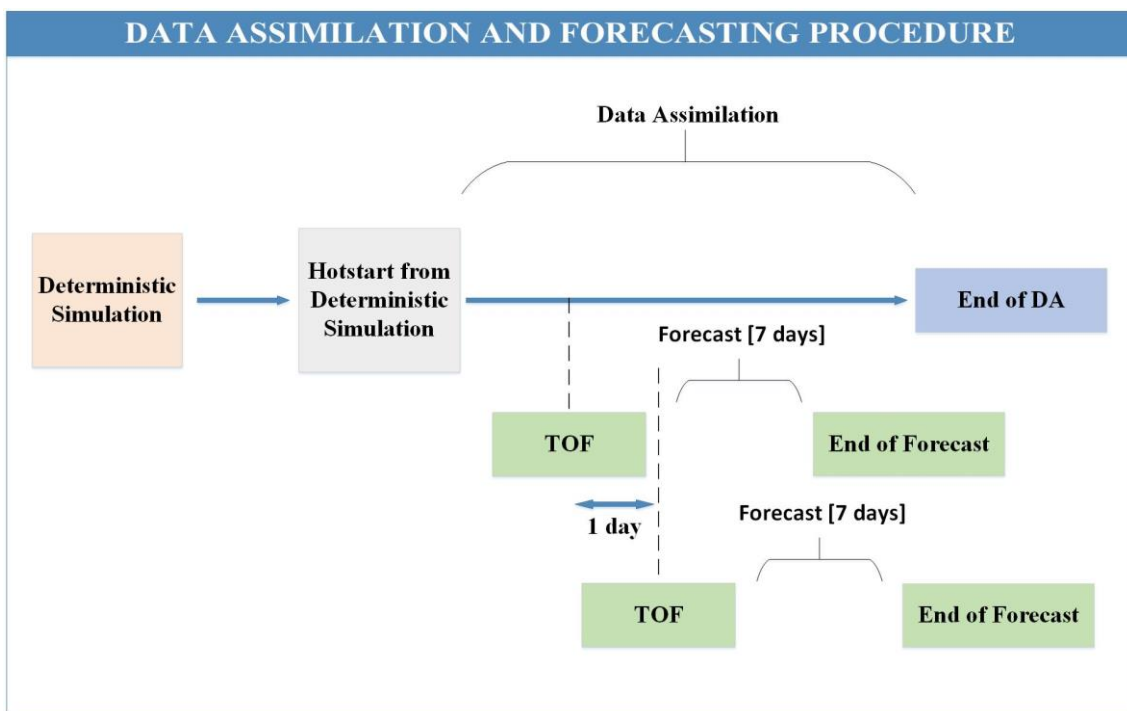


Figure 19: Data assimilation and forecasting procedure

5.6 Sensitivity Analysis

One of the challenges in the application of data assimilation methods is that the model and observational uncertainties are poorly known, and data assimilation systems operating under poor estimates of input uncertainties give forth a suboptimal estimate of the model states (Reichle et al., 2008). Thus, one of the objectives of this study is to investigate the sensitivity of the data assimilation to the filter parameters such as ensemble size, model uncertainty, model forcing uncertainty, as well as observation uncertainty. Obviously the data assimilation algorithm is highly influenced by the choice of input error parameters. Therefore, the sensitivity of the filter needs to be diagnosed thoroughly with respect to the input parameters (Kumar et al., 2008). The objective here is to find the best combination of filter parameters that represent the

model and measurement uncertainties more accurately in such a way that updated model states are close to the true state of the catchment just before the time of forecast (and beyond the time of forecast). (Sun et al., 2015) emphasized that proper error quantification of the model is a very important process in order to get acceptable results. Thus, the need for a sensitivity analysis arises to obtain the right filter parameters that represent the model and observation uncertainties.

A set of different parameter ranges will be defined for every parameter that will be tested in the sensitivity analysis. Using the selected values for the parameters, a data assimilation run will be made and saved as a separate file for forecast initiation. Following the data assimilation a sequence of forecasts will be made and the forecasts will be verified as a function of lead time. This will be done for every case, which is comprised of a set of different filter parameters.

5.6.1 First phase of sensitivity analysis

In the implementation of the data assimilation, the probability distribution of model states is approximated by ensemble members. The general rule of thumb is that as the ensemble size increases the algorithm will be able to accurately propagate the error information at the expense of a computational burden. Therefore, it is crucial to investigate the appropriate ensemble size in order to balance the estimation accuracy and the computational expense (Xie & Zhang, 2010). This marks the first phase of the sensitivity analysis in this study. To this end, for a range of ensemble sizes data assimilation is applied and forecasts are generated and the forecasts are verified to compare the trade-off between forecast accuracy and computational time for the various ensemble sizes that are chosen.

5.6.2 Second phase of sensitivity analysis

The second phase of the sensitivity analysis is devoted to finding the optimum filter parameters that will represent uncertainty in the forcing (precipitation) and in the observation. The sensitivity analysis was narrowed to focus on the above two categories in order to limit the degrees of freedom when specifying the model and observation errors to the Kalman filter. Thus, the impact of different forcing and observation uncertainties is examined by intentionally varying the corresponding filter parameters. 96 cases of different filter parameter combinations are defined and for each case data assimilation will be applied and sequential forecasts will be made. Figure 20 outlines the procedures used to implement data assimilation and forecasting.

The forecasting procedure used in the sensitivity analysis is a bit different than the one explained in Figure 19. This is mainly because, the data assimilation has to be run for every combination of filter parameters and followed by forecasts. Where as in the general case, the forecasts can be done just after running the data assimilation with one set of filter parameters combination.

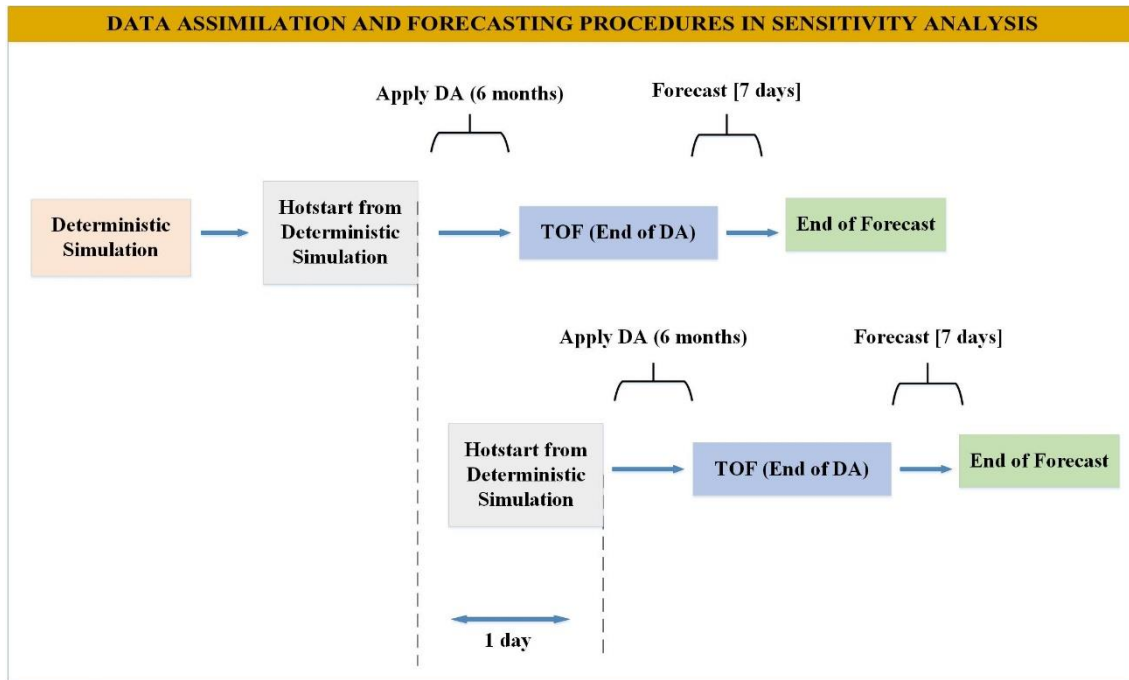


Figure 20: DA and forecasting procedures for sensitivity analysis

5.7 Verification Methods

This section outlines the different verification methods used to test the performance of the data assimilation (updating). Two different ways of verification were applied in this study; deterministic verification and probabilistic verification. The deterministic verification methods such as RMSE, MAE, PBIAS etc. evaluate for instance the mean of an ensemble with the single observed data. On the other hand, probabilistic verification methods such as the continuous ranked probability score evaluate the full ensemble against a single observation. Table 4 lists the verification methods used in this study.

Table 4: Verification methods used in this study

Verification Method	Type	Used for	Units
Nash-Sutcliffe efficiency (NSE)	Score	Deterministic simulations/Forecasts	%
Mean Error (ME)	Score	Deterministic simulations/Forecasts	Observed Variable
Mean Absolute Error (MAE)	Score	Deterministic simulations/Forecasts	Observed Variable
Percent Bias (PBIAS)	Score	Deterministic simulations/Forecasts	%
Root Mean Square Error (RMSE)	Score	Deterministic simulations/Forecasts	Observed Variable
Pearson Correlation Coefficient (r)	Score	Deterministic simulations/Forecasts	-
Continuous Ranked Probability Score (CRPS)	score	Ensemble simulations/Forecasts	Observed Variable
Root Mean Square Error Skill Score (RMSES)	Skill score	Deterministic simulations/Forecasts	-
Continuous Ranked Probability Skill Score (CRPSS)	Skill Score	Ensemble simulations/Forecasts	-

6. Results and Discussion

This section discusses the results obtained after implementing the research methodology described in 5. The first part (6.1) presents the results of the assessment made to select the appropriate precipitation product among the several precipitation products including rain gauge precipitation data. Upon selecting the appropriate precipitation product, as outlined in 5.4.1, two hydrologically different catchments were selected to show how the data assimilation works. The hydrological states of the individual catchments were updated by applying the ETKF data assimilation technique assimilating hourly discharge observations at the catchment outlets as shown in 6.2. The updated total runoff was verified by comparing it with the available observation at the catchment outlet. A forecast experiment was also done to test the performance of the assimilation in predicting the total runoff. Following this a sensitivity analysis was carried out (6.4) in order to configure the data assimilation filter with respect to several parameters as well as to find the optimum ensemble size that is computationally affordable and that gives a reasonable sampling space. In 6.5 discharge observations located along the river are assimilated to update the hydrodynamic states. Corresponding forecast experiments are also outlined with results. 6.6 shows the results of updating both hydrodynamic as well as hydrological states and the forecast improvements comparing the different updating categories.

6.1 Selecting appropriate precipitation product for data assimilation

6.1.1 Comparison of rainfall estimates

Sub-catchment level precipitation data from the three satellite products (TRMM, CHIRPS, and PERSIANN) was compared with the mean average rainfall from the rain gauges (computed using Theissen polygon approach). Comparison was done for the years 2013 to 2016 since the in-situ rainfall data is limited. The discrepancies of the satellite and rain gauge rainfall are further illustrated in Figure 21. The three satellite rainfall estimates are compared against the rain gauge rainfall data for the May – October 2015 period. In addition, the observed discharge at the sub-catchment outlet was used as a benchmark in order to check if any one of the rainfall estimates miss or overestimate a peak event.

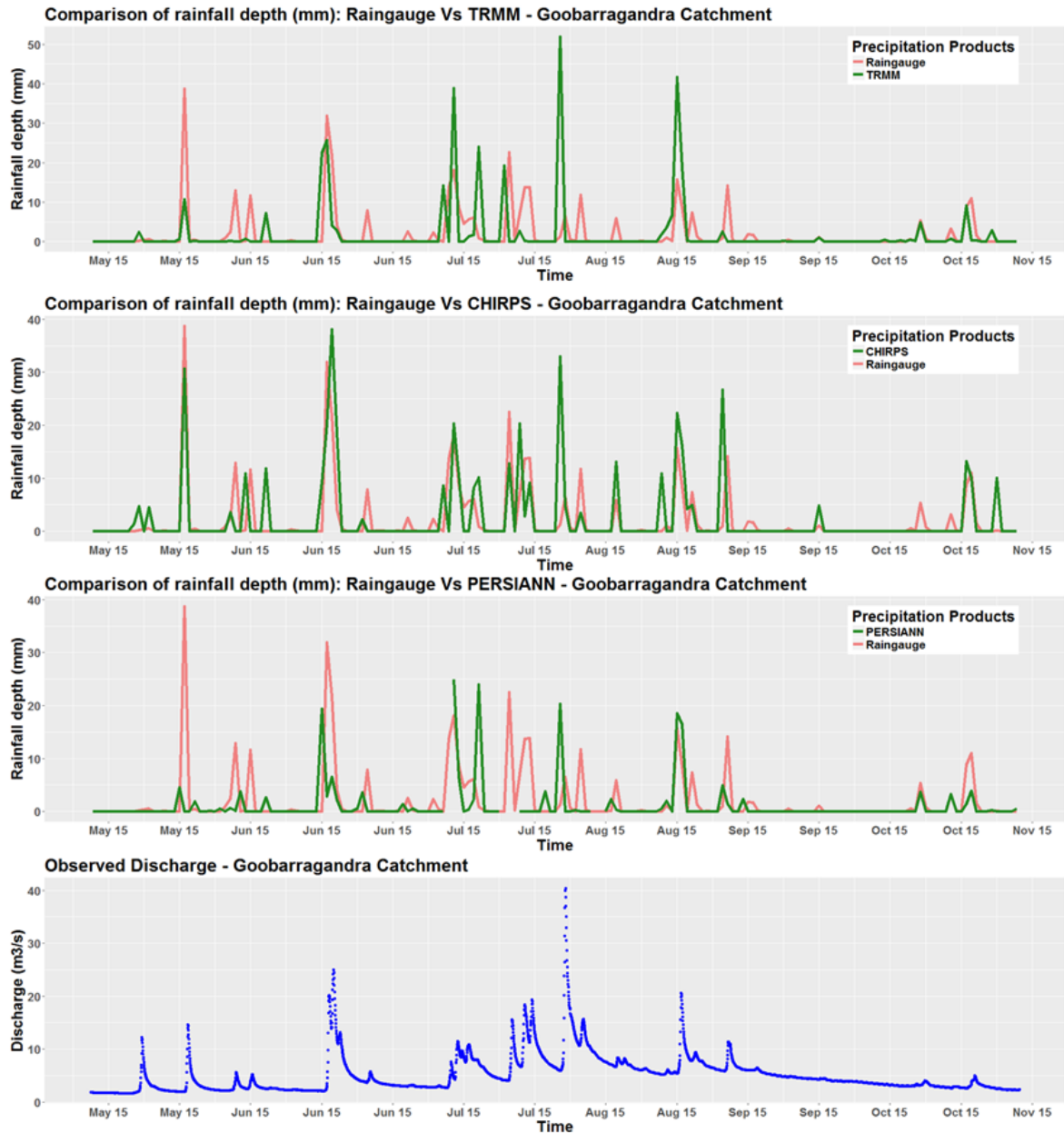


Figure 21: Comparison of the three satellite rainfall estimates with rain gauge rainfall

It is apparent that from Figure 21 that the PERSIANN product severely underestimates the rainfall in several cases, besides there are multiple missing data in the time series. Compared to PERSIANN, the TRMM 3B42 RT product captures some of the important rainfall events even though there is still some records with 0 mm of rainfall where in actuality there was some observed rainfall. Generally speaking, CHIRPS captures important rainfall events and has less records that miss rainfall events. This generalization holds true for the other three years too (2013, 2014 and 2016).

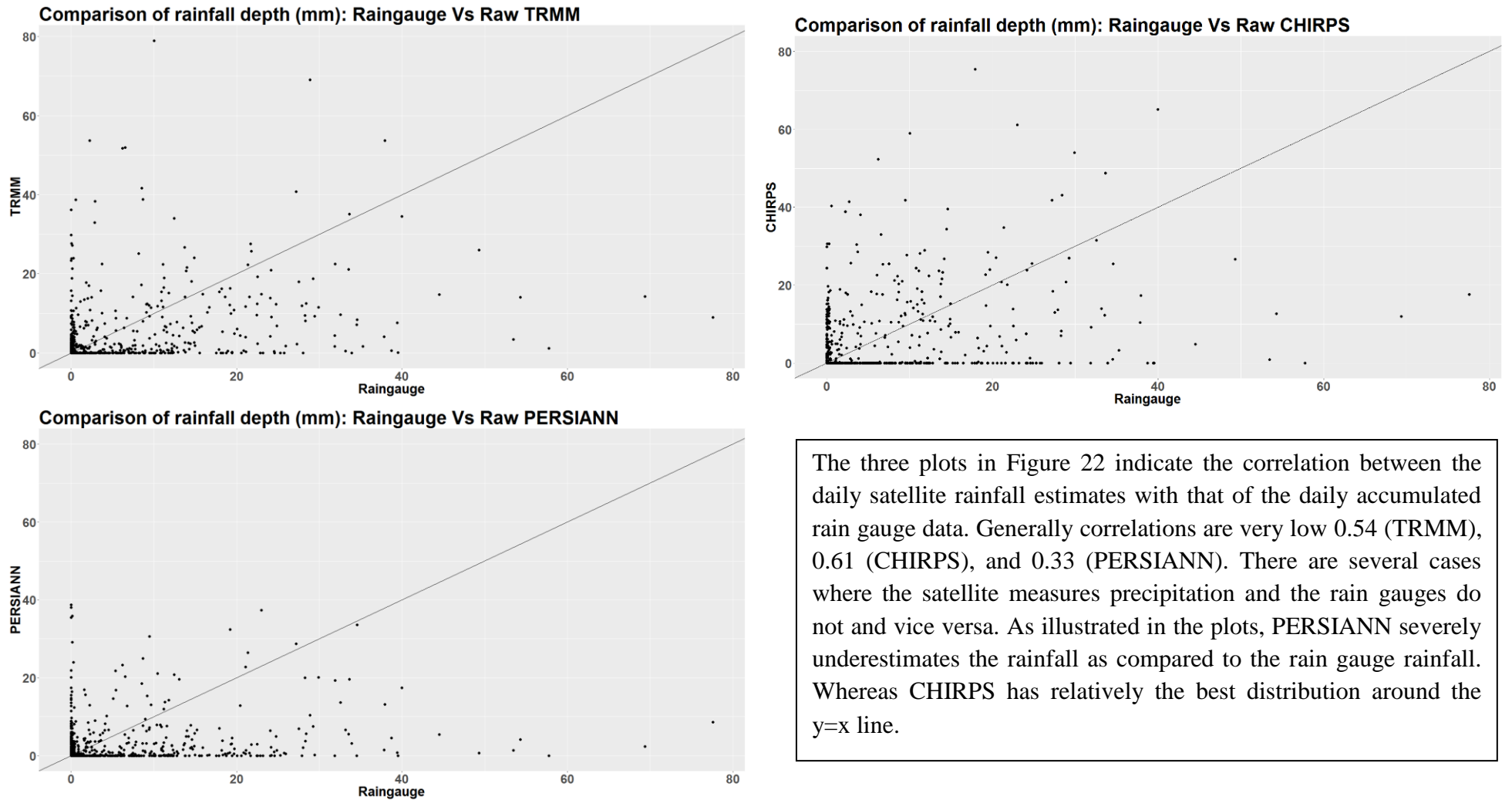


Figure 22: Comparison between daily rainfall from rain gauges and three satellite products TRMM (top left), CHIRPS (top right), PERSIANN (bottom left)

6.1.2 Bias correction of satellite rainfall estimates

Using the methodology in 5.1.1, the three satellite rainfall estimates were corrected and the accumulated mean daily rainfall over the Goobarragandra sub-catchment is displayed in Figure 23. In addition, the correlation between the bias corrected daily satellite rainfall products and the daily rain gauge rainfall was improved; 0.87 (TRMM), 0.94 (CHIRPS), and 0.78 (PERSIANN) (refer Figure A 4). Again it can be seen from the accumulated rainfall comparison that all the three products underestimate the rainfall with PERSIANN having the highest underestimation. Whereas the CHIRPS rainfall product more or less reproduces the accumulated rainfall for the entire period. Moreover, after the bias correction, almost all the satellite rainfall estimates show improvement, with PERSIANN showing slight bias.

6.1.3 Rainfall-runoff simulation

The bias corrected satellite rainfall products were used to simulate the rainfall-runoff process for the Goobarragandra sub-catchment. Due to the several missing data noticed in the PERSIANN rainfall product, only the TRMM 3B42 RT and CHIRPS products were used for the rainfall-runoff simulation. In line with this, the hydrological model (MIKE NAM) was re-calibrated just for the Goobarragandra sub-catchment with the bias corrected rainfall products. Specifically for the periods of (2005 - 2012) for TRMM and (1990 - 2012) for CHIRPS as shown in Figure 24. The peak event in the year 2012 could not be reproduced during calibration period (it was the major flooding event with an outlier 4000 m³/s discharge) when using any of the rainfall products. However when calibrating the model with CHIRPS dataset, the rainfall-runoff process is well captured also evidenced by the smaller volumetric error compared to that which used TRMM dataset for re-calibration. After re-calibration the hydrological model was forced with the two bias corrected satellite rainfall datasets and simulated for 4 years (2013 - 2016) on a daily time step. This is the period when the re-calibrated model was validated. Figure 25 illustrates the results of the rainfall-runoff simulation using three rainfall products, the TRMM, CHIRPS and the rain gauge. It can be seen that the satellite products have more or less represented the daily streamflow at Goobarragandra outlet. The simulation with rain gauge rainfall overestimates the streamflow throughout the simulation period, however the major peak events are captured well. Generally speaking, the simulation with CHIRPS rainfall has the lowest error statistics and highest efficiency (refer Figure 25) compared to the other simulations. However, like the TRMM simulation, the major peak events like that of the Oct 2016 were underestimated.

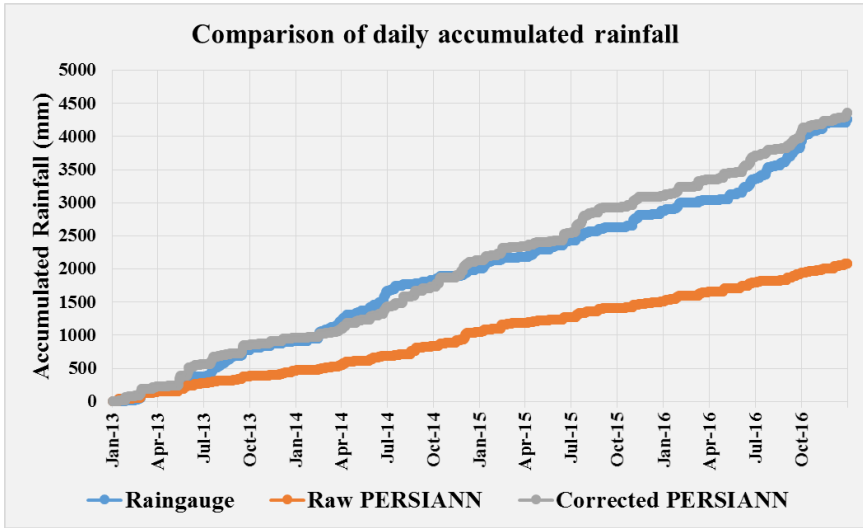
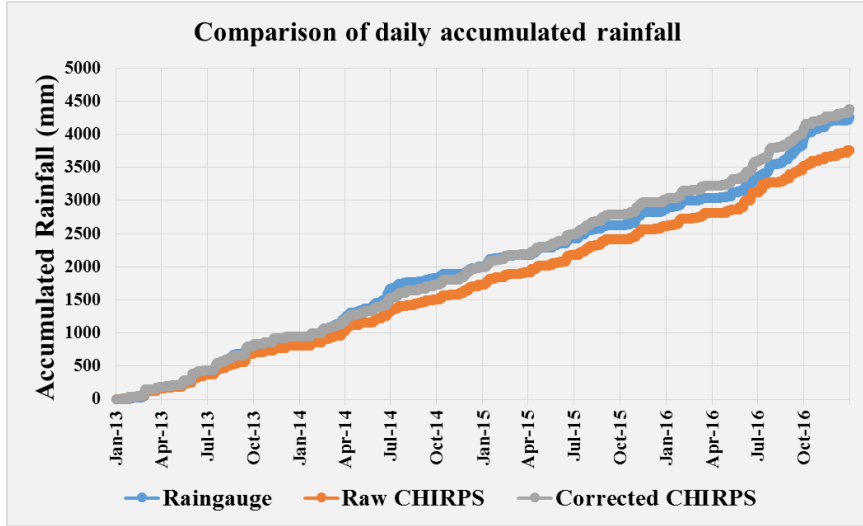
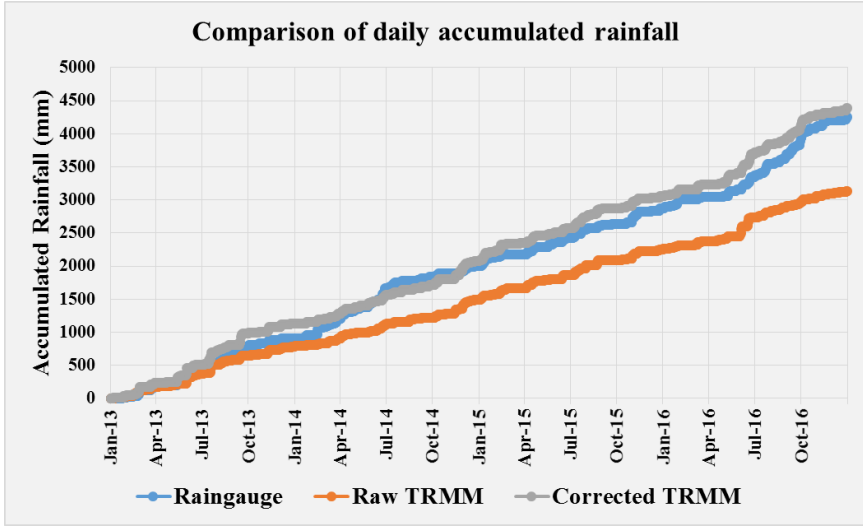


Figure 23: Accumulated mean daily rainfall over Goobarragandra sub-catchment before and after bias correction

Data Assimilation in Hydrodynamic-Hydrological Forecast Systems

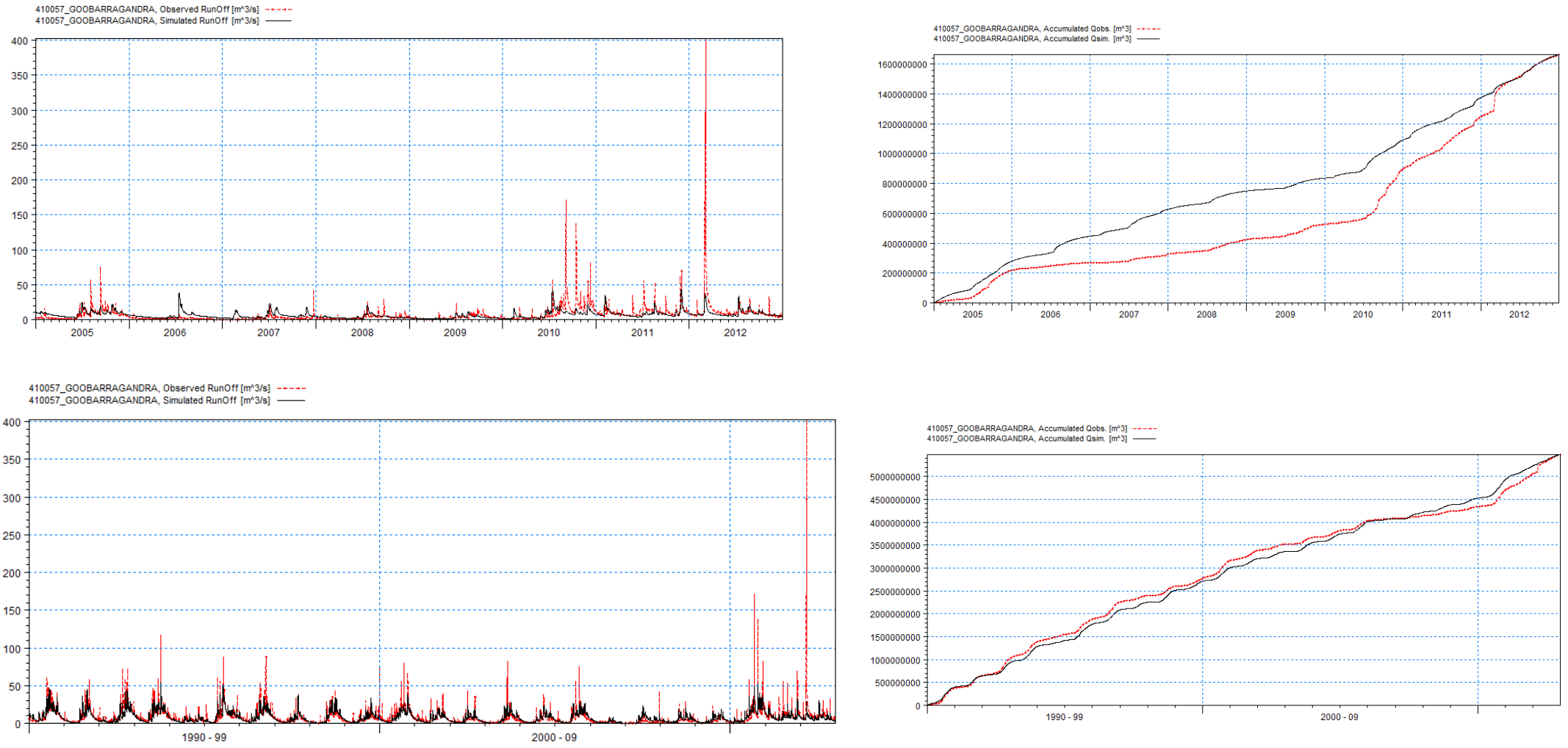
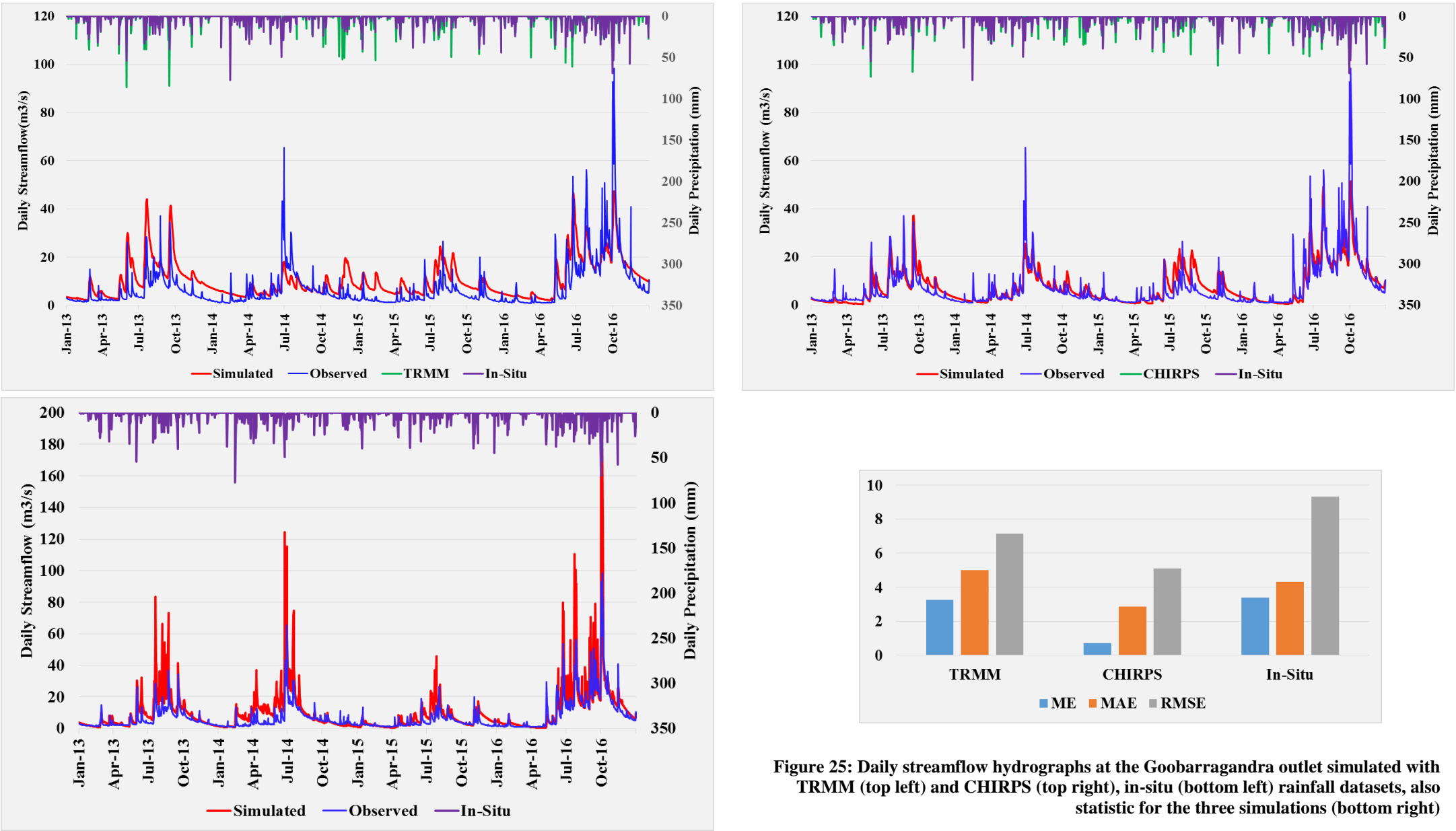


Figure 24: Re-calibration of rainfall-runoff model using TRMM (top) and CHIRPS (bottom) datasets (red and black lines represent observed and simulated flows)

Data Assimilation in Hydrodynamic-Hydrological Forecast Systems



This implies that even though the simulations with the two satellite products represented the rainfall-runoff process, they might not be suitable for flood prediction. Figure 26 demonstrates how the TRMM and CHIRPS forced model underestimates the Oct 2016 major peak as well as the small episodic events before and after the major event. The model forced with rain gauge rainfall, however, captures the small peak events before Oct 2016 however, it overestimates the Oct 2016 peak event.

Thus, it can be said that the use of the satellite rainfall estimates (TRMM, CHIRPS) generally produces a good estimate of the rainfall-runoff process and perhaps they can be used for large-scale hydrological modelling. However, for the sub-catchment in this study and the Murrumbidgee catchment in general accurate representation of initial states is very important to facilitate the reservoir operation system. Since the rainfall-runoff modelling forced with satellite rainfall estimates gives sub-optimal results compared to that of in-situ rainfall forced rainfall-runoff modelling, it is better to use rain gauge rainfall for the hydrological-hydrodynamic modelling in the catchment as well as the data assimilation and forecast experiments in the study.

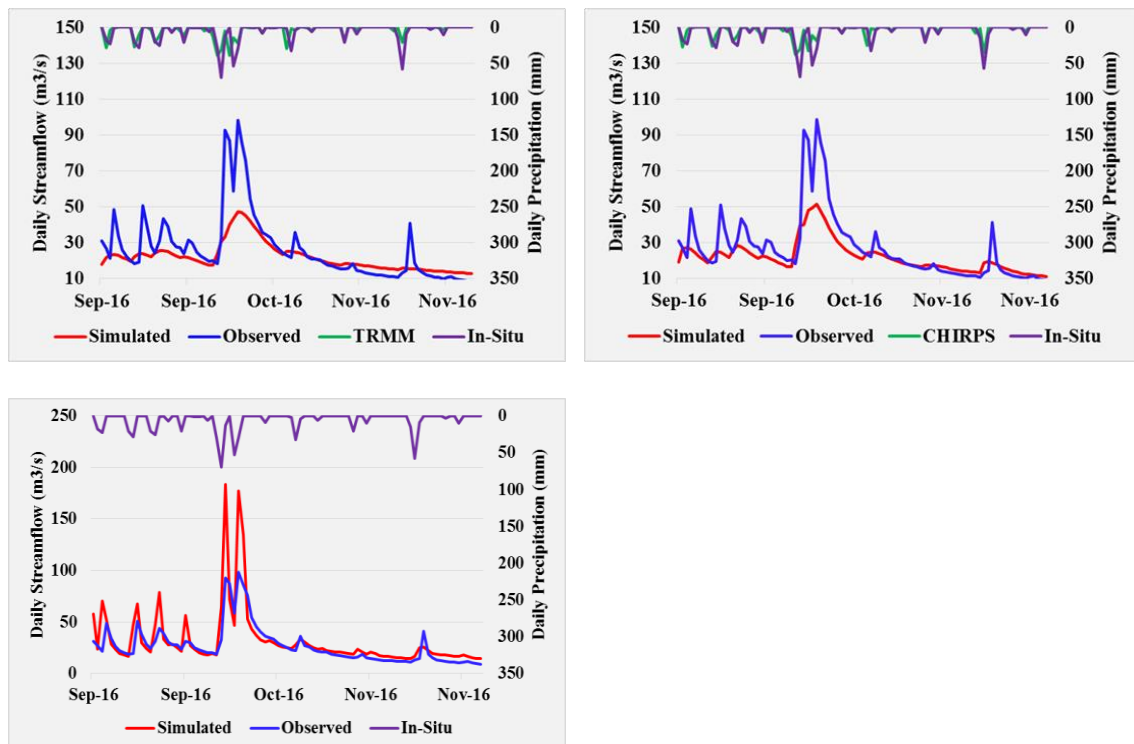


Figure 26: Streamflow hydrographs for the Oct 2016 peak event using TRMM (top left), CHIRPS (top right), and in-situ (bottom left) datasets

6.2 Hydrological model states update

For the two selected catchments (Jugiong and Goobarragandra), a three yearlong simulation was done with the calibrated model (using rain gauge rainfall). Figure 27 shows the simulation results, in addition specific events were chosen for both catchments in order to apply the data assimilation experiment. For Jugiong catchment the period from Jun-Aug 2016 was found to be of interest; 2016 was the wettest year for this catchment considering how dry it is. For the wet catchment, Goobarragandra, the Jun-Aug 2014 period was chosen for further analysis.

Data Assimilation in Hydrodynamic-Hydrological Forecast Systems

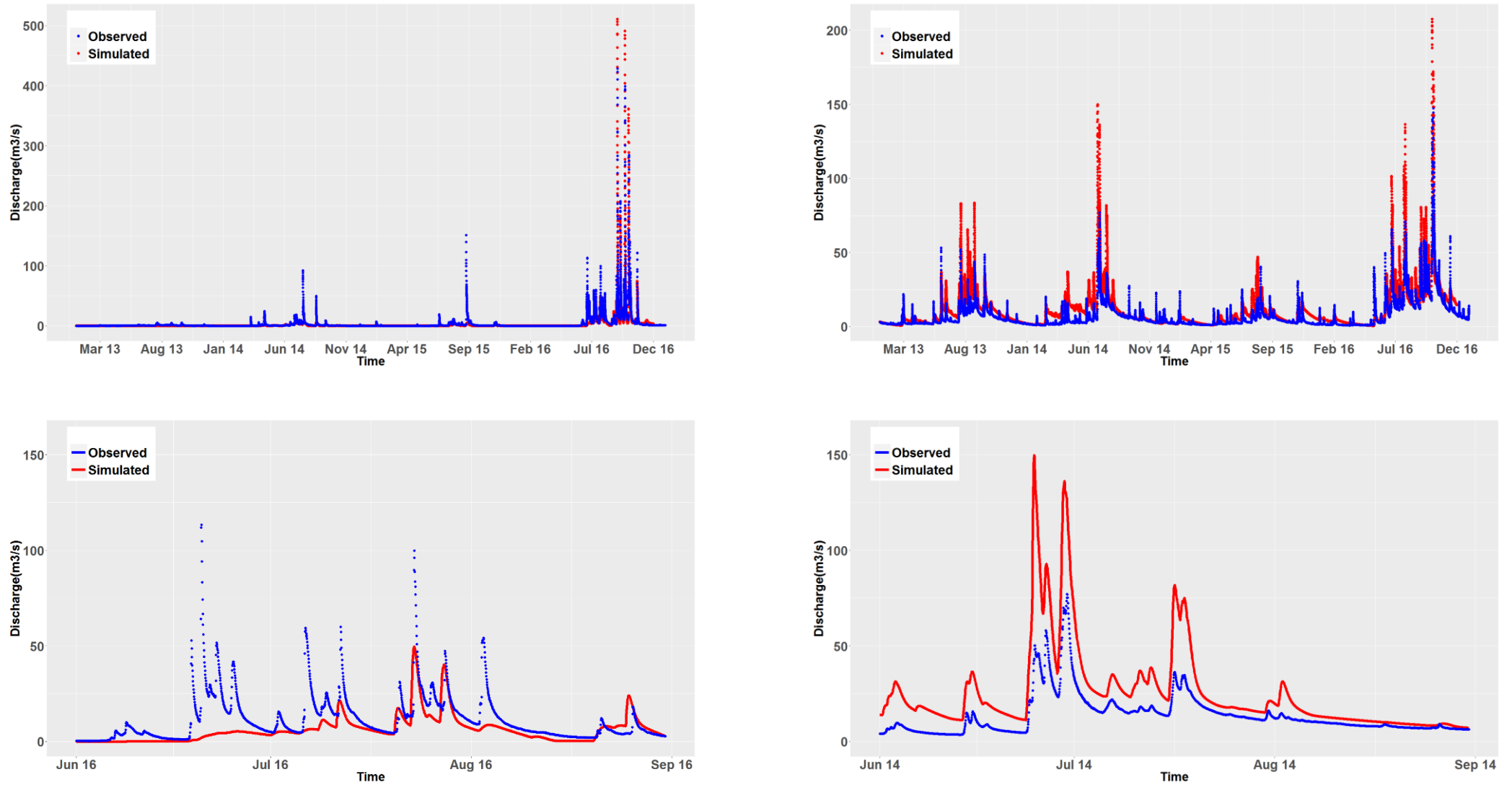


Figure 27: Comparison of observed and simulated discharge (three years) for Jugiong (top left) and Goobarrandra (top right) catchments; selected events for data assimilation for Jugiong catchment (bottom left) and for Goobarrandra catchment (bottom right)

The ETKF was configured with the parameters shown in Table 5 in order to update the hydrological model states. Different ensemble simulations were run for the selected period for the two sub-catchments in order to study the behavior of the ETKF. Figure 28 and Figure 29 show the control simulation (ensemble simulation where there is no data assimilation), for simulation of total runoff in the two sub-catchments. In the control simulation, the filter propagates every ensemble member forward in time without assimilating the available observations (discharges). This allows to see how the ensemble is spread throughout the simulation period and notice how uncertainty is propagated. It's where the assimilating/updating procedure is omitted.

In the control simulations, the black line, (referred to as open loop in this study) represents the deterministic model run, whereas the red line (MainModel) represents the mean of the ensemble members, the light grey lines signify the individual ensemble members and the observation is shown by the blue points. It can be seen that the open loop (black) is underestimating the runoff most of the time for Jugiong whereas it overestimates the runoff in the case of Goobarragandra. The behavior of the ensemble can also be viewed in all the hydrological states in Figure 30 as well as in Figure 31. It can be seen that when there is a substantial rainfall event, the ensemble spread becomes larger, increasing the background covariance error which in turn leads to a significant update after the assimilation of observations as displayed in Figure 33 and Figure 34.

Table 5: Selected Filter parameters for updating

Parameter	Unit	Value
Time Step	Min	5
Updating time step	Min	60
Forcing Uncertainty (σ_{forc})	-	0.5
Half-Time constant ($T_{1/2}$)	hr	12
Measurement Uncertainty (σ_{obs})	-	0.1
Ensemble size	-	20

Figure 30 and Figure 31 show the control simulation for the internal hydrological states for Jugiong and Goobarragandra sub-catchments respectively for the chosen period of simulation. Looking at Figure 30, for instance, there are eight different simulations presented. From top to bottom it shows the ensemble simulations of the following model states; surface storage (top row), root zone storage (2nd row), overland first reservoir storage (3rd row), overland second reservoir storage (4th row), interflow first reservoir (5th row), groundwater depth (6th row), total runoff (7th row), and perturbed precipitation (bottom row).

Generally, this control simulation is showing how each individual ensemble member is propagated forward in time. Looking at the control simulations of the two sub-catchments, one can see that ensemble spread in Jugiong is larger than that of Goobarragandra. This is owing to the fact that there are more precipitation events in the former sub-catchment in that particular period. If the duration of precipitation is not enough or if there is no precipitation at all, the data assimilation algorithm (ETKF) can't perturb precipitation of the ensemble members which leads to a reduced ensemble spread.

After selecting the parameters for the filter, data assimilation was implemented. At this point, the available observations (hourly discharges) have been assimilated and the

internal model states were updated. Figure 32 shows the updated total runoff at the outlet of the two sub-catchments. The update for Goobarragandra seems much better than that of Jugiong, evidenced by the graphical comparison as well as the statistical analysis of the updates quantified by ME, MAE and RMSE. This is partly due to the poor simulation of the open loop (deterministic model run) of Jugiong, especially in capturing major peak events. It underestimates the total runoff by big amounts. On the contrary, the deterministic run for Goobarragandra is relatively better (even though it overestimates the total runoff) and thus better total runoff update. In addition, the less satisfactory update shown for Jugiong sub-catchment could be attributed to the erroneous selection of filter parameters. The filter parameters selected in Table 5 were chosen by using educated guess, or engineering judgement, the incorrect choice of filter parameters could actually deteriorate the update. Thus a sensitivity analysis of the filter parameters needs to be done in order to select the fitting parameters for the filter. This is discussed in detail in Sensitivity Analysis.

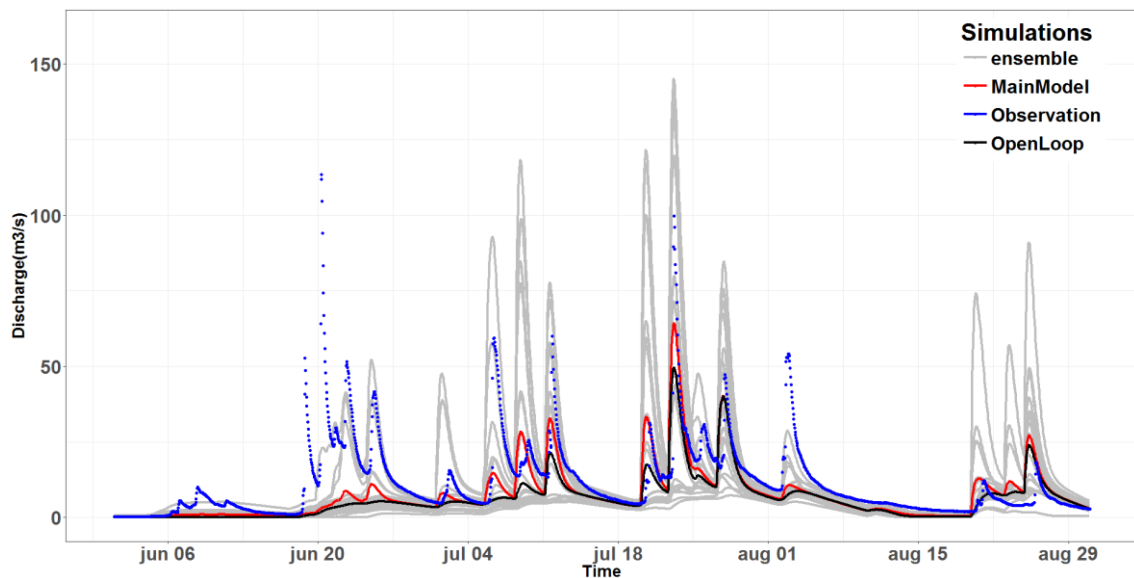


Figure 28: Control Simulation (no data assimilation): Total runoff for Jugiong catchment

Again looking at Figure 32, the updated total runoff, it can be seen that the ensemble spread is very much reduced compared to the control simulation. This is because every ensemble member is updated with the available observation and thus the variance of the ensemble members reduces at the update point.

Similarly, the hydrological model states update for both sub catchments is illustrated in Figure 33 and Figure 34. Looking at the update for Jugiong sub-catchment, the peaks are simulated better than the open loop. The recession part of the hydrograph is also well captured. For instance, in order to better simulate the peak runoff event in the month of June (for Jugiong sub-catchment), the two overland flow reservoirs were recharged, root zone storage was increased to up to 80%, interflow was also increased. One can also notice that, the updated ground water depth is higher than the one shown in the open loop, this accounts for the better simulation of the base flow (recession part of the hydrograph). Generally speaking, the open loop (deterministic model run) did not pick up the peaks and the base flows accurately, thus it can be said that data assimilation improved catchment state estimation. In comparison, the catchment states update for Goobarragandra (Figure 34) are much better than that of Jugiong. Generally in all the

storages (overland, root zone, interflow etc.) the model simulates more water than there is in actuality, which is also evidenced by the overestimation of the runoff by the open loop (deterministic model). The updated runoff simulates the peak events as well as the low flow events more accurately by adjusting the corresponding storages. For instance looking at the peak runoff in June 2014, it is updated by reducing overland flow storages, and lowering ground water depth, whereas in the small peak event in the first week of August, interflow storage and surface storage were increased to adjust to the observed runoff.

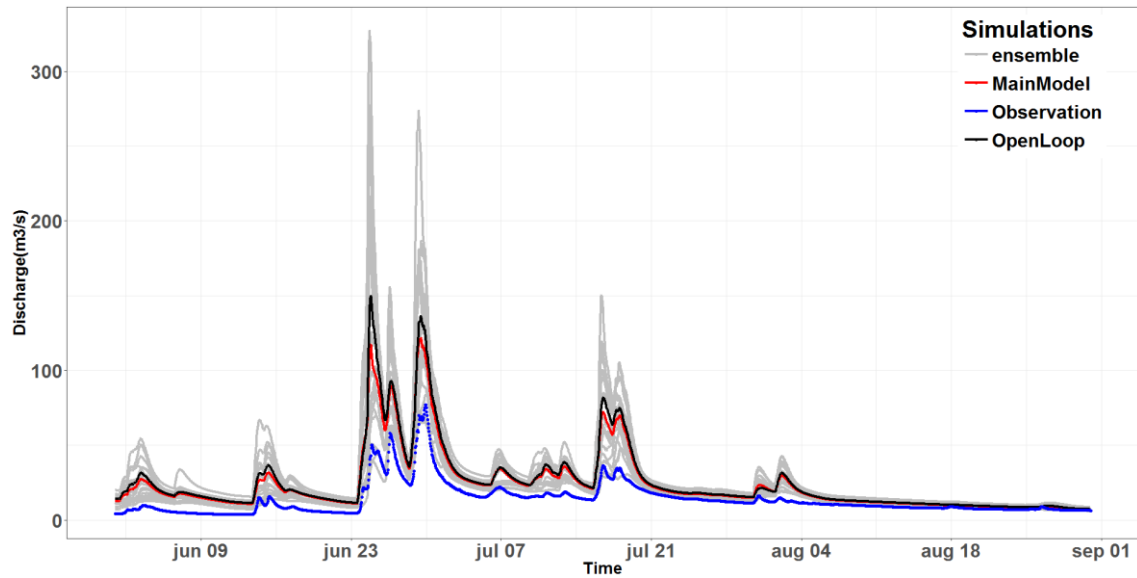


Figure 29: Control Simulation (no data assimilation): Total runoff for Goobarragandra catchment

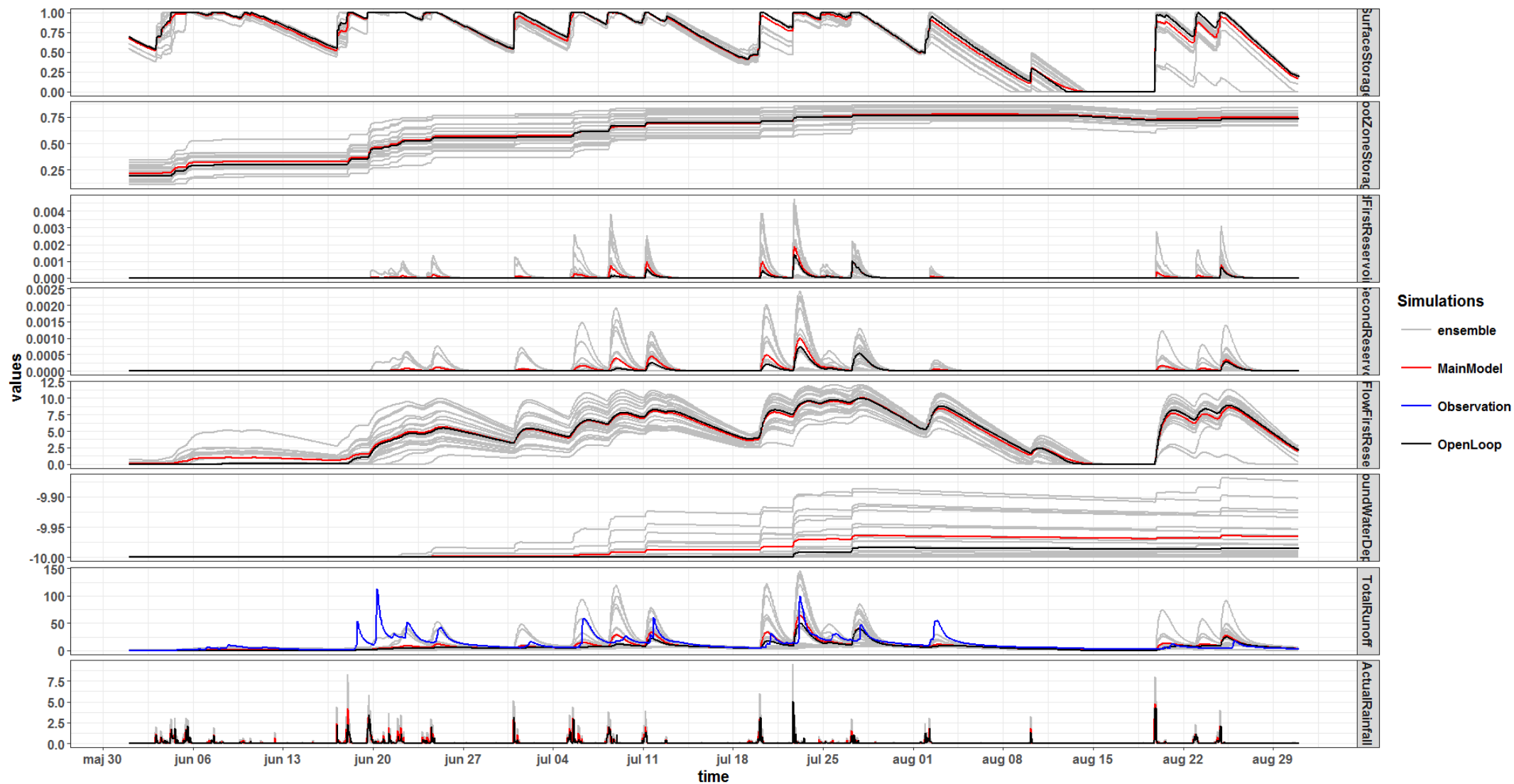


Figure 30: Control simulation for the hydrological model states - Jugiong sub-catchment

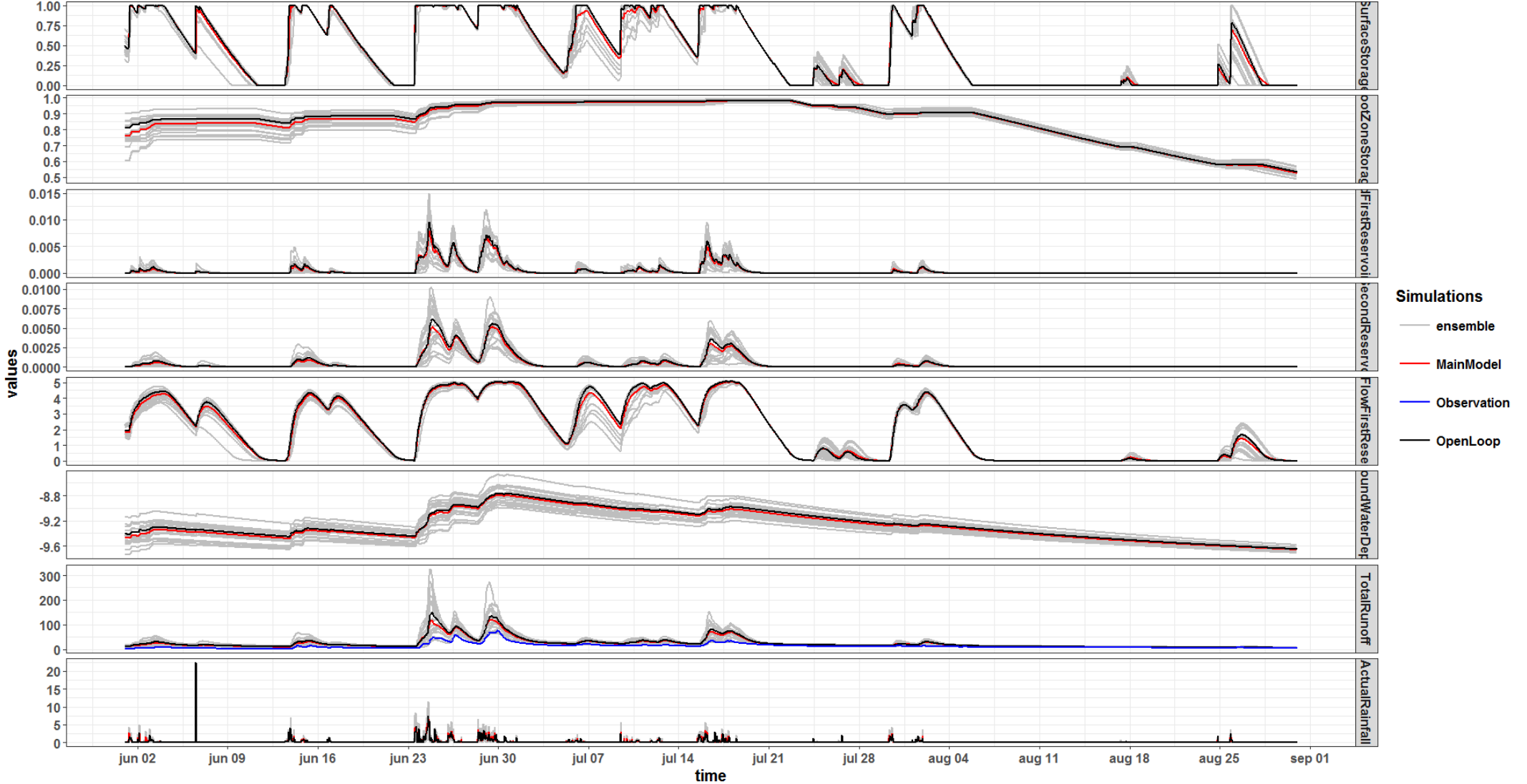


Figure 31: Control simulation for the hydrological model states - Goobarragandra sub-catchment

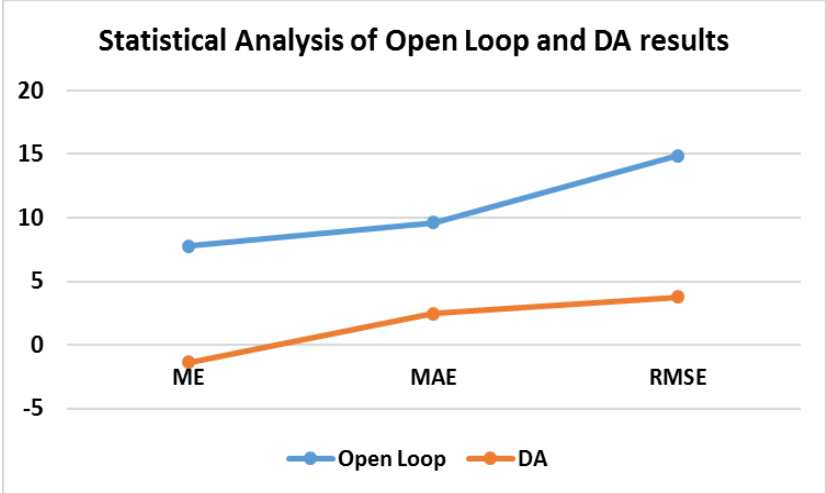
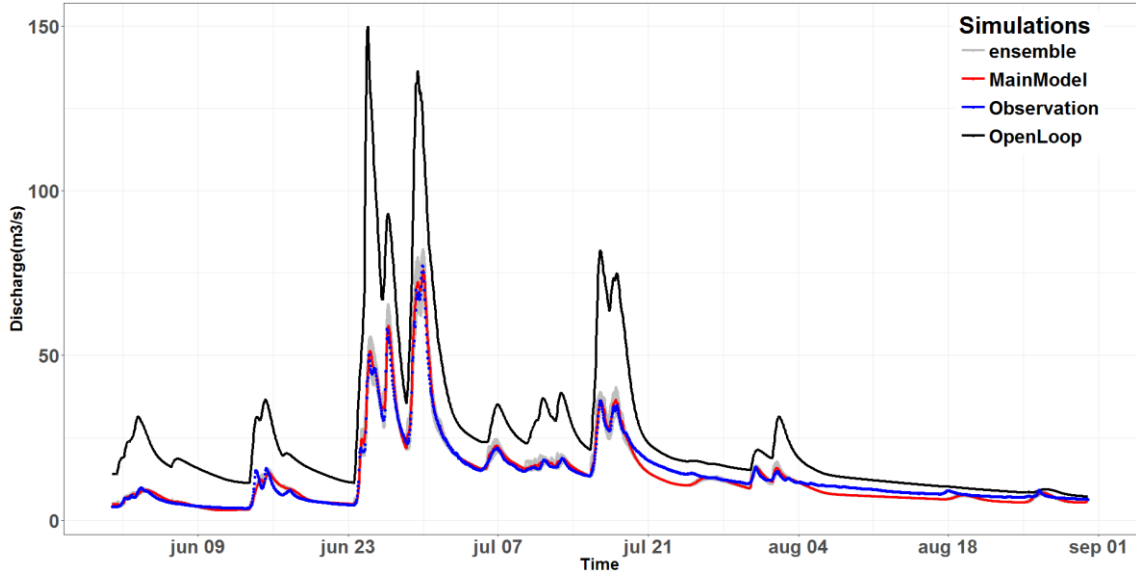
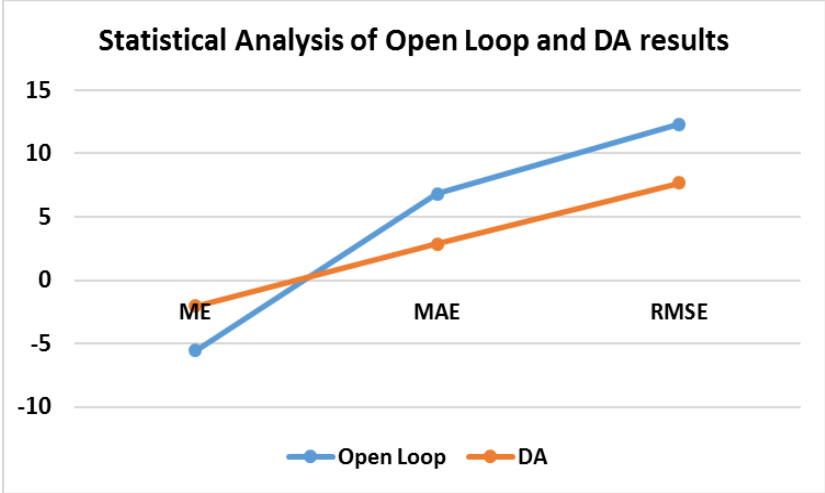
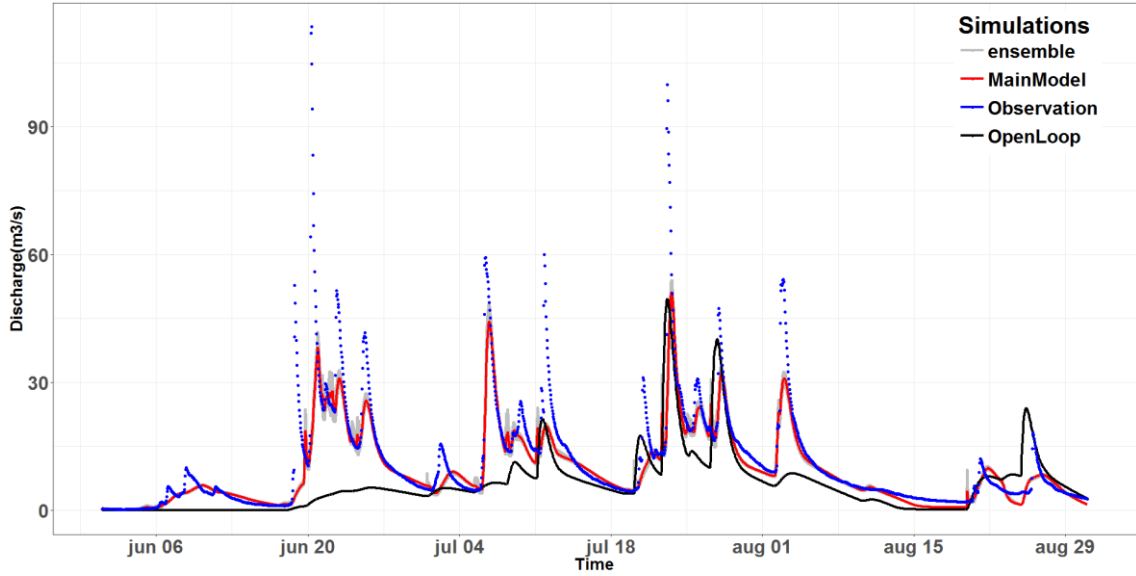


Figure 32: Updated total runoff for Jugiong (top left) and Goobarrandra (bottom left) and comparison of statistical analysis for both updates

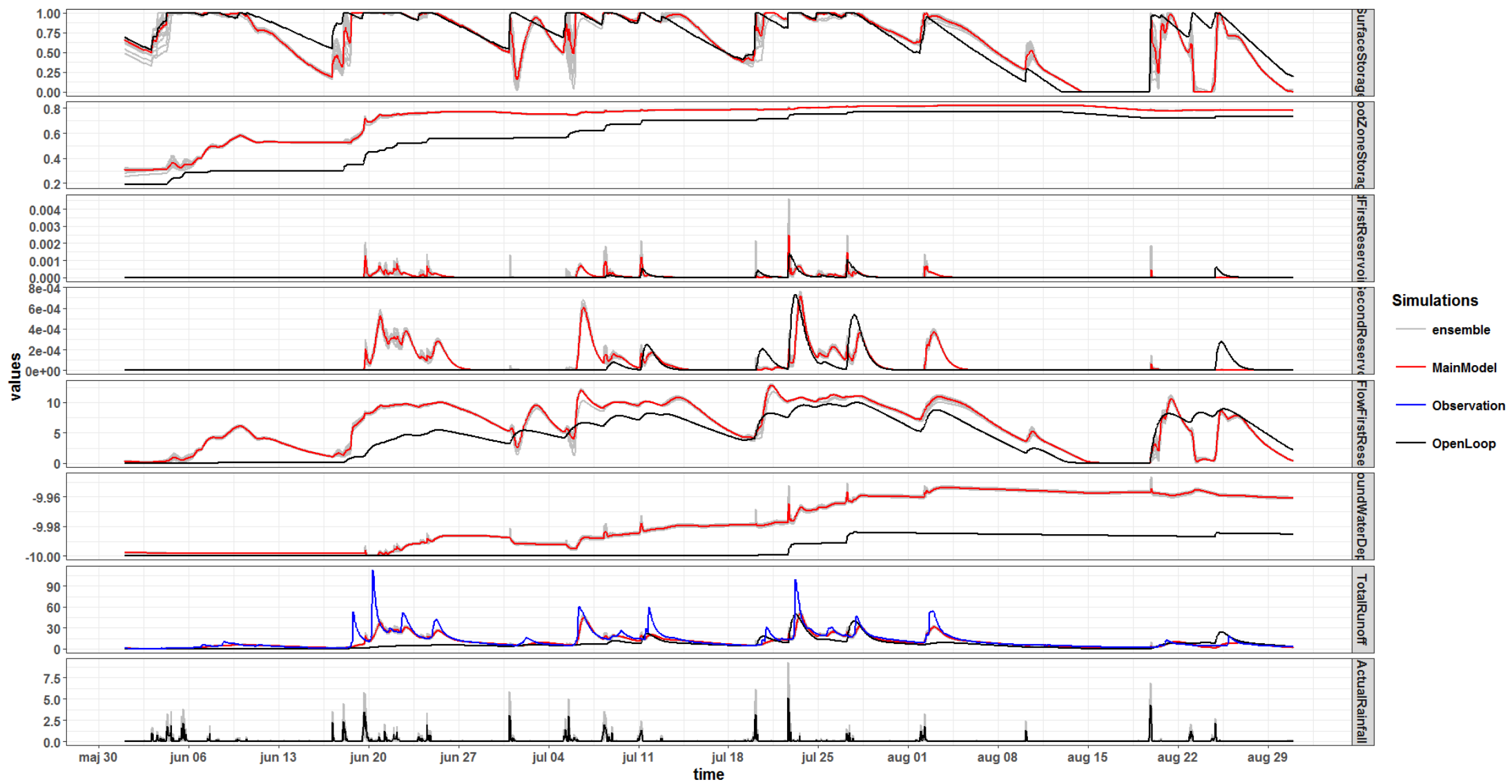


Figure 33: Updated hydrological states for Jugiong sub-catchment

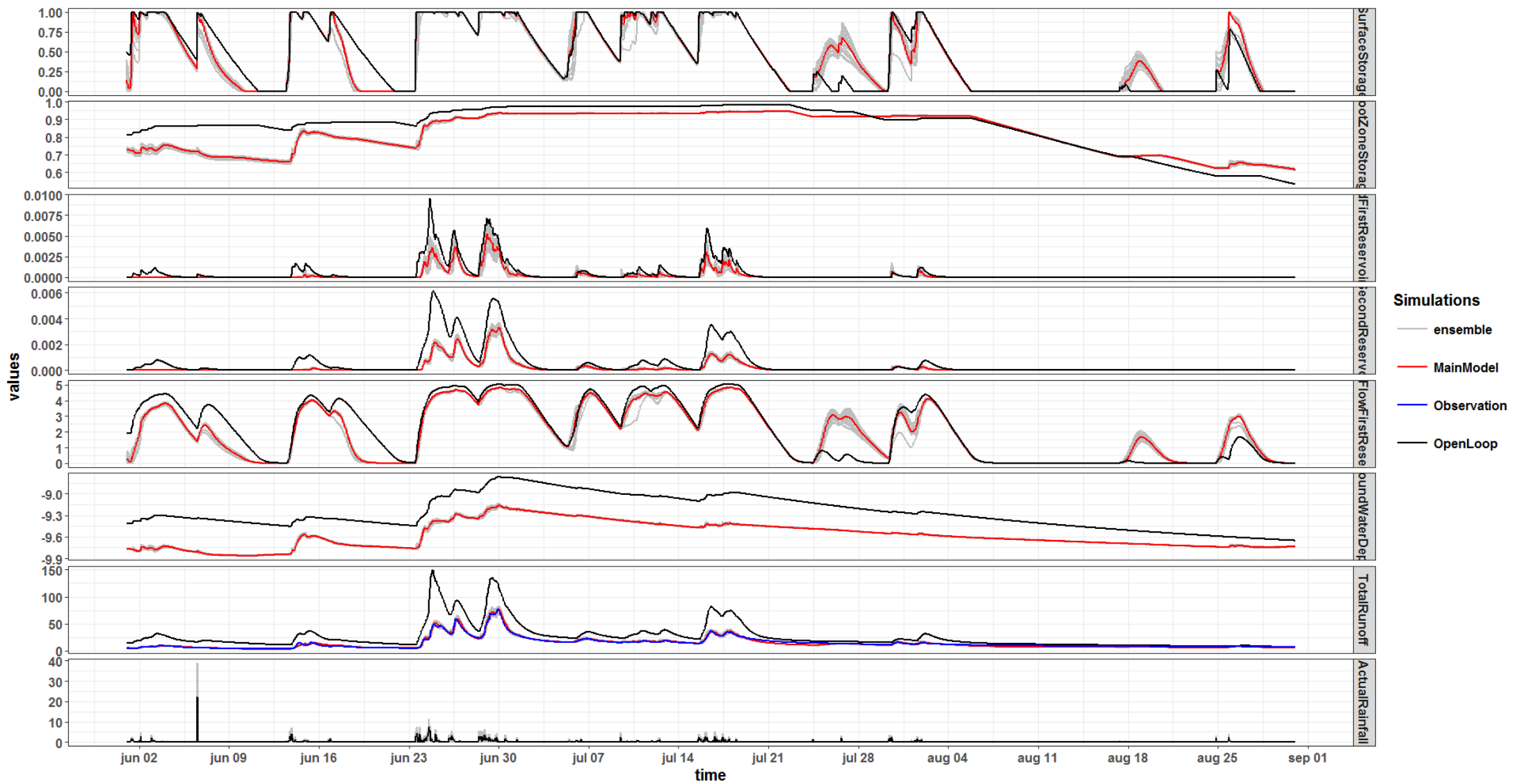


Figure 34: Updated hydrological states for Goobarragandra sub-catchment

6.3 Forecasting and Verification

In order to test the performance of the data assimilation, a series of simulated forecast experiments was made following the implementation of data assimilation. The forecast experiment is done for the Goobarragandra sub-catchment. Total runoff for this sub-catchment was forecast. Note that this is not a real time forecast since observed precipitation was used as forcing in the model instead of a forecast precipitation. The forecast total run off is verified by comparing it with the observed total runoff (discharge). The skill of forecast based on data assimilation was compared with the open loop (deterministic run) and skill scores were computed. The forecasting procedure is based on the methodology explained in 5.5; observed discharges were assimilated for the August 2012 to February 2014 period and a series of 245 forecasts were generated as of June 2013. The forecasts were made daily for 8 months each with a lead time of 7 days.

The series of forecasts was verified in two different ways; deterministically by comparing the mean of the ensembles against the observation and probabilistically comparing the whole ensemble against the observation using the appropriate verification method. RMSE and CRPS scores as well as skill scores were computed for deterministic and probabilistic verification. The forecasts were compared with the deterministic model run (open loop) in order to compute the forecast skill scores

Figure 35 shows the evaluation of the 245 simulated forecasts. The skill scores of the runoff forecast represented by RMSES and CRPSS indicate that the total runoff at the catchment outlet can be forecast with a reasonable accuracy. In addition the good accuracy persists for longer periods. Assuming that there is no uncertainty coming from forecast precipitation (since observed precipitation is used), a deterministic forecast made after data assimilation is at least 50% more skillful for a lead time of 4 days than the forecast made without data assimilation as shown by the RMSE skill score. Whereas an ensemble forecast made after data assimilation is at least 70% more skillful for the entire 7 days lead time as evidenced by the CRPS skill score.

6.4 Sensitivity Analysis

The sensitivity analysis was done in two phases; the first phase is to find the optimum ensemble size that fulfils both the computational and forecast accuracy requirements of the data assimilation. The second phase is to find the “best⁶” combination of filter parameters that represent the forcing and the observation uncertainty for a specific sub-catchment.

6.4.1 First Phase of Sensitivity Analysis

The first phase of the sensitivity analysis, is devoted to investigate the sensitivity of the data assimilation filter as well as the forecasts that are following data assimilation, with respect to ensemble size. Thus ensemble sizes ranging from 10 to 150 were chosen and DA was implemented followed by a series of ensemble forecasts.

⁶ This best filter parameters are unique to the chosen sub-catchment; they will not apply to other sub-catchments

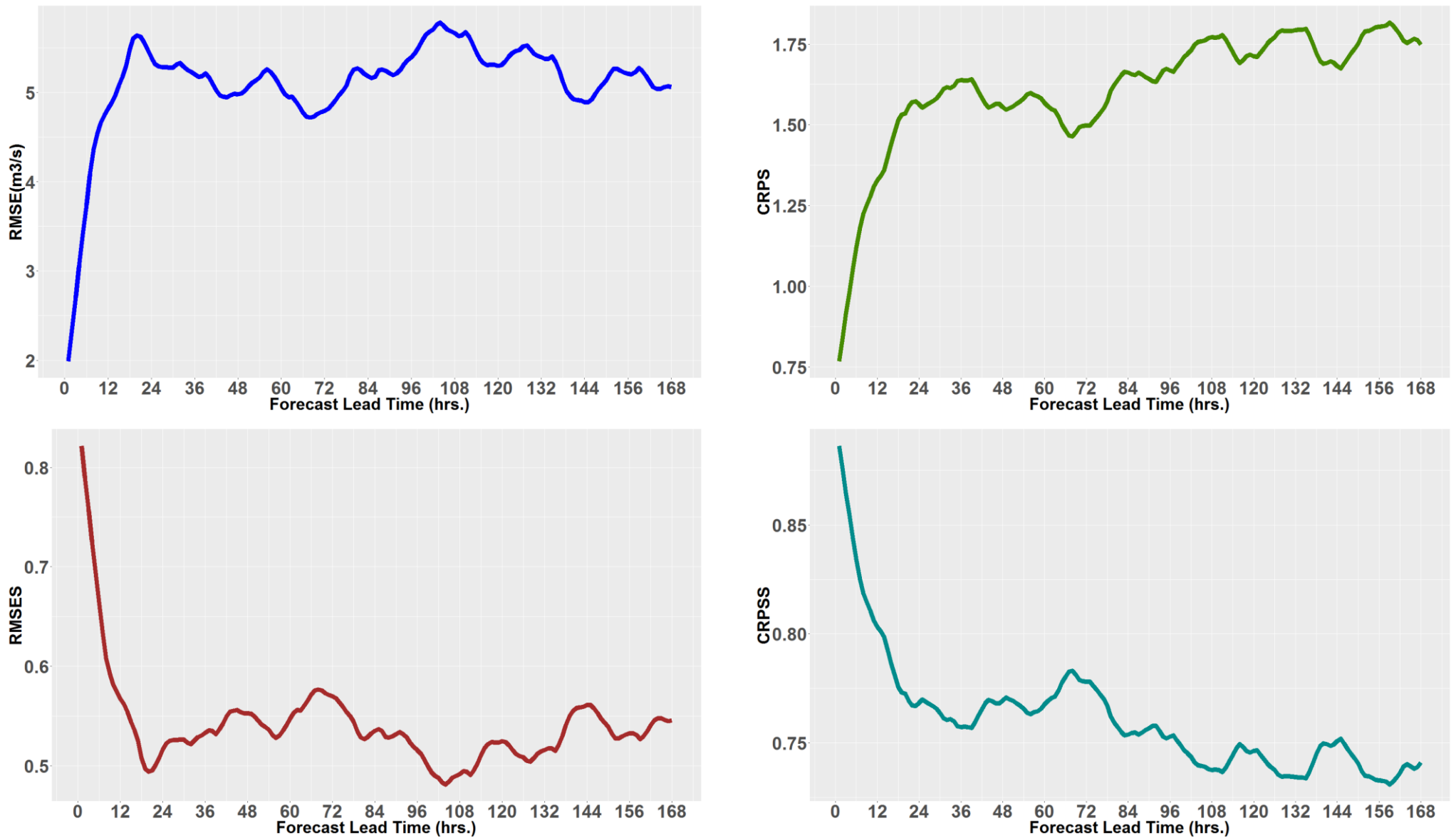


Figure 35: Forecast RMSE (top left), CRPS (top right), RMSES (bottom left), and CRPSS (bottom right) for Goobarragandra catchment

The mean RMSE of the ensemble forecasts was computed as a function of lead time which is shown in Figure 36. Figure 37 depicts the average 1 day, 3 days, 5 days and 7 days RMSEs for the different ensemble sizes. It can be seen that even though the forecast RMSE does not change significantly, it is reduced with increase in ensemble size. However, the RMSE starts to show a slight increase when more than 100 ensemble members are used. On the other hand, looking at the computational time required to perform ensemble simulations for the different ensemble sizes, it can be seen that the computational time increases non-linearly. Table 6 shows the computational time required to propagate the ensemble members on forecast mode for 30 days. But in general, considering the insignificant difference in forecast RMSE when using different ensemble sizes and taking into consideration the large amount of time it takes to run the forecast as the ensemble size increases, an optimal ensemble size of 20 is chosen for the sensitivity analysis as well as for the rest of the study.

Table 6: Amount of time (min) it takes to propagate the different ensemble members in forecast mode

Ensemble Size	10	20	50	70	100	150
Run-Time (min)	7	10	22	27	38	70

6.4.2 Second Phase of Sensitivity Analysis

Several combinations of different filter parameters were selected to run the sensitivity analysis. There are several filter parameters the value of which can be altered, however, this was limited to only three of them, viz. forcing uncertainty (quantified by standard deviation), forcing half-time constant (hours), and observation uncertainty (standard deviation). The three filter parameters were chosen after a broader sensitivity analysis which included all the filter parameters. It was found that the above three variables had stronger correlation with forecast error and thus, they were chosen for further investigation. Based on the procedures explained in detail in 5.6, for every combination of filter parameters data assimilation was done for the March to August 2013 (6 months) period followed by a sequence of 30 daily forecasts with a lead time of 7 days starting on July 15, 2013 (time of forecast). Then RMSE and CRPS scores for the forecasts are computed as a function of lead time and these scores are compared for every combination of filter parameters chosen at the outset of the sensitivity analysis. The combination which brings forth the lowest RMSE & CRPS scores is considered to represent the model and observation error in a better way and thus will be chosen as the “best” combination of filter parameters.

The filter parameters for the observation and the forcing (precipitation) are varied to represent different error magnitudes. To this end, 96 cases are designed with the combination of different values of the three filter parameters as shown in Table 7.

Table 7: Filter parameter ranges for sensitivity analysis

Filter Parameter	Range	Remark
Forcing Uncertainty	0.1 – 0.8	Standard Deviation (0.1 increment)
Forcing Half-Time constant	2, 4, 8, 16	Hours
Observation Uncertainty	0.05 – 0.15	Standard Deviation (0.05 increment)

Forecast Error (RMSE) for Different Ensemble Sizes

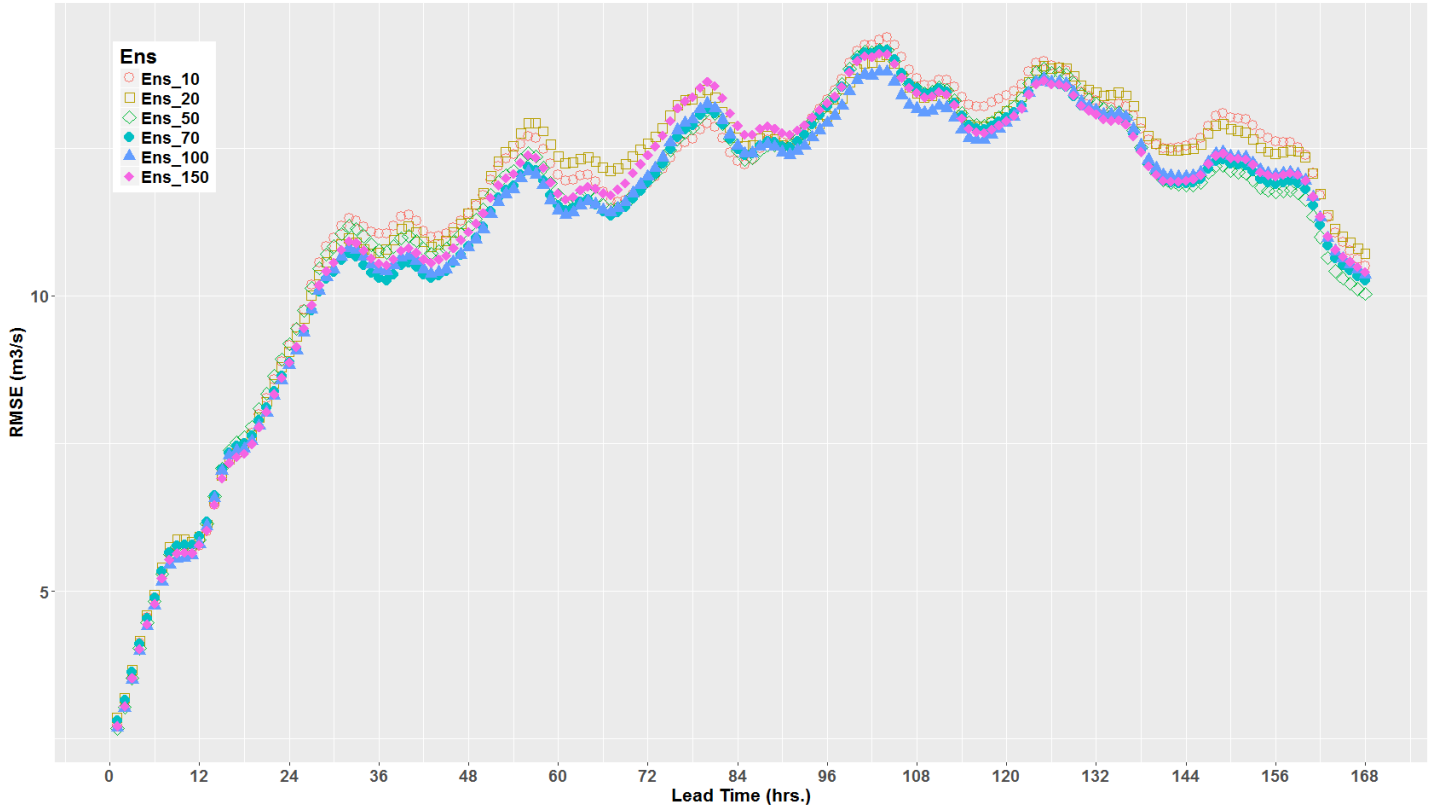


Figure 36: Forecast error as a function of lead time for different ensemble sizes

Forecast Error (RMSE) for Different Ensemble Sizes

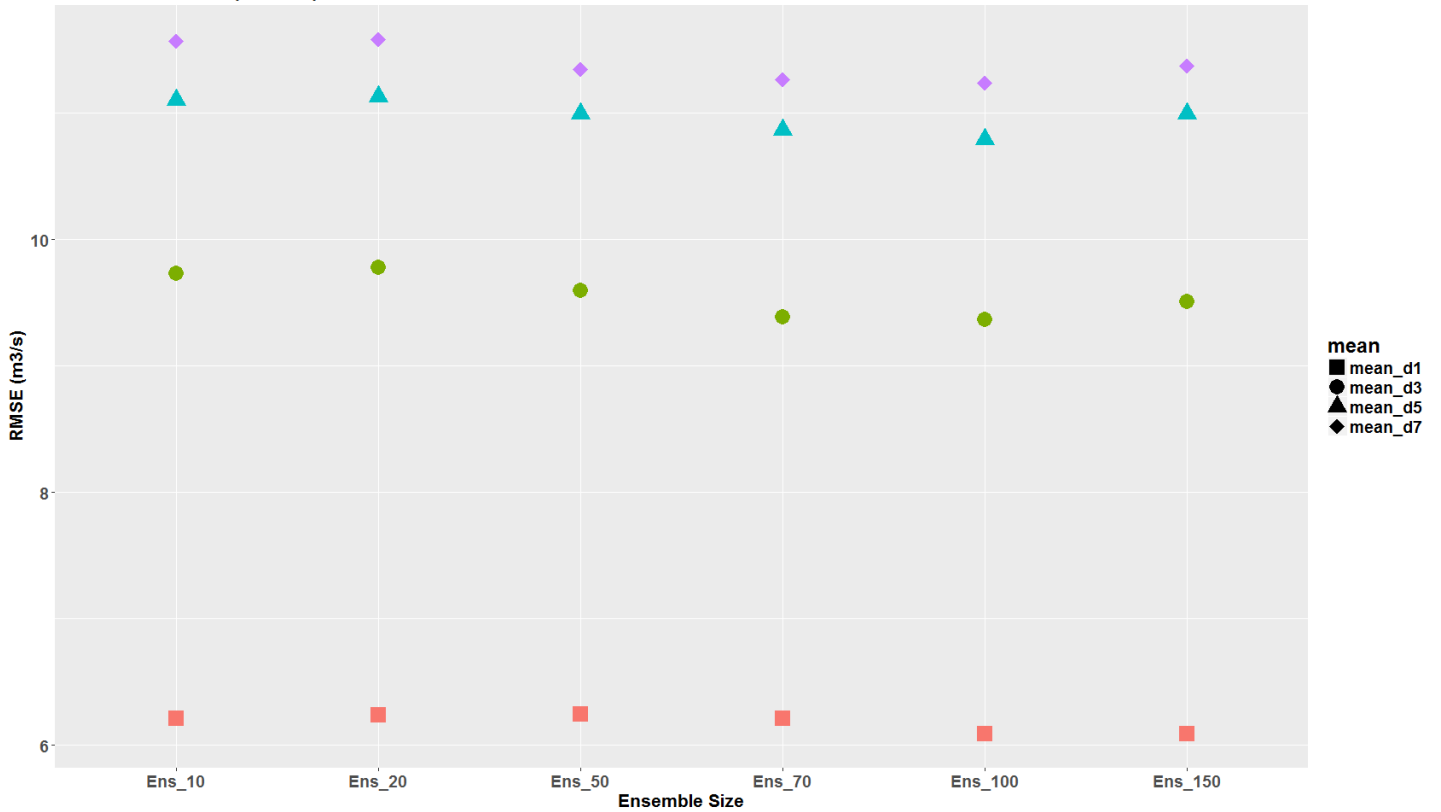


Figure 37: Average RMSE of forecasts for different ensemble sizes

This part of the analysis is carried out in two steps, first the data assimilation filter parameters will be calibrated or tuned to find the best forecast results for a chosen calibration period (March – August 2013) as shown in Figure 38 and data assimilation will be implemented on another period to validate its performance on forecast accuracy. The full result of the above analysis is displayed in appendix A with Figure A 1 and Figure A 2, the cases with the lowest RMSE and CRPS are chosen as the best cases and are taken for further investigation. The cases that led to the lowest forecast error verified by RMSE and CRPS are shown in Table 8.

Table 8: Best filter combination with low forecast errors (forcing and observation uncertainty are standard deviation values)

Case	Forcing Uncertainty	Forcing Half-Time constant	Observation Uncertainty
Case 28	0.4	16hrs.	0.05
Case 32	0.8	16hrs.	0.05
Case 63	0.7	16hrs.	0.10
Case 93	0.5	16hrs.	0.15
Case 95	0.7	16hrs.	0.15

In order to select a single case for further implementation of data assimilation, the average RMSE for 1 day, 3 days, and 7 days was computed for the above cases and case 63 came out to be the best solution (results are displayed in Figure A 3). From the analysis, one can learn that the forcing uncertainty obtained from the sensitivity analysis, is very large (70%). This indicates that the precipitation observed in this specific catchment (Goobarragandra) has a considerable uncertainty.

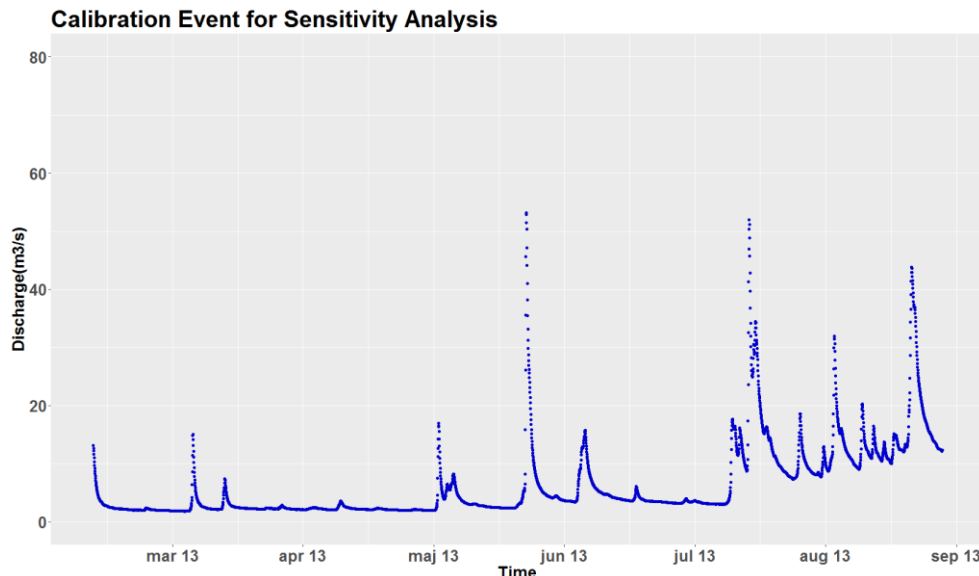


Figure 38: Calibration period for sensitivity analysis

After selecting the filter combinations represented by case 63 (refer to Table 8), the newly configured data assimilation scheme was tested. Thus a validation period (shown in Figure 39) from January 2013 to December 2014 is chosen and data assimilation was applied followed by the consecutive forecasts of one year each with a lead time of 7 days. The forecasts are then verified using RMSE and CRPS. Skill scores of the forecasts are also calculated with the open loop (deterministic run) being the reference simulation.

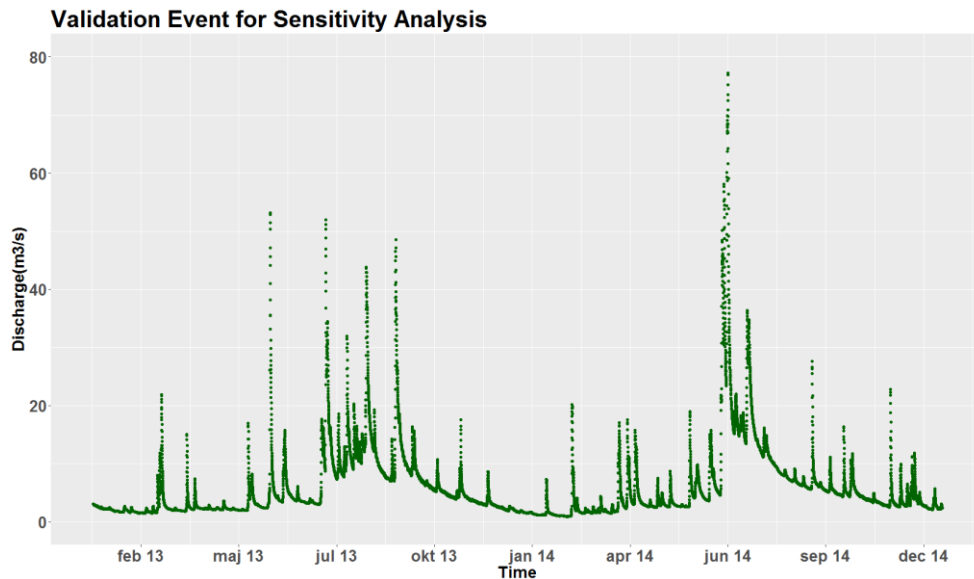


Figure 39: Validation period for sensitivity analysis

Figure 40 shows the graphical representation of DA in red, observations in blue, ensemble members in grey, the deterministic run (open loop) in black and the 7 day forecasts in green after the application of DA for the validation period. It can be seen that almost all the time the forecasts are performing better than the open loop simulation. Full results of the analysis are depicted in Figure 41; for instance looking at the first 24 hours of forecast, according to RMSE results, the forecasts made after applying DA are 55% more skilful than the open loop run. Whereas CRPSS results tell that for the first 24 hours, the forecasts are 82% more skilful than the forecast made with the open loop.

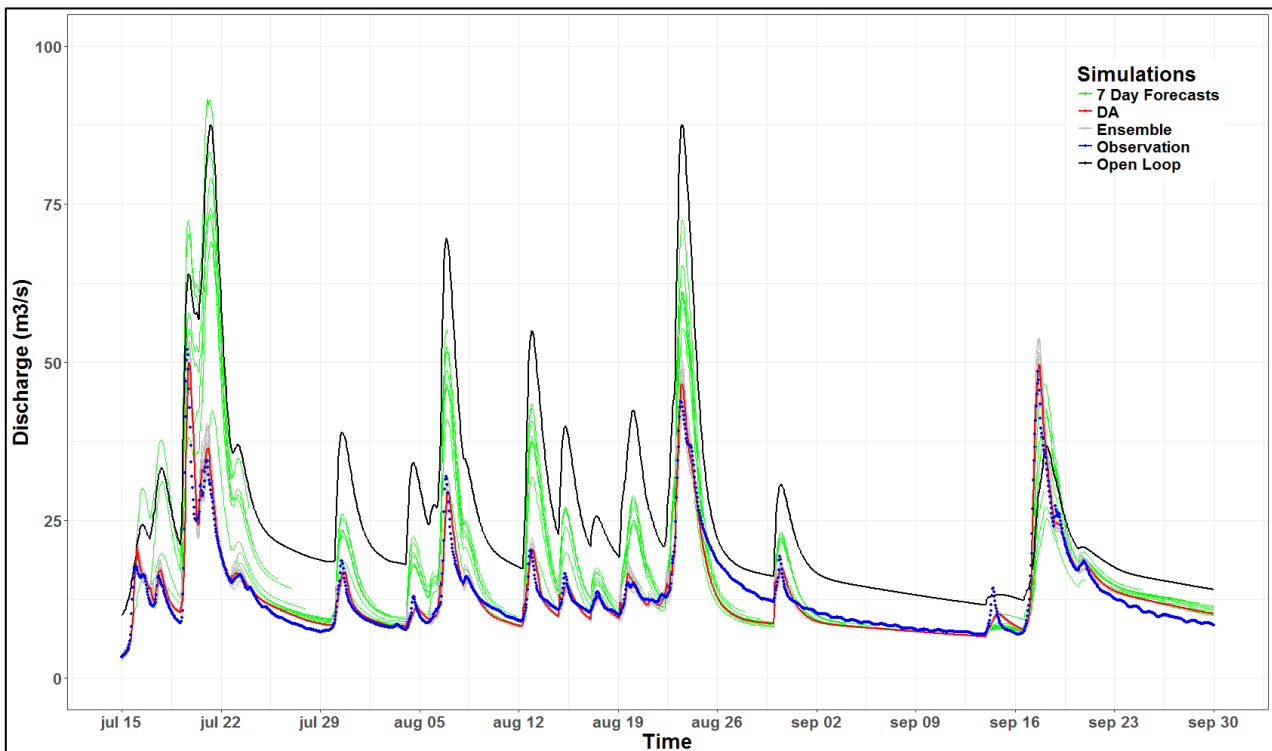


Figure 40: Sequence of forecasts made in the validation period

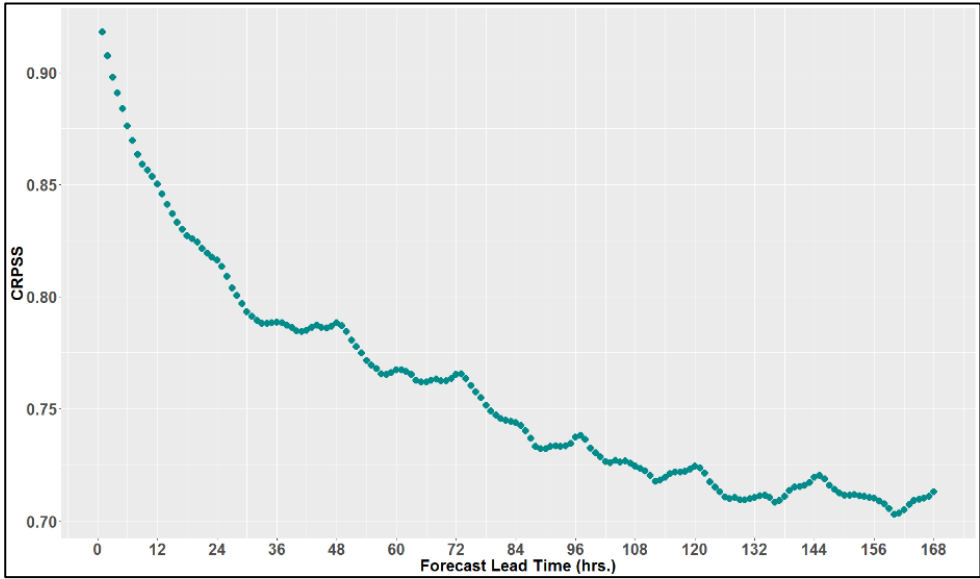
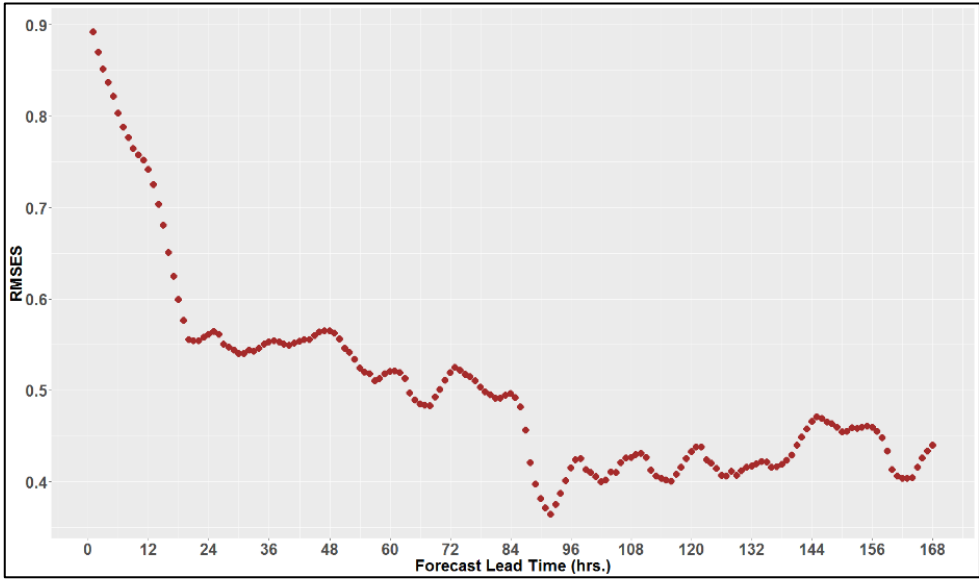
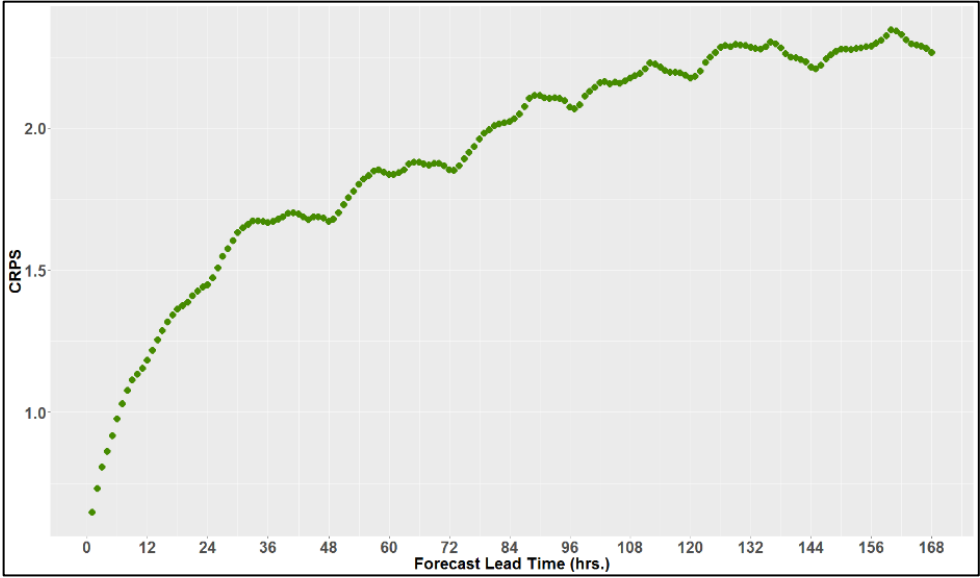
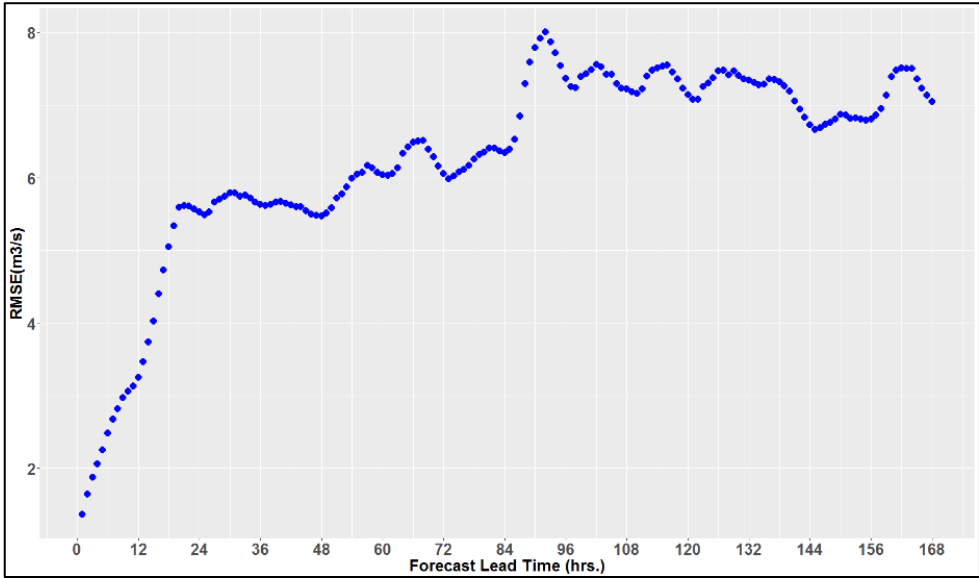


Figure 41: RMSE (Top left) and CRPS (Top right) of 1 year forecast on validation period, RMSES (lower left) and CRPSS (lower right) skill score of forecast



6.5 Hydrodynamic model states update

6.5.1 Model Area

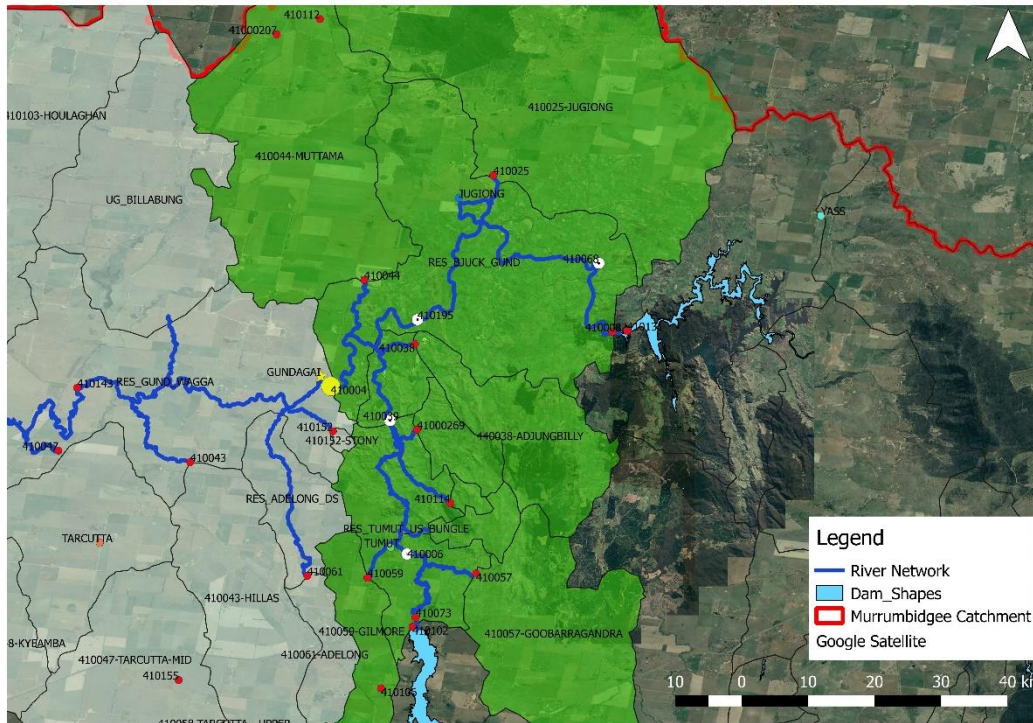


Figure 42: Murrumbidgee catchment and the subdivision into eleven sub catchments. Gauging stations are also shown in white and red circles

The model domain for the hydrodynamic model states update covers the upstream part of the Murrumbidgee catchment. Eleven rainfall-runoff sub catchments (marked green in Figure 42) were chosen for this specific study. These catchments feed the Murrumbidgee River and two other tributaries. The precipitation used for each catchment is the result of the mean area weighting of precipitation measured in multiple gauges within the sub-catchments. As outlined in Table 9, in-situ discharges from four gauging stations, (white circles) in Figure 42 are used for assimilation, whereas discharge observation downstream of the sub catchments, (yellow circle, at Gundagai), is used for validation of the assimilation.

Table 9: Gauging stations used for assimilation and validation

ID	Gauging Station	Placed at	River	Q-chainage	Remark
410068	Glendale	HD inlet	Murrumbidgee	17398.61	Assimilation
410195	U/S Gobarra	HD inlet	Murrumbidgee	84561.01	Assimilation
410039	Brungle Bdge	Branch connection	Tumut	61400	Assimilation
410006	Tumut	HD inlet	Tumut	25434.98	Assimilation
410004	Gundagai	HD inlet	Murrumbidgee	117646	Validation

6.5.2 Major Peaks

The discharge at the outlet of the model domain, which is at Gundagai was studied to identify major peak events. Data assimilation will be implemented for the (2013 - 2016) period in order to reduce the uncertainty when predicting the major peak events. Table 10 shows the details of the selected peak events. The precipitation peak is representing the rainfall intensity of all the sub-catchments within the model domain.

Table 10: Major peak events at Gundagai station (2013 - 2016)

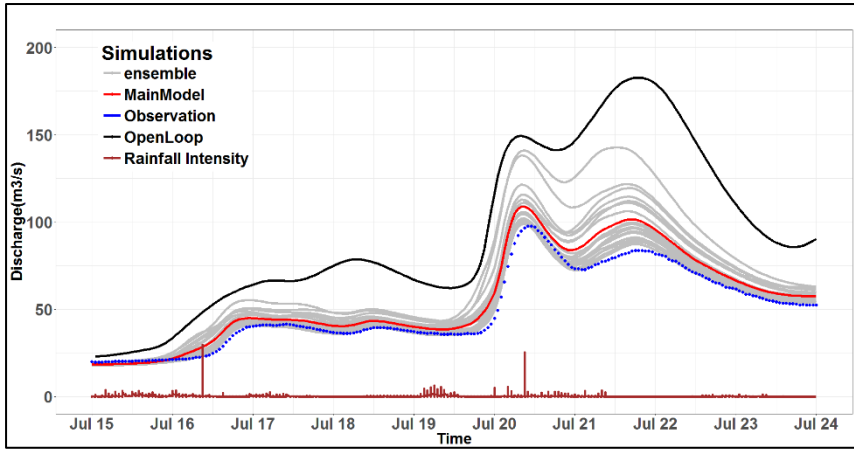
	Jul 2013	Dec2013	Apr 2014	Jun 2014
Observed Peak (m3/s)	97.62	186.01	51.27	114.94
Peak Time	Jul 20	Dec 24	Apr 13	Jun 25, 27
Precipitation Peak Time	Jul 16, 20	Dec 23	Apr 11	Jun 24
Precipitation Peak (mm/hr)	62.74	11.22	20.678	33.38
	Oct 2014	Jul 2015	Aug 2015	Sep 2016
Observed Peak (m3/s)	182.69	94.06	187.21	749.57
Peak Time	Oct 03	Jul 23, 25, 28	Aug 26	Sep 22
Precipitation Peak Time	-	Jul 22, 25	Aug 24	Sep 21
Precipitation Peak (mm/hr)	-	29.42	22.28	34.56

6.5.3 Analysis Parameters

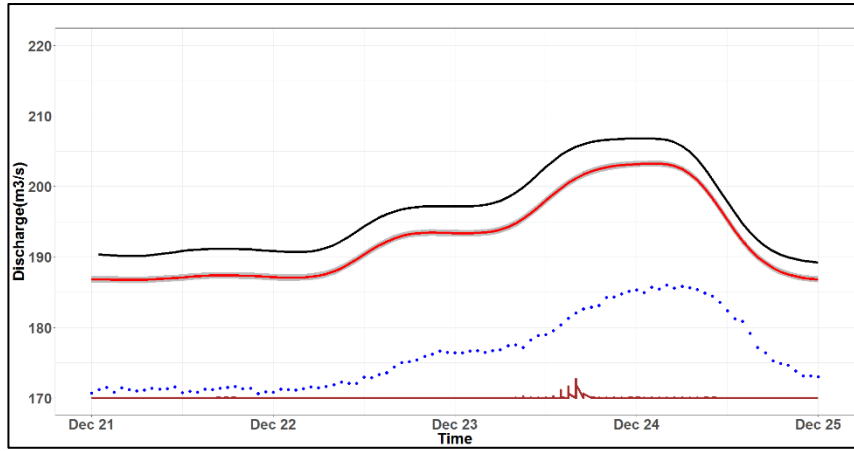
After choosing the major peaks, data assimilation was implemented with the error parameters obtained from the sensitivity analysis in 6.4. The filter parameters found in 6.4 were unique to the Goobarragandra sub-catchment, however, due to time constraints the error parameters obtained for the Goobarragandra sub-catchment in Table 8 are assumed to be the same for all the other sub-catchments too. Perturbation of precipitation is sampled from a Gaussian distribution of $N(0, (0.7*P)^2)$ where P is the precipitation value. Spatial correlation of catchment rainfall was activated in the data assimilation scheme. Perturbation of observed discharge is sampled from a Gaussian distribution of $N(0, (0.1*O)^2)$, where O represents the observed value. In order to account for the temporal correlation of the forcing errors, a first order autoregressive model is used as explained in 5.3.1 and a half-time constant of 16 hrs is used as obtained from the sensitivity analysis. Data assimilation was applied for the 2013 to 2016 period and the graphical representation of the DA is shown in Figure 43.

It can be seen from Figure 43 that compared to the open loop, the performance of the data assimilation is significantly better. For most of the peak events, RMSE, MAE, and PBIAS statistics were reduced especially for the June 2013, July 2015 and August 2015 peak events as shown in Figure 45. However for the peaks in December 2013 and October 2014, the data assimilation did not improve the simulation. The reason for the poor performance of the data assimilation in these events is because the duration of rainfall is very much short (for the October 2014 event, there was no precipitation recorded) compared to the other events. Besides the flow during these periods is mostly governed by flow from the two reservoirs upstream. Thus the forcing cannot be perturbed appropriately and its uncertainty cannot be defined properly which leads to inadequate assimilation result.

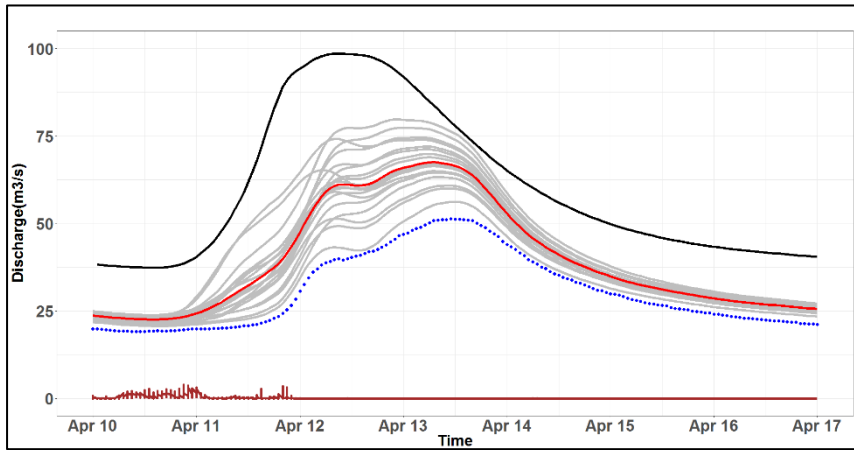
Data Assimilation in Hydrodynamic-Hydrological Forecast Systems



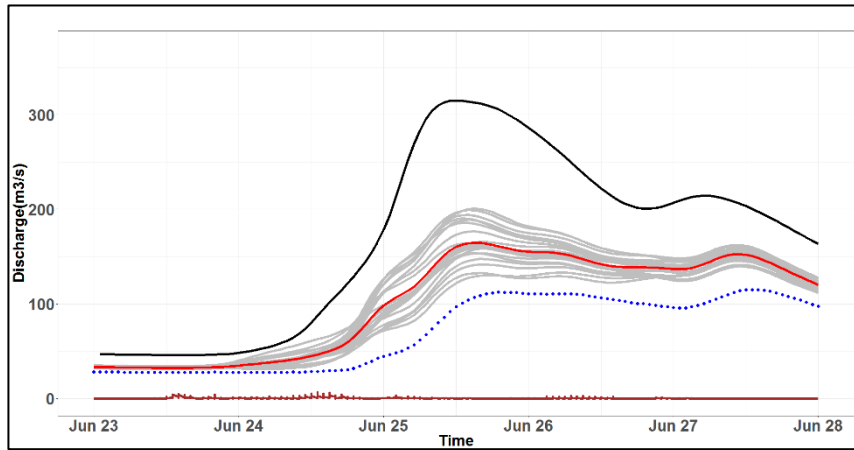
Jul 2013



Dec 2013

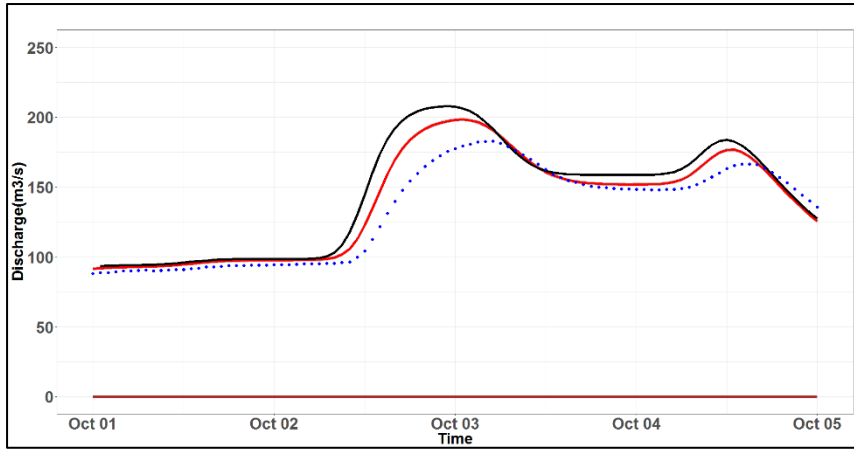


Apr 2014

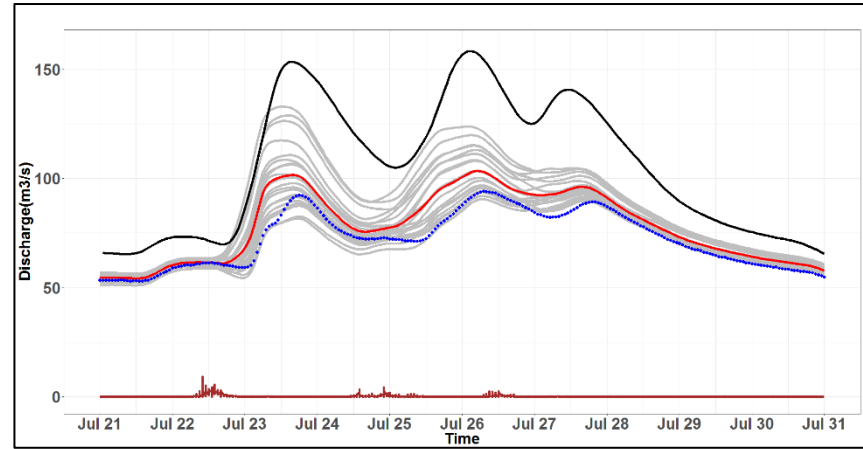


Jun 2014

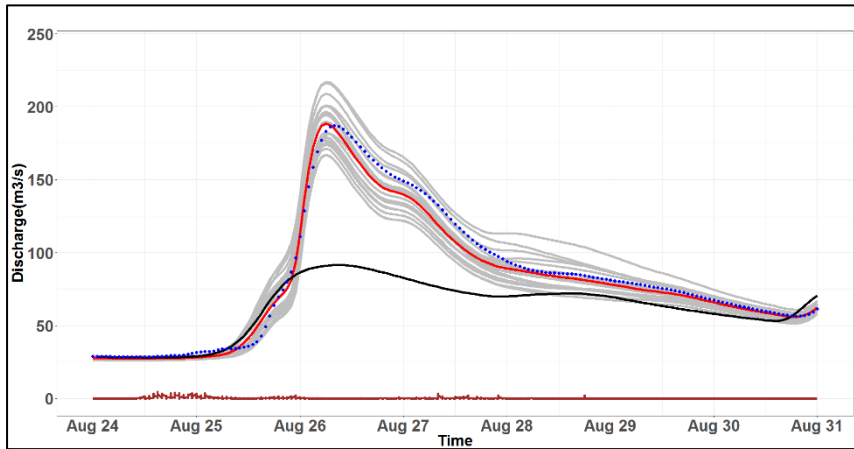




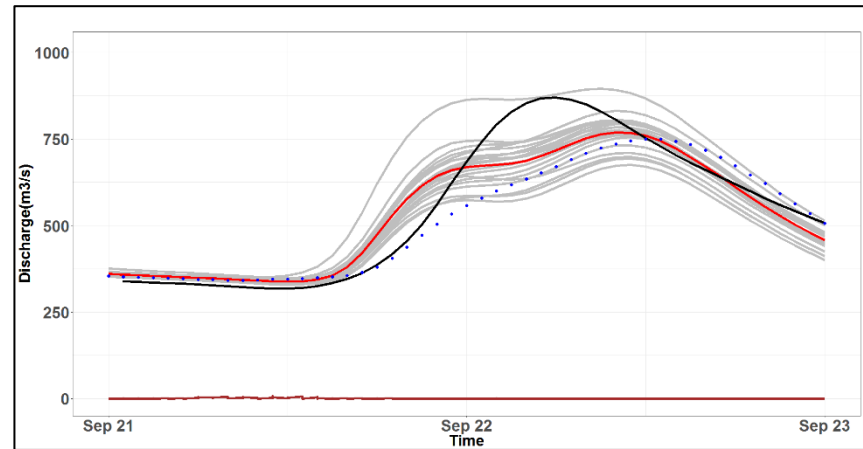
Oct 2014



Jul 2015



Aug 2015



Sep 2016

Figure 43: Implementation of data assimilation on the major peaks

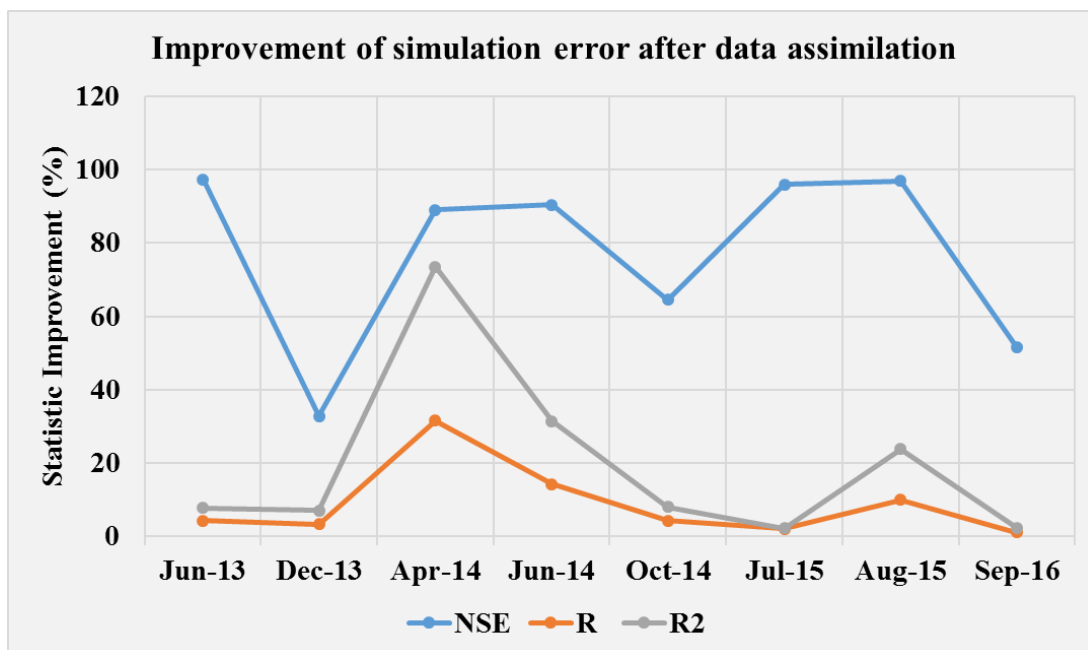
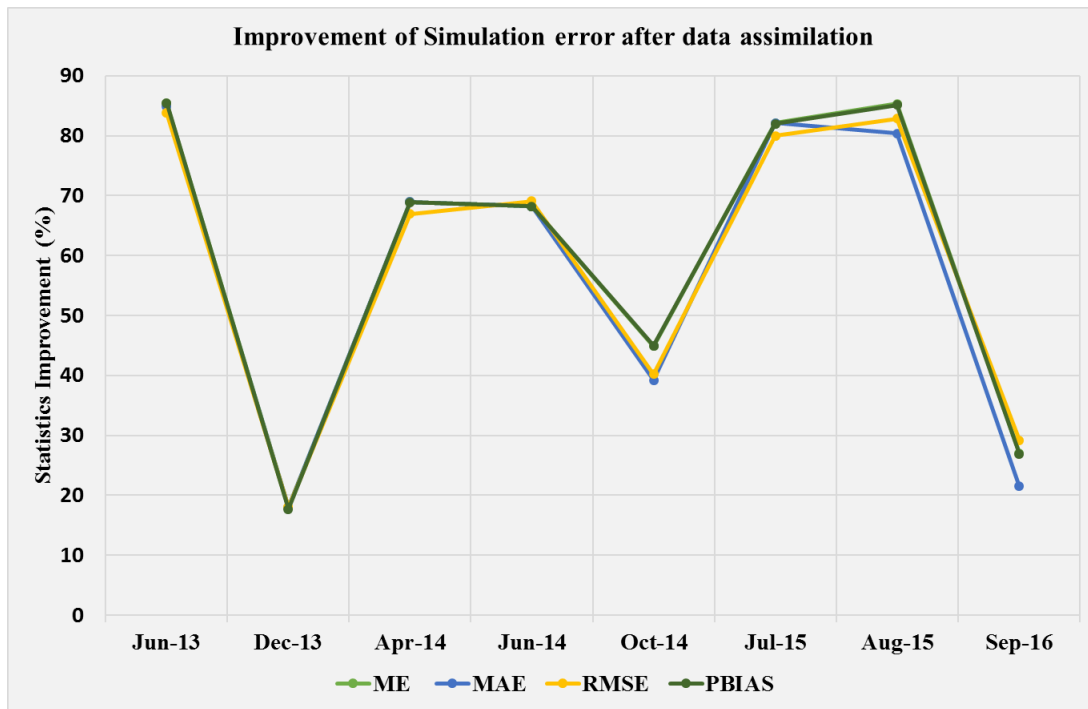


Figure 44: Improvement of statistical errors for the eight major peaks after DA

6.5.4 Streamflow Forecast

Here it is intended to evaluate the effect of updating only hydrodynamic states on stream flow prediction. Forecasting strategy is the same as the one explained in 5.5. Before the forecast is made, the observed discharge measurements in the 4 locations (refer Figure 42) are assimilated for the period of May 2013 to December 2016. Following the assimilation, daily forecasts were issued as of May 2014 for one year with a lead time of 7 days, giving a sequence of 365 forecasts. The discrepancy of the forecasts from the measured discharges is quantified by RMSE and CRPS statistics as a function of forecast lead time. In addition skill scores are computed for the forecasts.

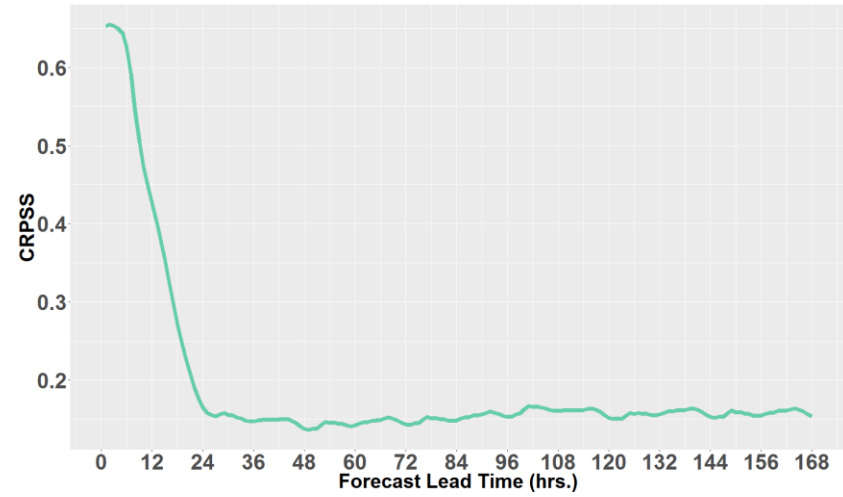
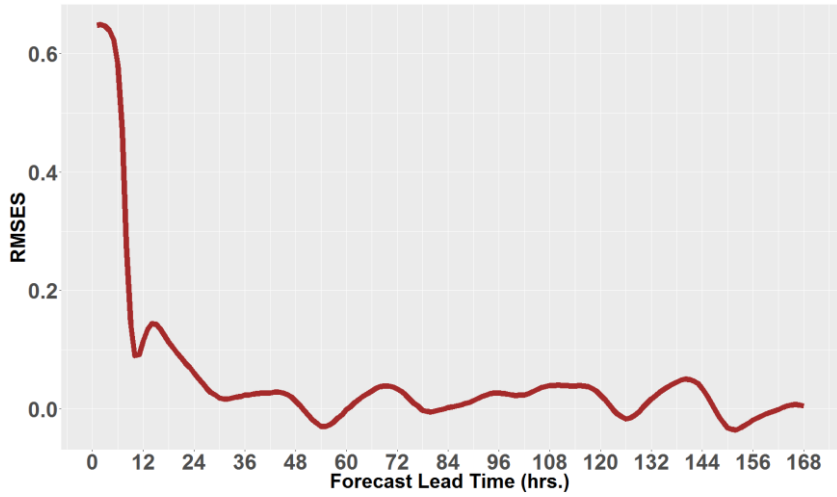
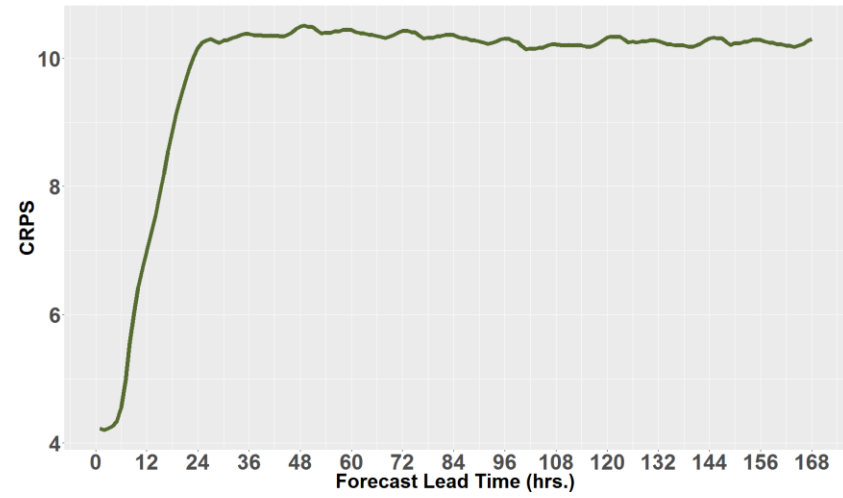
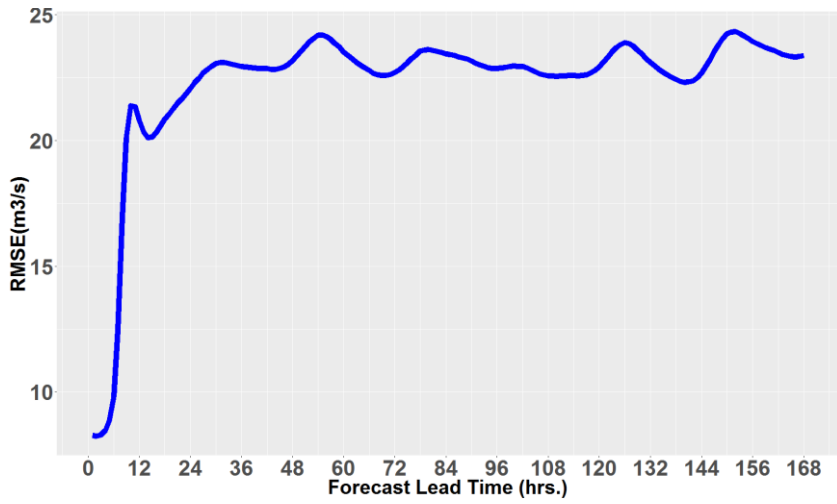


Figure 45: Verification of forecast based on HD update as a function of lead time

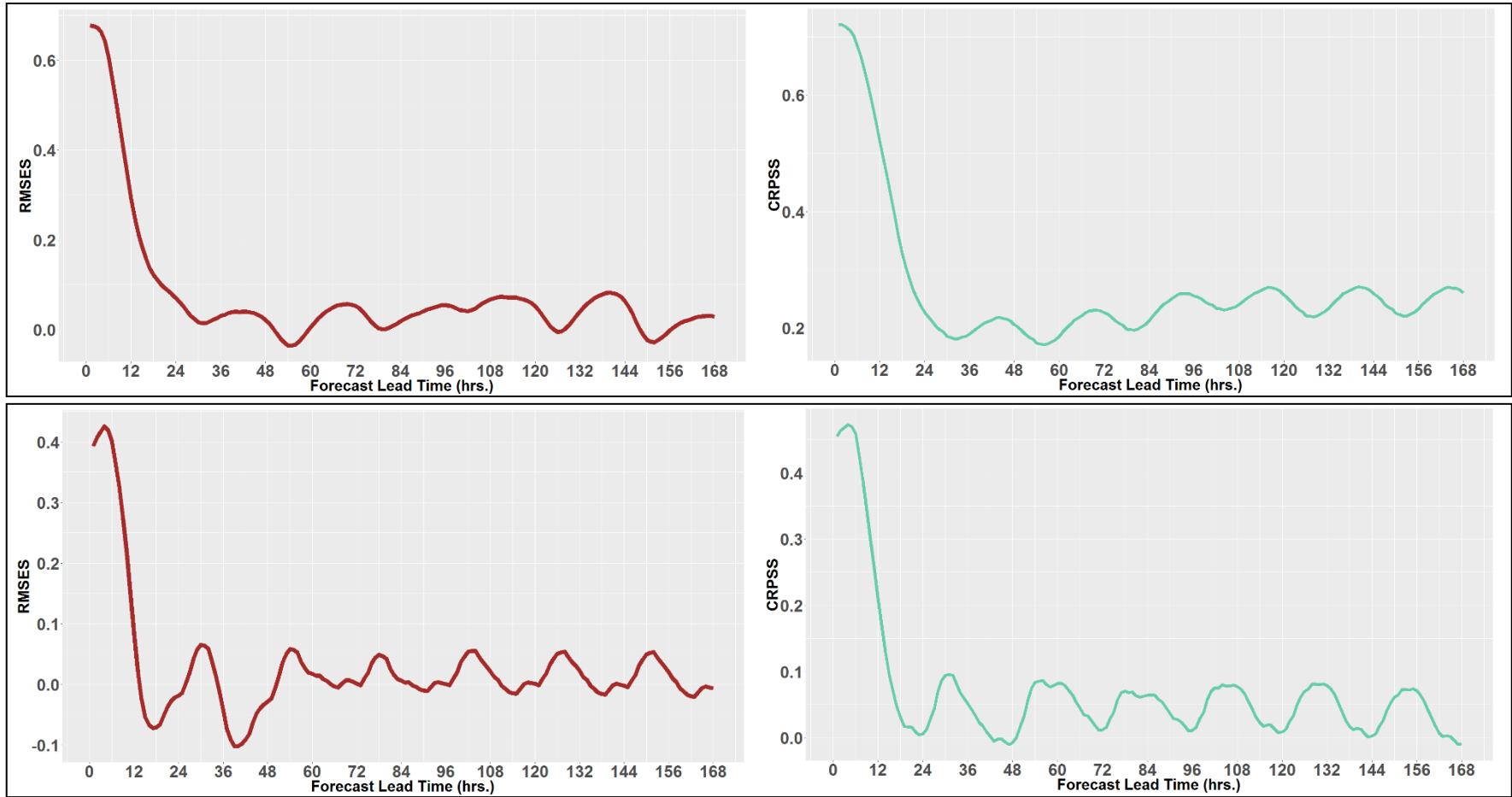


Figure 46: Comparison of forecast skills in high-flow (the top-most plots) and low-flow periods (bottom plots) for HD update

The one year forecast was separated into high-flow period and low-flow period in order to study the impact of data assimilation in the two periods. The top-most plots in Figure 46 represent the skill of the forecasts during the high-flow period whereas the bottom-most plots are showing the skill of the forecasts for the low-flow period. Comparing the forecast skills for the two periods, one can see that during the high-flow period (dominated by precipitation events) skilful forecasts can be made up to 48 hrs. However, during the low-flow periods skilful forecasts could be made up to only 12 hrs. This could be explained by the fact that, during the low-flow period (which is mainly governed by reservoir releases), there is not enough precipitation; which makes it difficult to represent the hydro-meteorological uncertainty using the ETKF. Hence the data assimilation and forecasts experiments are unsatisfactory.

Looking at Figure 45, one can notice that the forecast RMSE statistic deteriorates dramatically within the first 12 hours after which it saturates to an RMSE of 25 m³/s. Similarly CRPS statistic deteriorates within the first 24 hours. Discrepancies between forecasts and observed values increases with lead time. RMSE and CRPS skill scores depreciate drastically within the first 24 hours, meaning its better off using the calibrated model (without data assimilation) than implement data assimilation for forecast lead times longer than 24 hours. Thus, updating only the hydrodynamic states has improved the forecasts until a lead time of 24 hours tops. This could be because the hydrodynamic update improves the subsequent forecasts only for the duration corresponding to the travel time of the flood wave. Thus the effect of updating the river states on subsequent forecasts is only transient.

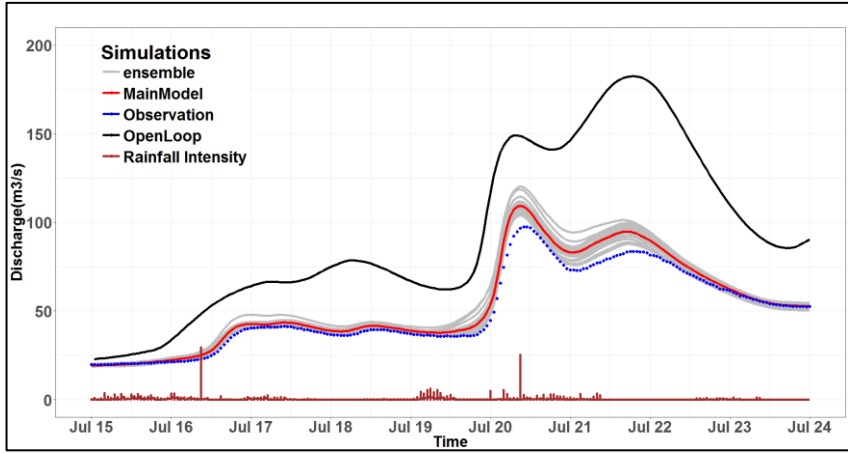
6.6 Hydrodynamic-Hydrological model states update

This part of the study discusses the results obtained after implementing a combined hydrodynamic-hydrological model state updating. In this case, both the catchment and the river states will be updated by assimilating available discharge observations. Table 11 outlines the details of the gauging stations. The model forcing (precipitation) is perturbed according to the error parameters selected in 6.5.3. The difference between the combined update and the hydrodynamic update is that, the ensemble (generated by perturbing the precipitation) will be updated using available observation in catchment outlets thereby reducing the hydrological uncertainty. As opposed to the hydrodynamic update, inherent hydrological uncertainty will not be propagated as the river is routed downstream.

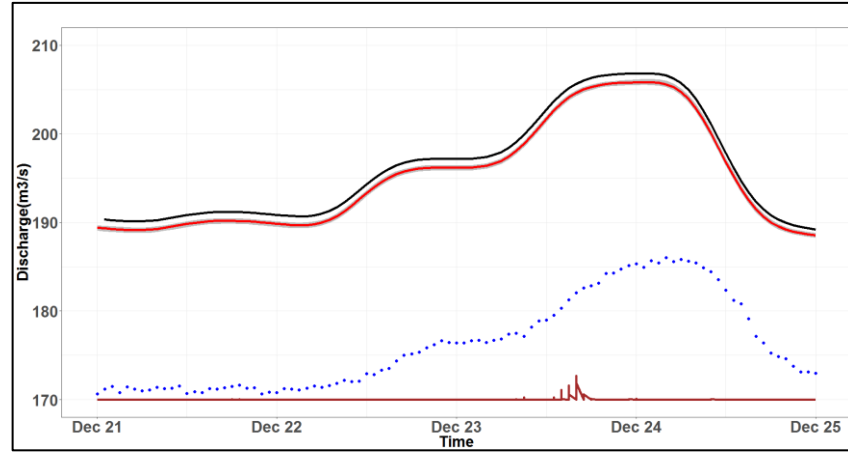
Table 11: Gauging stations used for assimilation and validation in the combined update

ID	Gauging Station	Placed at	River	Q-chainage	Remark
410068	Glendale	HD inlet	Murrumbidgee	17398.61	Assimilation
410195	U/S Gobarra	HD inlet	Murrumbidgee	84561.01	Assimilation
410039	Brungle Bdge	Branch connection	Tumut	61400	Assimilation
410006	Tumut	HD inlet	Tumut	25434.98	Assimilation
410044	Coolac	Catchment outlet	Muttama Creek	0	Assimilation
410114	Wyangle	Catchment outlet	Killimcat Creek	0	Assimilation
41000269	Redhill	Catchment outlet	Brungle Creek	0	Assimilation
410059	Gilmore	Catchment outlet	Gilmore Creek	0	Assimilation
410038	Adjungbilly Dbalara	Catchment outlet	Adjungbilly Creek	0	Assimilation
410025	Jugiong	Catchment outlet	Jugiong Creek	0	Assimilation
410057	Gndra Lacmalac	Catchment outlet	Goobarragandra river	0	Assimilation
410004	Gundagai	HD inlet	Murrumbidgee	117646	Validation

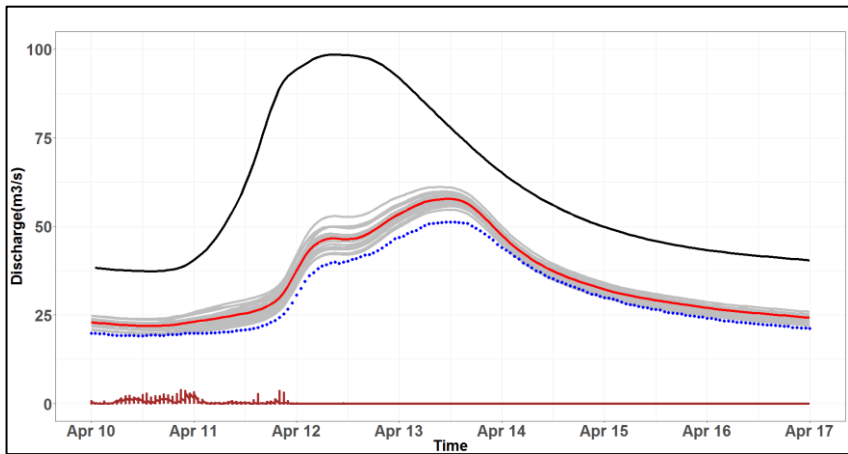
The same major peak events shown in Table 10 are used to test the performance of the data assimilation for the combined update. The results of the combined update on the major peaks is shown below in Figure 47.



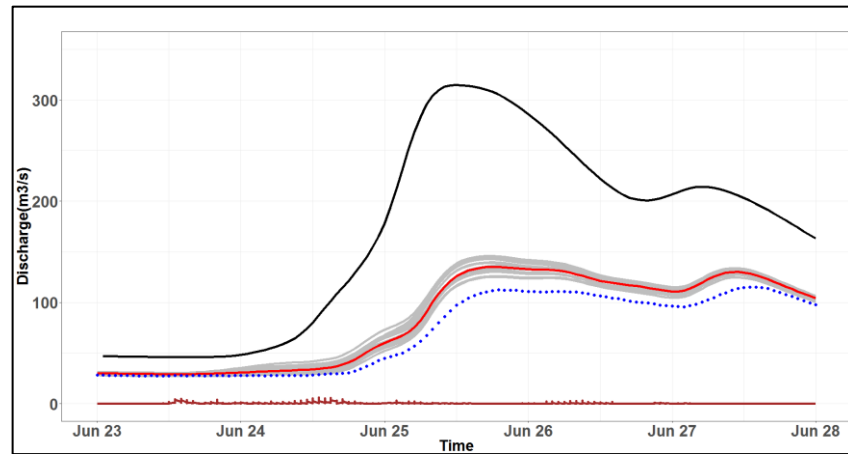
Jul 2013



Dec 2013

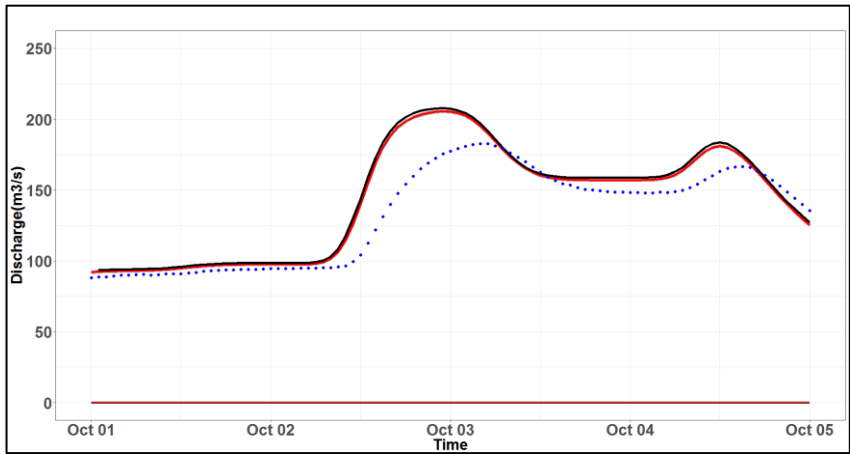


Apr 2014

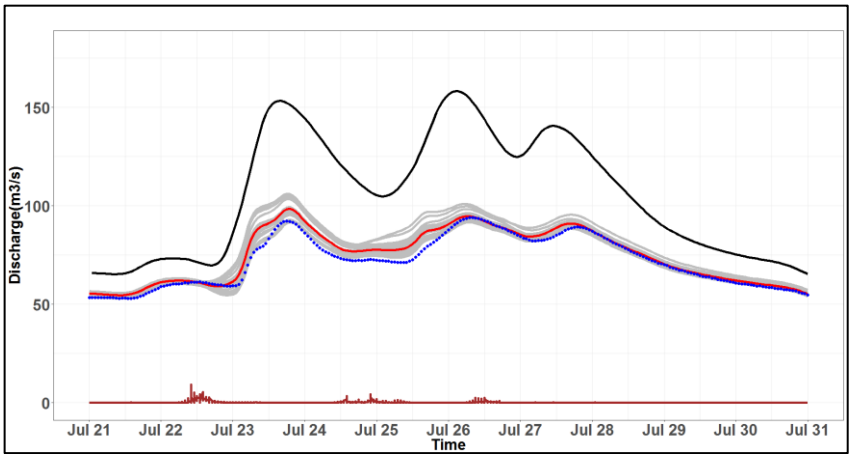


Jun 2014

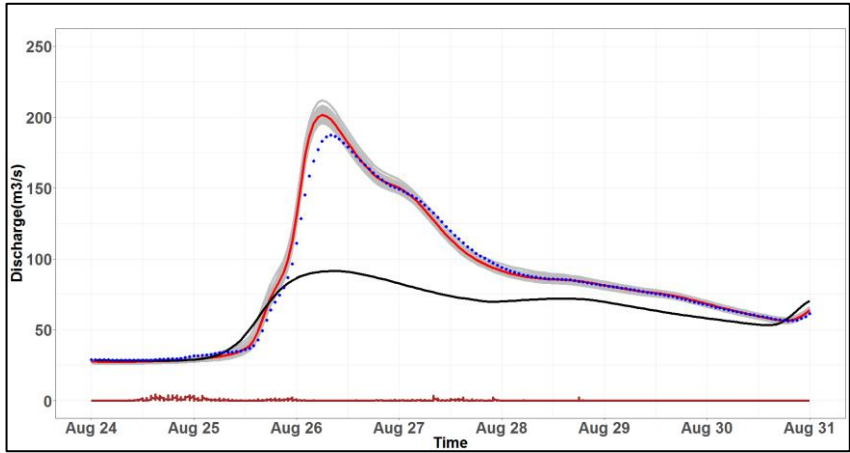




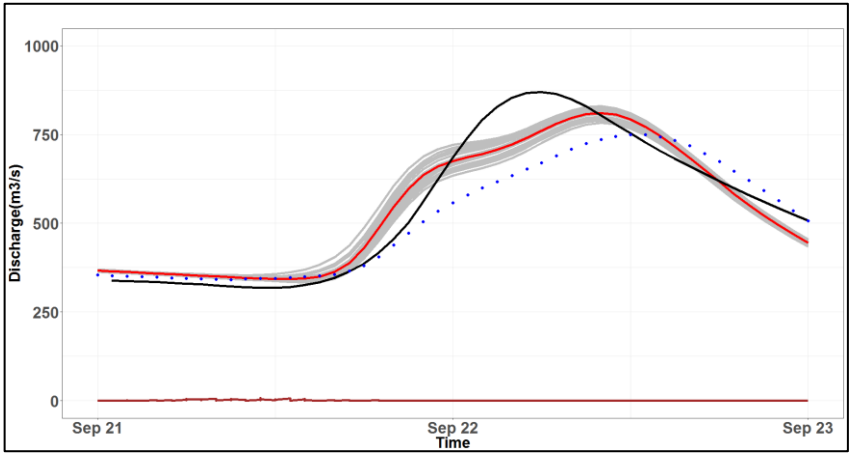
Oct 2014



Jul 2015



Aug 2015



Sep 2016

Figure 47: Assimilation results after combined HD+RR update

Comparing the assimilation results of the hydrodynamic update with the combined update, one can see that the recession part of the hydrograph was improved for the Jul 2013, Apr 2014 and Aug 2015 peak events. The peaks in Apr 2014 and the three peaks of Jul 2015 were reproduced very well after the combined update. However, the August 2015 peak event was slightly over-estimated even though the mis-phasing problem was solved after the combined update. As expected the dry period events of Dec 2013 and Oct 2014 where the flow is dominated by reservoir release saw no improvement after the combined update. Another interesting difference is the ensemble spread; comparing the hydrographs for the two updates in Figure 43 and Figure 47, it can be seen that the ensemble spread is comparatively low after the combined update meaning there is relatively less uncertainty in streamflow simulation after hydrological-hydrodynamic update. This is because the inherent meteorological uncertainty (arising from uncertainty in precipitation estimation) was reduced when the six hydrological model states were updated. Thus less uncertainty was propagated from the rainfall-runoff to towards the river routing.

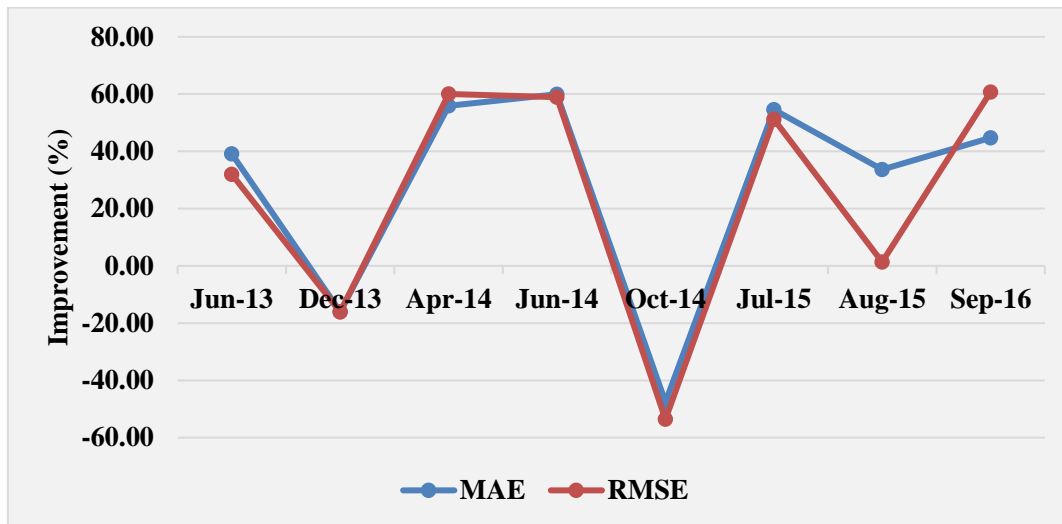


Figure 48: Improvement MAE & RMSE after combined HD+RR update

Overall, after the combined HD+RR update there was a significant improvement compared to the HD only update in the error statistics. The MAE and RMSE statistics for instance, were very much reduced after the combined update as shown in Figure 48. The RMSE statistic for the Apr and Jun 2014 peak events was for instance reduced by almost 60% after the implementation of the combined update. On the contrary, the Dec 2013 and Oct 2014 events saw a deterioration in both MAE and RMSE statistics.

Another experiment was done to further test the performance of the combined HD+RR update. Before assimilating the observed discharges, a small chunk of observed data was deliberately omitted from the observation time series and the update was done separately on HD and HD+RR schemes. This was done to test how far would the update go before deteriorating to the open loop. In other words, in order to test the longevity of the HD and HD+RR updates. Results are shown in Figure 49, it's interesting to see that in the HD only update, as soon as the observations are omitted, the MainModel (marked by red) quickly reverts back to the open loop simulation (deterministic run without data assimilation) at both the high and low flow events.

Data Assimilation in Hydrodynamic-Hydrological Forecast Systems

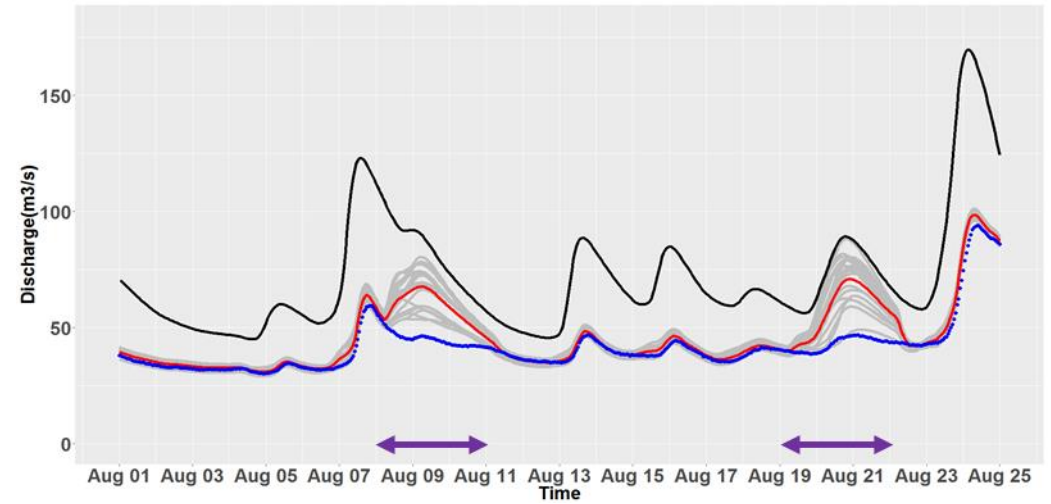
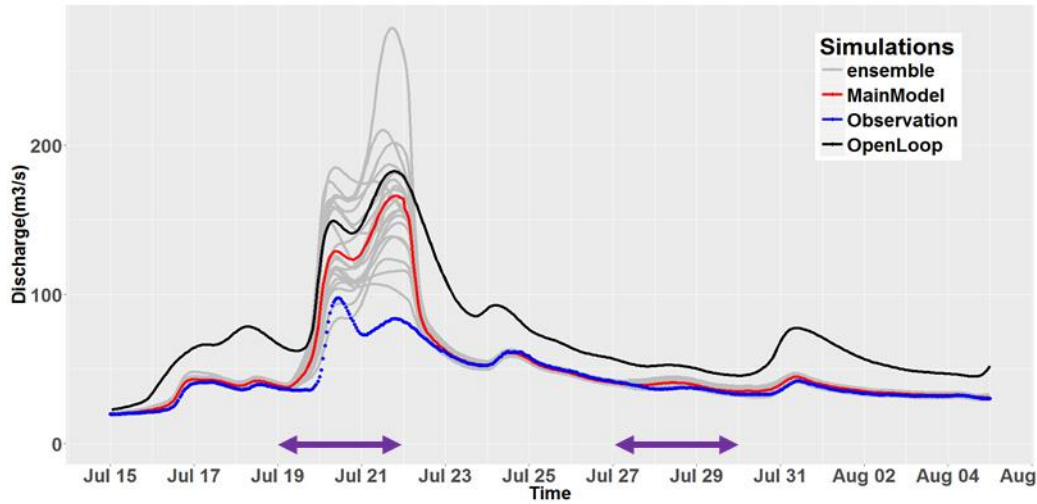
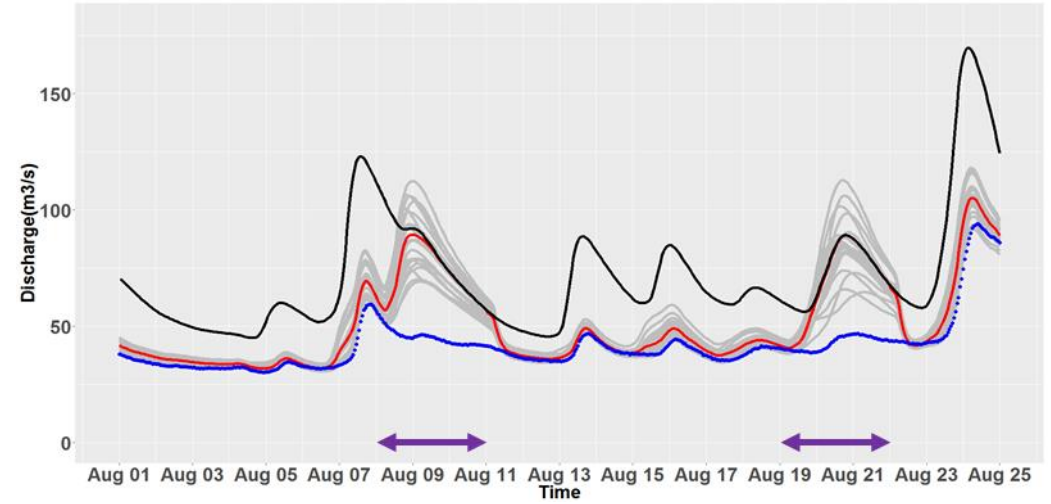
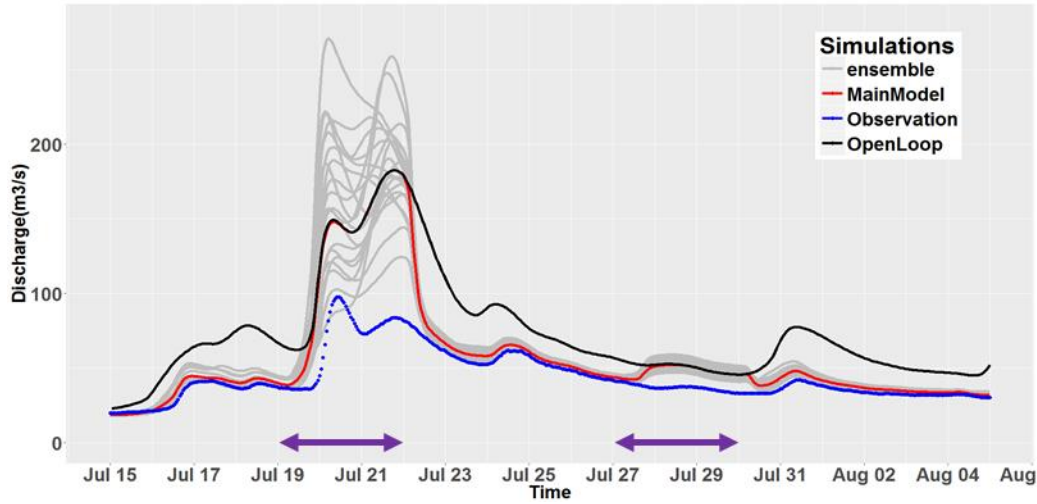


Figure 49: Top left and right show the HD update results with missing observations (purple) and bottom left and right show the HD+RR update results with missing observations

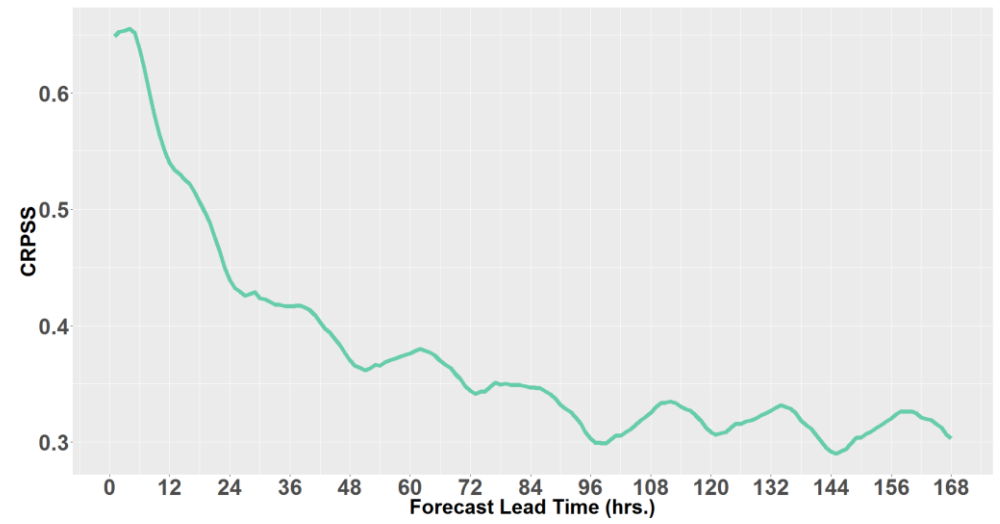
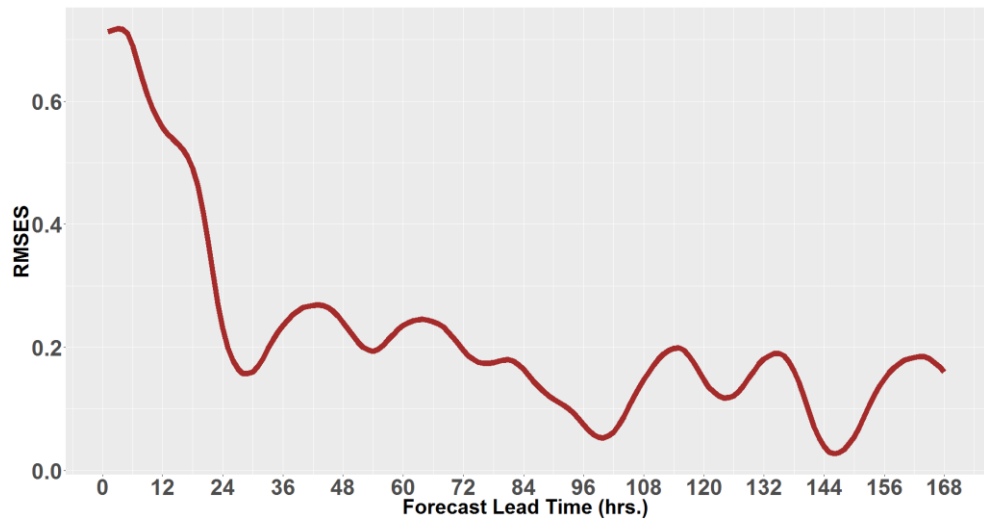
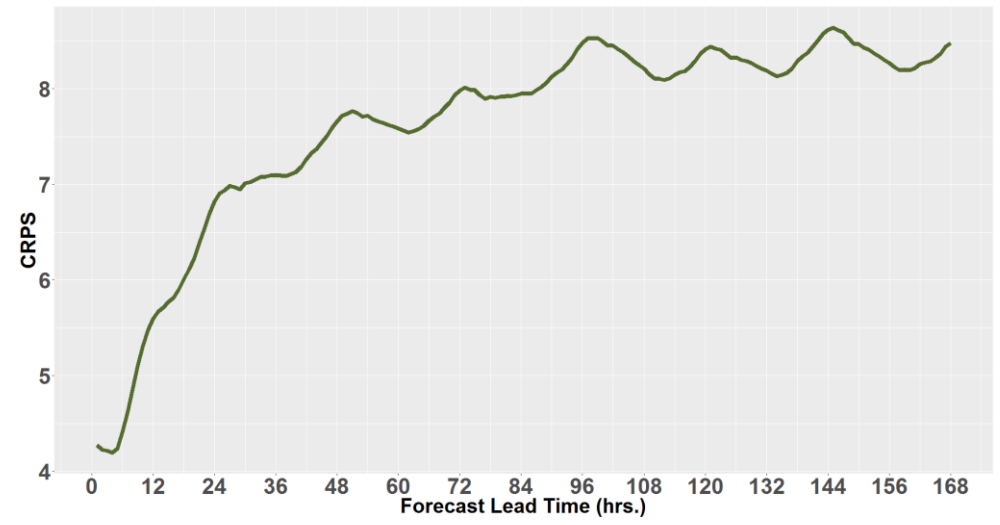
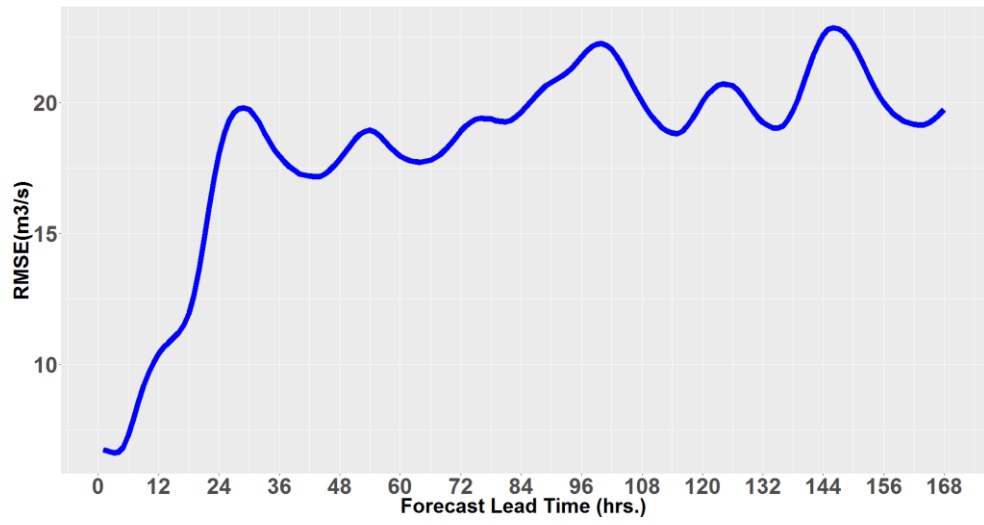
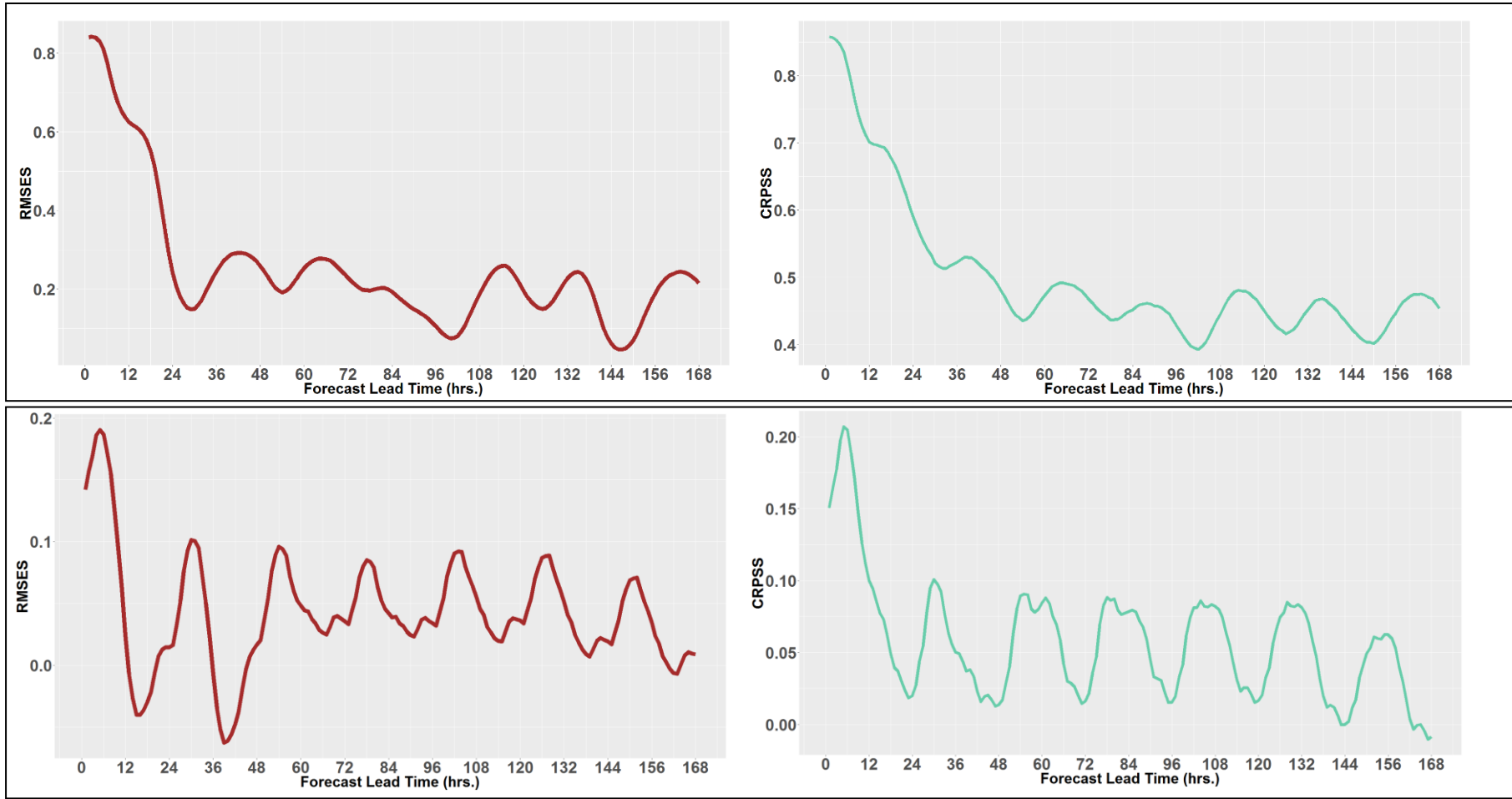


Figure 50: Verification of hindcast results based on HD+RR update as a function of lead time





High-flow
Period
(Jun - Aug)

Low-flow
Period
(Oct - Dec)

Figure 51: Comparison of forecast skills in high-flow (the top-most plots) and low-flow periods (bottom plots) for HD+RR update

Similar to the plots shown in Figure 46, the one year forecast that was made after HD+RR update was separated into high-flow and low-flow periods. The forecast skills were calculated (RMSES and CRPSS). The top row of plots in Figure 51 represents the skill of the forecasts made during the high-flow period and the bottom row of plots represent the skill of the forecasts for the low-flow period. During the high-flow period, skilful forecasts can be made for up to 96 hrs lead time, however, for the low-flow period it's only about 12 hrs. This is owing to the very low precipitation events in the low period. This makes it difficult to accurately represent hydro-meteorological uncertainty using the ETKF since there is very little precipitation of the ensembles to perturb.

However, during the combined HD+RR update, one can see that the updating effect lasts much longer especially during the low flow periods. This could be due to the fact that catchment hydrological memory does not change as rapidly as the states in the river and since the combined update adjusts the catchment states to their “true” states, the effect of the update persists longer than just the HD update only.

6.6.1 Streamflow Forecast

Similar to the HD only update, the performance of the combined update needs to be tested by generating a series of forecast experiments. The forecasts were done on the same period as for the HD only update in order to compare results. Eventually the forecasts were evaluated with the verification methods and forecast skill scores were calculated accordingly. Figure 50 shows the forecast results for the HD+RR update; generally speaking the forecast RMSE and CRPS are lowered compared to the case of HD only update. The maximum forecast RMSE score was reduced to 22.5 m³/s (HD+RR) from 25m³/s (HD), whereas the maximum forecast CRPS score was reduced to 9 m³/s (HD+RR) from 10.5 m³/s (HD). Moreover, the RMSE and CRPS statistics degrade less rapidly as opposed to the drastic deterioration observed in HD only update (refer Figure 45). The forecast skill scores illustrate that there is a significant improvement; for instance looking at the RMSES results, the deterministic forecasts were more skillful than the reference simulation for the first 96 hours, which is additional 72 hours as compared to the HD only update. CRPS skill score tell that the ensemble forecasts made after HD+RR update are at least 30% more skillful for the entire 7 days lead time.

Thus, it has been shown that updating both hydrological and hydrodynamic model states improved the deterministic forecasts (looking at RMSES results, taking the mean of the ensemble as a deterministic forecast) up to a lead of 96 hours (4 days) and ensemble forecasts (looking at CRPSS results) for the entire 7 days lead time. This implies that due to the combined update, the lead time for skillful forecasts was extended significantly (from 48hrs to 96hrs, RMSES). This extension of forecast lead time was achieved as follows; by updating the catchment states the catchment runoff can be forecast with reasonable accuracy up to the time of concentration. Further downstream when the catchment runoff is routed along the river and gets updated by the available river discharge, streamflow can be forecast with a reasonable accuracy up until the flood wave travel time. Thus, by updating both states, the lead time for skillful forecasts was extended by the time of concentration. This will come in handy in flood forecasting as well as reservoir operating systems within the Murrumbidgee catchment. On the other hand hydrodynamic updates can produce skillful forecasts within the time frame of flood wave travel time.

Figure 52 is showing the comparison of forecast accuracy and skill for the first 48 hours. Regarding the accuracy measured by RMSE and CRPS, the HD+RR forecasts show lower forecast errors on average 28% lower RMSE compared with the HD forecasts. Similarly HD+RR forecasts have on average 22% lower CRPS as compared with the HD forecasts. Looking at the forecast skill scores, one can see that for the first 48 hours only, the HD+RR forecasts are 23% (RMSES) and 18% (CRPSS) more skilful than the HD forecasts. This suggests that streamflow forecasts and more importantly floods can be forecast with a reasonable accuracy for larger lead times.

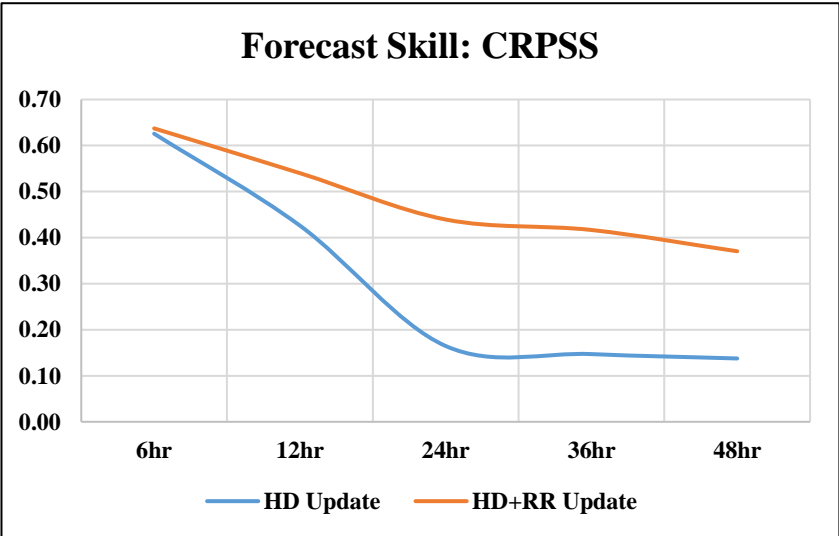
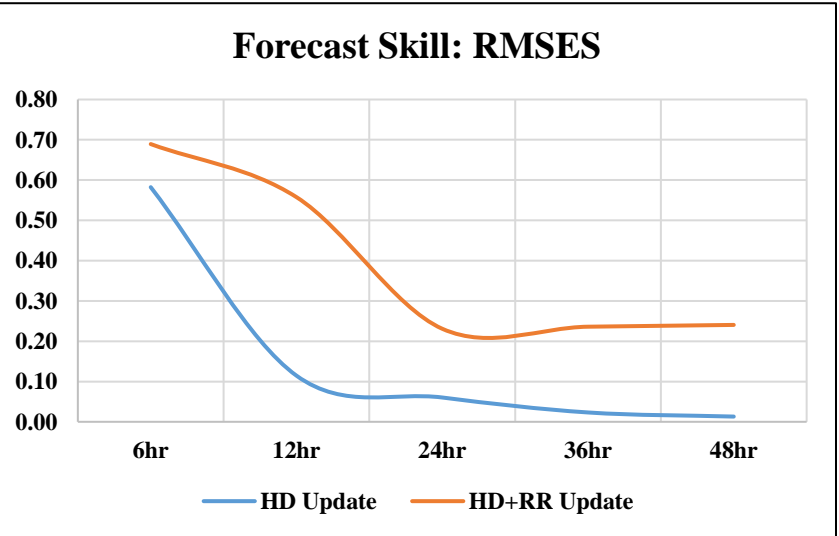
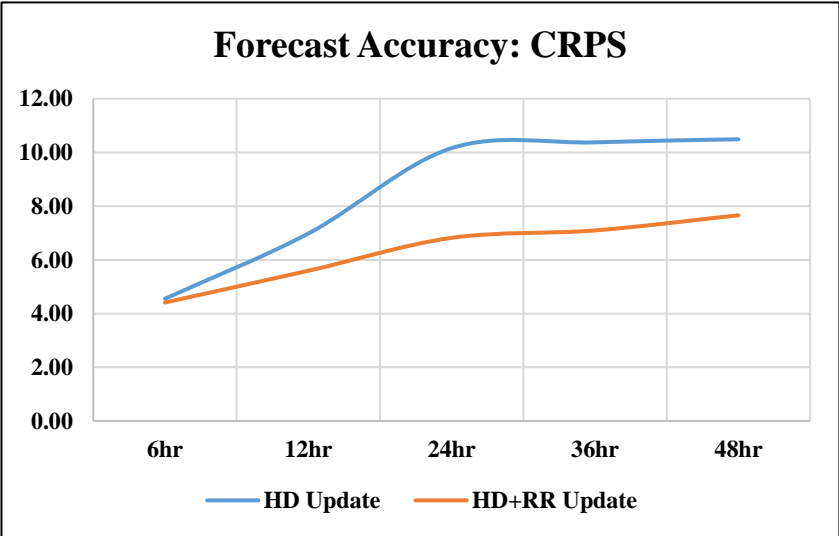
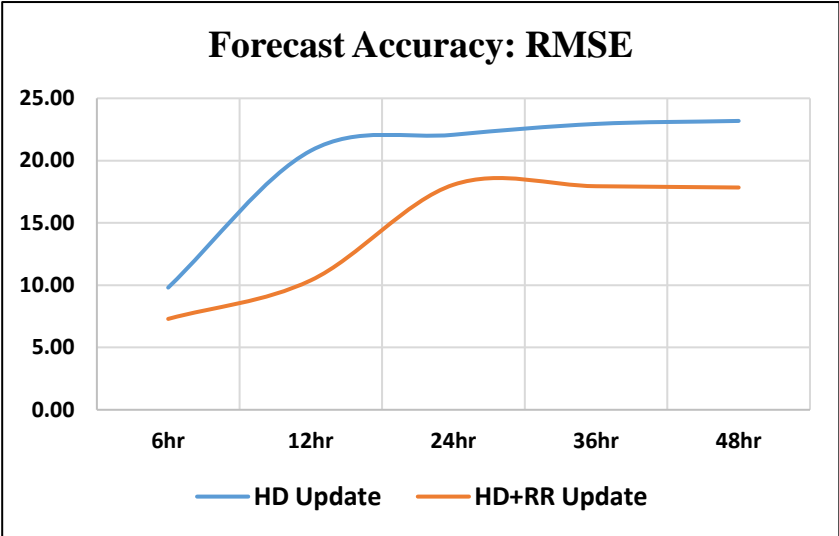


Figure 52: Forecast skill Comparison for HD and HD+RR update

7. Conclusions

The main objectives of this study were the following: investigating the potential benefit of combined hydrological-hydrodynamic update on streamflow forecast improvement; optimizing the data assimilation filter parameters for improved forecast; and studying the potential of using satellite precipitation products for rainfall runoff modelling. To this end, the following conclusions were reached:

1. Rainfall-runoff processes can be represented at large using daily satellite rainfall estimates, however major peak events were not captured rendering the rainfall products unsuitable for flood forecasting/reservoir management systems.
 - Three satellite rainfall products (TRMM, CHIRPS, & PERSIANN) with daily temporal resolution were studied for an alternative precipitation as a substitute for in-situ rainfall data. Raw satellite data had very low correlation with in-situ rainfall data. Almost all the three products underestimate/miss the rainfall compared to the in-situ rainfall data. Comparatively speaking raw CHIRPS had better correlation ($r = 0.61$). On the contrary, raw PERSIANN product has several gaps and highly underestimates the rainfall.
 - It was noted that the daily temporal resolution of the satellite products is not suitable to simulate the rainfall-runoff process for the sub-catchment since the sub-catchment responds more frequently than a daily time scale and thus daily rainfall data cannot capture the episodic events caused by moderate/high intensity rainfall.
 - Bias correction factors were calculated and the satellite products were corrected after which better correlation was achieved. The bias corrected rainfall products were used to re-calibrate the hydrological model for a specific sub-catchment.
 - A rainfall-runoff simulation was done for the (2013 to 2016) period using the bias corrected rainfall products. It was shown that the rainfall-runoff process can be represented at large, the model forced with bias corrected CHIRPS product even reproduced some parts of the observed hydrograph. However, the major peak events were severely underestimated. As a result, the daily satellite rainfall products were regarded as unsuitable for flood forecasting/reservoir management systems. Thus, for the purposes of flood forecasting/reservoir management systems in the Murrumbidgee catchment it is better to use in-situ rainfall data. Perhaps for sub-catchments with poor gauge distribution or no gauges at all, the satellite rainfall estimates can be an excellent alternative source of rainfall data.
2. Appropriate filter parameters were optimized for a specific sub-catchment in such a way that the hydrological forecast errors are minimized.
 - An ensemble size sensitivity analysis showed that optimal results can be achieved with an ensemble size of 20 members. The tradeoff between sampling error and computational expense was balanced with the optimal ensemble size. Increasing ensemble size did not show significant improvement in forecast while the computational time soared with increased in ensemble size.

- Forcing uncertainty (precipitation uncertainty) was found to be the most dominant filter parameter since it is highly correlated with streamflow forecast errors.
 - For the case of Goobarragandra sub-catchment, precipitation forcing uncertainty of 70%, half-time constant of 16 hrs. and observation uncertainty of 10% were found to be the best combination of filter parameters that minimized the forecast error.
3. Hydrological-hydrodynamic model states update improved streamflow simulation and forecasts.
- Updating the hydrodynamic model states alone or together with the hydrological model states improved streamflow simulation as well as streamflow forecast. Updating the hydrodynamic states alone corrected volumetric errors as well as phase errors of the hydrographs for the selected eight major peak events. Simulation error statistics were also improved after the update. Skillful deterministic forecasts (better than just using the calibrated model for forecast) could be made up to a lead time of 48 hours. Whereas skillful (at least 10% more skillful) ensemble forecasts could be made for the entire 7 days lead time.
 - Similarly updating both the hydrodynamic and the hydrological model states improved the simulation and forecast of streamflow. Simulation error statistics for some of the peak events were reduced by up to 60% compared to updating the hydrodynamic states alone. An updating experiment where observations were deliberately removed showed that, the effect of the combined states update persisted longer compared to the hydrodynamic states update alone. It was possible to make skillful deterministic forecasts up to a lead time of 96 hours; whereas skillful (at least 30% more skillful) ensemble forecasts could be made for the entire 7 days lead time. Looking at 48 hours lead time alone, deterministic forecasts based on combined states update are on average 23% more skillful than the forecasts that are based on only hydrodynamic states update. Similarly the ensemble forecasts are 18% more skillful than their counterparts.
 - Even though hydrodynamic states update alone improved streamflow forecast, comparatively speaking its effect was only transient. This is due to the fact that the effect of hydrodynamic states update persists only within the flood wave travel time. On the other hand, the effect of combined states update persists within the duration which is the sum of concentration time and flood wave travel time. Thus the combined states update has extended the lead time for skillful forecasts by time of concentration. This will come in handy for flood forecasting systems and reservoir operation systems in Murrumbidgee catchment.
 - The impact of the two different data assimilation methods on streamflow forecasts was further investigated for high-flow and low-flow events. The high-flow period is governed by moderate/high precipitation events, whereas the low-flow period is governed by reservoir releases from the two dams upstream. The skill of streamflow forecast during the high-flow period is satisfactory for up to a lead time of 48 hrs. (after HD only update) and 96 hrs. (after HD+RR update). On the other hand, during the low-flow period the skill of streamflow forecast

deteriorated just after 12 hrs. The poor streamflow forecast skill during the low-flow period is due to the fact that there is very little precipitation. In this case the ETKF cannot quantify the hydro-meteorological uncertainty appropriately.

8. Limitation of the study and further recommendation

1. A sensitivity analysis was carried out to find the filter parameters that represent the forcing precipitation and observation uncertainty accurately. However, this analysis was done for only one of the sub-catchments in the model domain. Due to the shortage of time, the optimal filter parameters which are unique to the sub-catchments were used for the other ten sub-catchments when the hydrodynamic-hydrological model states updating were done. This however will not give the best results since each sub-catchment has its own unique precipitation and measurement uncertainty. Thus, for future studies, it is better to run the sensitivity analysis for all the sub-catchments so that the forcing and observation uncertainty can be defined for each sub-catchment appropriately.
2. Regarding the representation of the precipitation forcing uncertainty, it was shown that a first order autoregressive error model was used to perturb the forcing. Besides, the temporal and spatial correlation of the errors was considered. However, it was found later in the study, that when there was no observed precipitation, the ensemble members are set to zero (first order autoregressive error models are used). This approach as noted by (Maggioni et al., 2017) does not represent precipitation errors appropriately. For future research and development, it is recommended to use more advanced precipitation error models.
3. Comparative study was done on rain gauge rainfall data and three satellite rainfall products in pursuit of a precipitation product with less uncertainty. The daily time scale comparison showed that the satellite products severely underestimate precipitation. The rainfall-runoff simulation using the satellite products didn't capture major events. The daily temporal resolution is not adequate enough to capture the dynamic runoff process in the catchment to the required accuracy. It is recommended that finer temporal resolution satellite data should be used for rainfall-runoff modelling as well as data assimilation/forecast experiments. In addition, the potential of radar data should be explored for future data assimilation experiments. Besides, advanced bias correction methods can be applied to fully exploit the data rich remotely sensed precipitation products.
4. In order to quantify model uncertainty, in this study, only model forcing was perturbed to generate the ensembles in order to study the effect of forcing uncertainty on streamflow forecast. This methodology assigns that model uncertainty is mainly due to forcing uncertainty. However, for future studies, both forcing and model state perturbation should be incorporated.
5. Observed precipitation was used for all the data assimilation and forecast experiments. Thus, the streamflow forecasts are not influenced by uncertainty from forecast precipitation. But operational forecasting needs forecast precipitation as one of the main inputs. Thus for future studies, forecast precipitation should be used for the data assimilation experiments.
6. Time didn't allow for the implementation of more verification methods to evaluate the performance of the ensemble forecasts. Therefore, it is recommended to implement several verification tools to evaluate the forecasts in depth.

9. References

- Anderson, J. L. (n.d.). Localization and Sampling Error Correction in Ensemble Kalman Filter Data Assimilation. <https://doi.org/10.1175/MWR-D-11-00013.1>
- Arias-Hidalgo, M., Bhattacharya, B., Mynett, A. E., & Van Griensven, A. (2013). Experiences in using the TMPA-3B42R satellite data to complement rain gauge measurements in the Ecuadorian coastal foothills. *Hydrol. Earth Syst. Sci.*, *17*, 2905–2915. <https://doi.org/10.5194/hess-17-2905-2013>
- Ashouri, H., Hsu, K.-L., Sorooshian, S., Braithwaite, D. K., Knapp, K. R., Dewayne Cecil, L., ... Prat, O. P. (2014). PERSIANN-CDR Daily Precipitation Climate Data Record from Multisatellite Observations for Hydrological and Climate Studies. <https://doi.org/10.1175/BAMS-D-13-00068.1>
- Aubert, D., Loumagne, C., & Oudin, L. (2003). Sequential assimilation of soil moisture and streamflow data in a conceptual rainfall - Runoff model. *Journal of Hydrology*, *280*(1–4), 145–161. [https://doi.org/10.1016/S0022-1694\(03\)00229-4](https://doi.org/10.1016/S0022-1694(03)00229-4)
- Behrangi, A., Andreadis, K., Fisher, J. B., Joseph Turk, F., Granger, S., Painter, T., & Das, N. (2014). Satellite-based precipitation estimation and its application for streamflow prediction over mountainous western U.S. basins. *Journal of Applied Meteorology and Climatology*, *53*(12), 2823–2842. <https://doi.org/10.1175/JAMC-D-14-0056.1>
- Blasone, R.-S. (2014). *Coupling groundwater and ecological models (MIKE-SHE & ECO Lab) - Roberta-Serena Blasone (DHI)*.
- Brocca, L., Moramarco, T., Melone, F., Wagner, W., Hasenauer, S., & Hahn, S. (2012). Assimilation of surface- and root-zone ASCAT soil moisture products into rainfall-runoff modeling. *IEEE Transactions on Geoscience and Remote Sensing*, *50*(7 PART1), 2542–2555. <https://doi.org/10.1109/TGRS.2011.2177468>
- Bröcker, J. (2012). Evaluating raw ensembles with the continuous ranked probability score. *Quarterly Journal of the Royal Meteorological Society*, *138*(667), 1611–1617. <https://doi.org/10.1002/qj.1891>
- Butts, M. B., Falk, A. K., Hartnack, J., Madsen, H., Klitting, A., Van Kalken, T., ... Price, D. (2005). ENSEMBLE-BASED METHODS FOR DATA ASSIMILATION AND UNCERTAINTY ESTIMATION IN THE FLOODRELIEF PROJECT, *17*, 17–19. Retrieved from https://www.mikepoweredbydhi.com/upload/publications/mike11/Butts_Ensemble-based.pdf
- Carney, M., & Cunningham, P. (2006). Evaluating Density Forecasting Models. Retrieved from <https://pdfs.semanticscholar.org/6d63/81c37496c26d1ce471fc5aeb9757fd06e77d.pdf>
- Chen, H., Yang, D., Hong, Y., Gourley, J. J., & Zhang, Y. (2013). Hydrological data assimilation with the Ensemble Square-Root-Filter: Use of streamflow observations to update model states for real-time flash flood forecasting. *Advances in Water Resources*, *59*, 209–220. <https://doi.org/10.1016/j.advwatres.2013.06.010>
- Clark, M. P., Rupp, D. E., Woods, R. A., Zheng, X., Ibbitt, R. P., Slater, A. G., ... Uddstrom, M. J. (2008). Hydrological data assimilation with the ensemble Kalman filter: Use of streamflow observations to update states in a distributed hydrological model. *Advances in Water Resources*, *31*(10), 1309–1324. <https://doi.org/10.1016/j.advwatres.2008.06.005>
- Deliu, C., & Giurma, I. O. N. (2014). DATA ASSIMILATION APPLICATIONS IN HYDROLOGY, (Lxiv).
- Dhi. (2007). Mike 11, 278–325.

- DHI. (2016). *Murrumbidgee Computer Aided River Management System (CARM)*.
- DHI. (2017). *DHI Data Assimilation Framework: Reference Manual*. Horsholm.
- DPI. (2017). Real-time water data. Retrieved from <http://realtimedata.water.nsw.gov.au/water.stm>
- Evensen, G. (2003). The Ensemble Kalman Filter: Theoretical formulation and practical implementation. *Ocean Dynamics*, 53(4), 343–367. <https://doi.org/10.1007/s10236-003-0036-9>
- Evensen, G. (2009). *Data Assimilation: The Ensemble Kalman Filter 2nd Edition*.
- FloodList. (2013). Gundagai Floods 1852. Retrieved from <http://floodlist.com/australia/gundagai-floods-1852>
- Funk, C., Peterson, P., Landsfeld, M., Pedreros, D., Verdin, J., Shukla, S., ... Michaelsen, J. (2015). The climate hazards infrared precipitation with stations—a new environmental record for monitoring extremes Background & Summary. <https://doi.org/10.1038/sdata.2015.66>
- Gillijns, S., Mendoza, O. B., Chandrasekar, J., De, B. L. R., Bernstein, D. S., & Ridley, A. (2006). What Is the Ensemble Kalman Filter and How Well Does it Work? Retrieved from <http://citeseerx.ist.psu.edu/viewdoc/download?doi=10.1.1.146.801&rep=rep1&type=pdf>
- Guzzi, R. (2015). *Data Assimilation: Mathematical Concepts and Instructive Examples*. *Data Assimilation: Mathematical Concepts and Instructive Examples*. <https://doi.org/10.1007/978-3-319-22410-7>
- Habib, E., Haile, A. T., Sazib, N., Zhang, Y., & Rientjes, T. (2014). Effect of bias correction of satellite-rainfall estimates on runoff simulations at the source of the Upper Blue Nile. *Remote Sensing*, 6(7), 6688–6708. <https://doi.org/10.3390/rs6076688>
- Hamill, T. (2010). *Common verification methods for ensemble forecasts*.
- Hamill, T. M. (2006). *Ensemble-based atmospheric data assimilation*. *Predictability of Weather and Climate*. <https://doi.org/10.1017/CBO9780511617652.007>
- Hong, Y., Gochis, D., Cheng, J., Hsu, K., Sorooshian, S., Hong, Y., ... Sorooshian, S. (2007). Evaluation of PERSIANN-CCS Rainfall Measurement Using the NAME Event Rain Gauge Network. *Journal of Hydrometeorology*, 8(3), 469–482. <https://doi.org/10.1175/JHM574.1>
- Hunt, B. R., Kostelich, E. J., & Szunyogh, I. (2007). Efficient data assimilation for spatiotemporal chaos: A local ensemble transform Kalman filter. *Physica D: Nonlinear Phenomena*, 230(1–2), 112–126. <https://doi.org/10.1016/j.physd.2006.11.008>
- Investopedia. (n.d.). Spurious Correlation. Retrieved from http://www.investopedia.com/terms/s/spurious_correlation.asp
- Jo, H., Jung, HyungsikKim, S., Ahna, J., Lee, K., & Choe, J. (2016). History matching of channel reservoirs using ensemble Kalman filter with continuous update of channel information. *Journal of Petroleum Science and Engineering*, 154(February), 19–37. <https://doi.org/10.1016/j.petrol.2017.04.016>
- Jolliffe, I. T. (2003). *Forecast Verification A Practitioner's Guide in Atmospheric Science*. Wiley.
- Kamel, A. H. (2008). APPLICATION OF A HYDRODYNAMIC MIKE 11 MODEL FOR THE EUPHRATES RIVER IN IRAQ. Retrieved from https://www.svf.stuba.sk/docs/sjce/2008/2008_2/file4.pdf
- Katrine, A., Falk, V., Butts, M. B., Madsen, H., & Hartnack, J. N. (1994). Data Assimilation To Improve Forecast Quality of River Basin Models, 1–8.
- Katzfuss, M., Stroud, J. R., & Wikle, C. K. (2016). Understanding the Ensemble Kalman Filter. *The American Statistician*, 1–14.

- <https://doi.org/10.1080/00031305.2016.1141709>
- Kimani, M. W. (2017). An Assessment of Satellite-Derived Rainfall Products Relative to Ground Observations over East Africa.
- Kleeman, L. (1996). Understanding and applying Kalman filtering. *Proceedings of the Second Workshop on Perceptive ...*, 17. [https://doi.org/10.1016/S0167-9473\(99\)00020-1](https://doi.org/10.1016/S0167-9473(99)00020-1)
- Kneis, D., Chatterjee, C., & Singh, R. (2014). Evaluation of TRMM rainfall estimates over a large Indian river basin (Mahanadi). *Hydrol. Earth Syst. Sci*, 18, 2493–2502. <https://doi.org/10.5194/hess-18-2493-2014>
- Kumar, S. V., Reichle, R. H., Peters-Lidard, C. D., Koster, R. D., Zhan, X., Crow, W. T., ... Houser, P. R. (2008). A land surface data assimilation framework using the land information system: Description and applications. *Advances in Water Resources*, 31(11), 1419–1432. <https://doi.org/10.1016/j.advwatres.2008.01.013>
- Liu, X., Liu, F. M., Wang, X. X., Li, X. D., Fan, Y. Y., Cai, S. X., & Ao, T. Q. (2015). Combining rainfall data from rain gauges and TRMM in hydrological modelling of Laotian data-sparse basins. *Applied Water Science*. <https://doi.org/10.1007/s13201-015-0330-y>
- Liu, X., Yang, T., Hsu, K., Liu, C., & Sorooshian, S. (2017). Evaluating the streamflow simulation capability of PERSIANN-CDR daily rainfall products in two river basins on the Tibetan Plateau. *Hydrol. Earth Syst. Sci*, 21, 169–181. <https://doi.org/10.5194/hess-21-169-2017>
- Liu, Y., & Gupta, H. V. (2007). Uncertainty in hydrologic modeling: Toward an integrated data assimilation framework. *Water Resources Research*, 43(7), 1–18. <https://doi.org/10.1029/2006WR005756>
- Liu, Y., Weerts, A. H., Clark, M., Hendricks Franssen, H. J., Kumar, S., Moradkhani, H., ... Restrepo, P. (2012). Advancing data assimilation in operational hydrologic forecasting: Progresses, challenges, and emerging opportunities. *Hydrology and Earth System Sciences*, 16(10), 3863–3887. <https://doi.org/10.5194/hess-16-3863-2012>
- Madsen, H., & Bauer-gottwein, P. (n.d.). *Hydrological-hydrodynamic modelling and data assimilation system*.
- Madsen, H., Hartnack, J., & Sørensen, J. V. T. (2006). Data Assimilation in a Flood Modelling System Using the Ensemble Kalman Filter, 1–8.
- Madsen, H., Rosbjerg, D., Damgård, J., Frands, & Hansen, S. (2003). Data assimilation in the MIKE 11 Flood Forecasting system using Kalman filtering. *Water Resources Systems—Hydrological Risk, Management and Development*, (281), 75–81.
- Madsen, H., & Sørensen, J. T. (2007). RECENT ADVANCES IN DATA ASSIMILATION IN LARGE SCALE HYDRODYNAMIC AND HYDROLOGICAL FORECASTING MODELS (pp. 1–11).
- Maggioni, V., & Houser, P. R. (2017). Data Assimilation for Atmospheric, Oceanic and Hydrologic Applications, Volume 3.
- Moriasi, D. N., Arnold, J. G., Liew, M. W. Van, Bingner, R. L., Harmel, R. D., Veith, T. L., ... Moriasi, D. N. (2007). MODEL EVALUATION GUIDELINES FOR SYSTEMATIC QUANTIFICATION OF ACCURACY IN WATERSHED SIMULATIONS. *Transactions of the ASABE*, 50(3), 885–900. Retrieved from <https://pubag.nal.usda.gov/pubag/downloadPDF.xhtml?id=9298&content=PDF>
- Munier, S., Polebistki, A., Brown, C., Belaud, G., & Lettenmaier, D. P. (2015). SWOT data assimilation for operational reservoir management on the upper Niger River Basin. *Water Resources Research*, 51(1), 554–575. <https://doi.org/10.1002/2014WR016157>
- NASA. (2015). No Title. Retrieved from <https://pmm.nasa.gov/trmm>
- NSW Office of Water. (2011). *Water resources and management overview: Murrumbidgee*

- catchment. Sydney. Retrieved from http://www.water.nsw.gov.au/___data/assets/pdf_file/0020/548012/catchment_overview_murrumbidgee.pdf
- Petrie, R. E. (2008). Localization in the ensemble Kalman Filter. Retrieved from [http://www.met.rdg.ac.uk/mscdissertations/Localization in the ensemble Kalman Filter.pdf](http://www.met.rdg.ac.uk/mscdissertations/Localization_in_the_ensemble_Kalman_Filter.pdf)
- Rasmussen, J., Madsen, H., Jensen, K. H., & Refsgaard, J. C. (2015). Data assimilation in integrated hydrological modeling using ensemble Kalman filtering: evaluating the effect of ensemble size and localization on filter performance. *Hydrology and Earth System Sciences*, *19*(7), 2999–3013. <https://doi.org/10.5194/hess-19-2999-2015>
- Reichle, R. H., Crow, W. T., & Keppenne, C. L. (2008). An adaptive ensemble Kalman filter for soil moisture data assimilation. *Water Resources Research*, *44*(3), 1–13. <https://doi.org/10.1029/2007WR006357>
- Ridler, M. E., Madsen, H., Stisen, S., Bircher, S., & Fensholt, R. (2014). Assimilation of SMOS-derived soil moisture in a fully integrated hydrological and soil-vegetation-atmosphere transfer model in Western Denmark. *Water Resources Research*, *50*(11), 8962–8981. <https://doi.org/10.1002/2014WR015392>
- Seo, D. J., Cajina, L., Corby, R., & Howieson, T. (2009). Automatic state updating for operational streamflow forecasting via variational data assimilation. *Journal of Hydrology*, *367*(3–4), 255–275. <https://doi.org/10.1016/j.jhydrol.2009.01.019>
- Stroud, J. (2015). *Understanding the Ensemble Kalman Filter*. Retrieved from <http://www.stat.osu.edu/~oksana/docs/STATMOS-SSDA/Stroud-ncar-2015.pdf>
- Sun, L., Seidou, O., Nistor, I., & Liu, K. (2015). Review of the Kalman type hydrological data assimilation. *Hydrological Sciences Journal*, *66*(7)(December), 02626667.2015.1127376. <https://doi.org/10.1080/02626667.2015.1127376>
- Turner, M. R. J., Walker, J. P., & Oke, P. R. (n.d.). Ensemble member generation for sequential data assimilation. Retrieved from <http://www.elsevier.com/copyright>
- Wagener, T., McIntyre, N., Lees, M. J., Wheater, H. S., & Gupta, H. V. (2003). Towards reduced uncertainty in conceptual rainfall-runoff modelling: Dynamic identifiability analysis, *17*, 455–476. <https://doi.org/10.1002/hyp.1135>
- Welch, G., & Bishop, G. (2006). An Introduction to the Kalman Filter. *In Practice*, *7*(1), 1–16. <https://doi.org/10.1.1.117.6808>
- Xie, X., & Zhang, D. (2010). Data assimilation for distributed hydrological catchment modeling via ensemble Kalman filter. *Advances in Water Resources*, *33*(6), 678–690. <https://doi.org/10.1016/j.advwatres.2010.03.012>
- Zhang, D., Madsen, H., Ridler, M. E., Kidmose, J., Jensen, K. H., & Refsgaard, J. C. (2016). Multivariate hydrological data assimilation of soil moisture and groundwater head. *Hydrology and Earth System Sciences*, *20*(10), 4341–4357. <https://doi.org/10.5194/hess-20-4341-2016>

10. Glossary

1. Adaptive localization:
2. Autoregressive model:
3. Background Error Covariances
4. Correlation Length Scale (L):
5. Decorrelation time:
6. Filter Divergence:
7. Filtering/Filter: The process of finding the “best estimate” from noisy data amounts to “filtering out” the noise
8. Fractional Error:
9. Hotstart:
10. Inflation:
11. Localization: used to reduce spurious correlations
12. Noise (Error) Models:
13. Perturbation:
14. Spatial and Temporal Correlation of errors
15. Spurious Correlation: when the correlation cannot be properly described by the ensemble of models, having a detrimental effect on the filter performance (J.Rasmussen et al., 2015)
16. State Vector: a collection of the variables we are interested to update the model state
17. Warm-up period: A model might need this to reach its balanced state (from the poorly known initial conditions)
18. White Noise:
19. Filtering:
20. Smoothing:
21. Control Simulation:
22. Open Loop Simulation:
23. MainModel:
- 24.

Appendix

SENSITIVITY ANALYSIS OF FILTER PARAMETERS

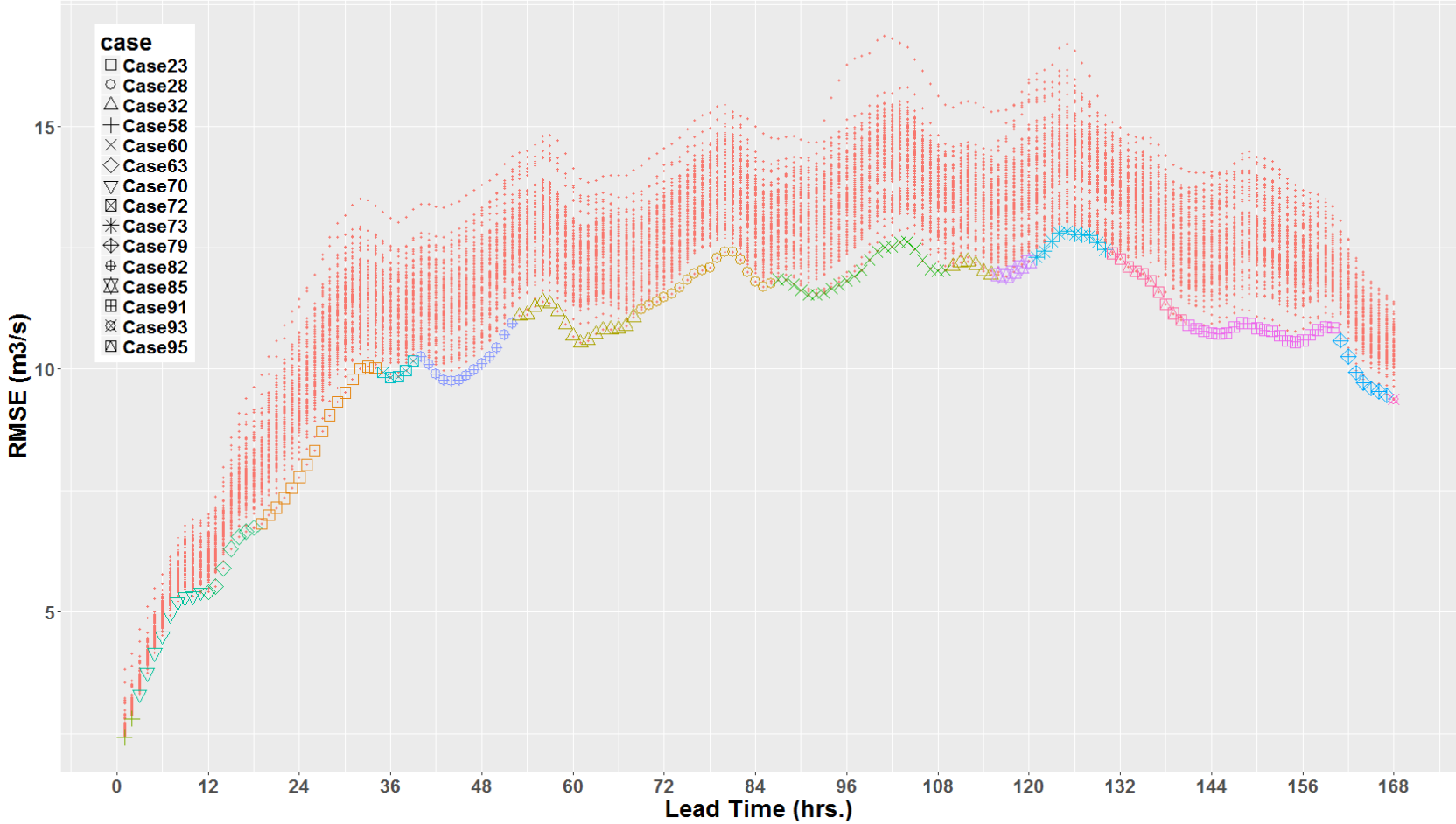


Figure A 1: Forecast RMSE for different combination of filter parameters

SENSITIVITY ANALYSIS OF FILTER PARAMETERS

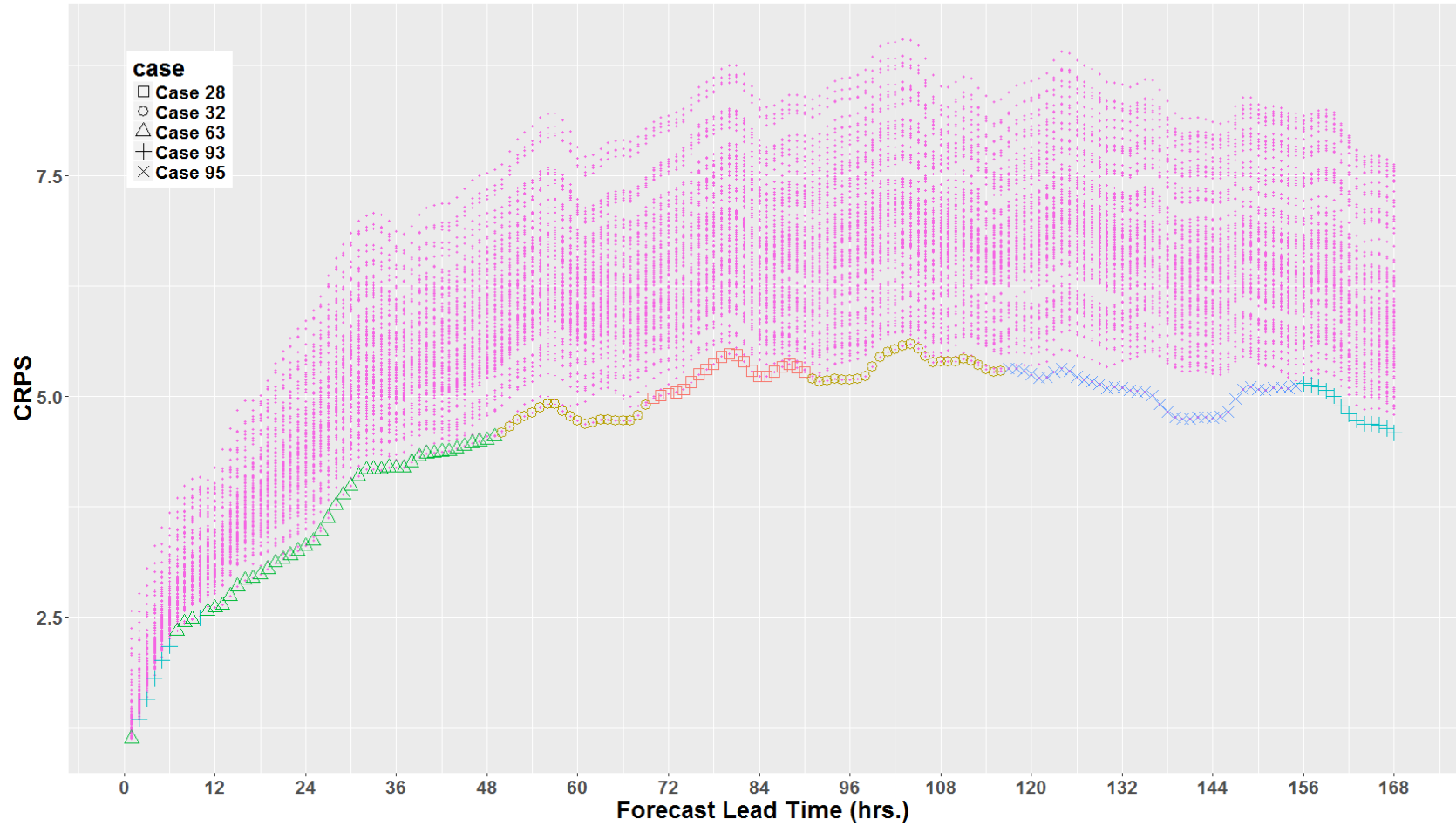


Figure A 2: Forecast RMSE for different combination of filter parameters

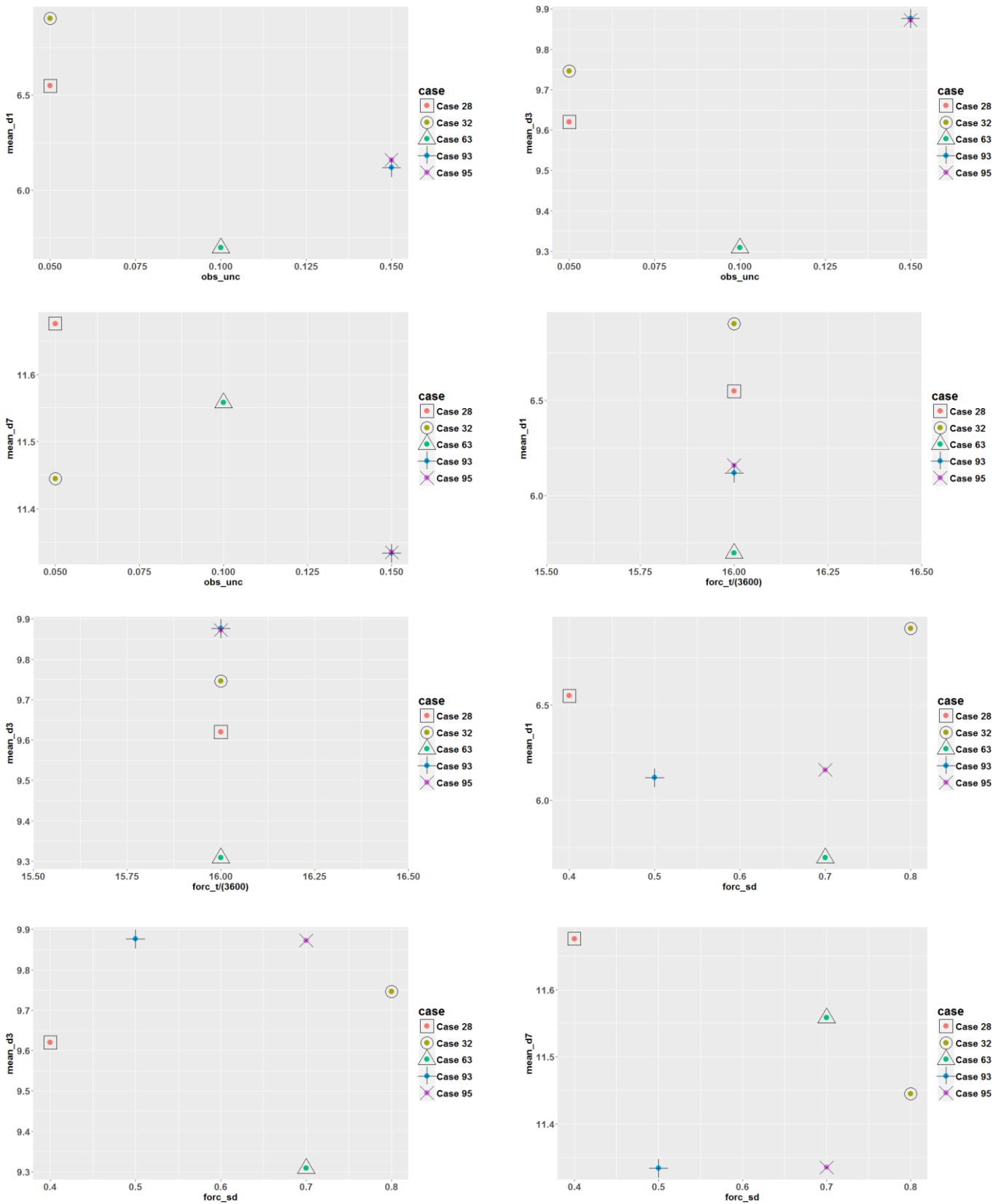


Figure A 3: Average RMSE for 1 day, 3 days, and 7 days for the 5 best cases. On the x axis the three filter parameters are represented, y axis represents forecast RMSE

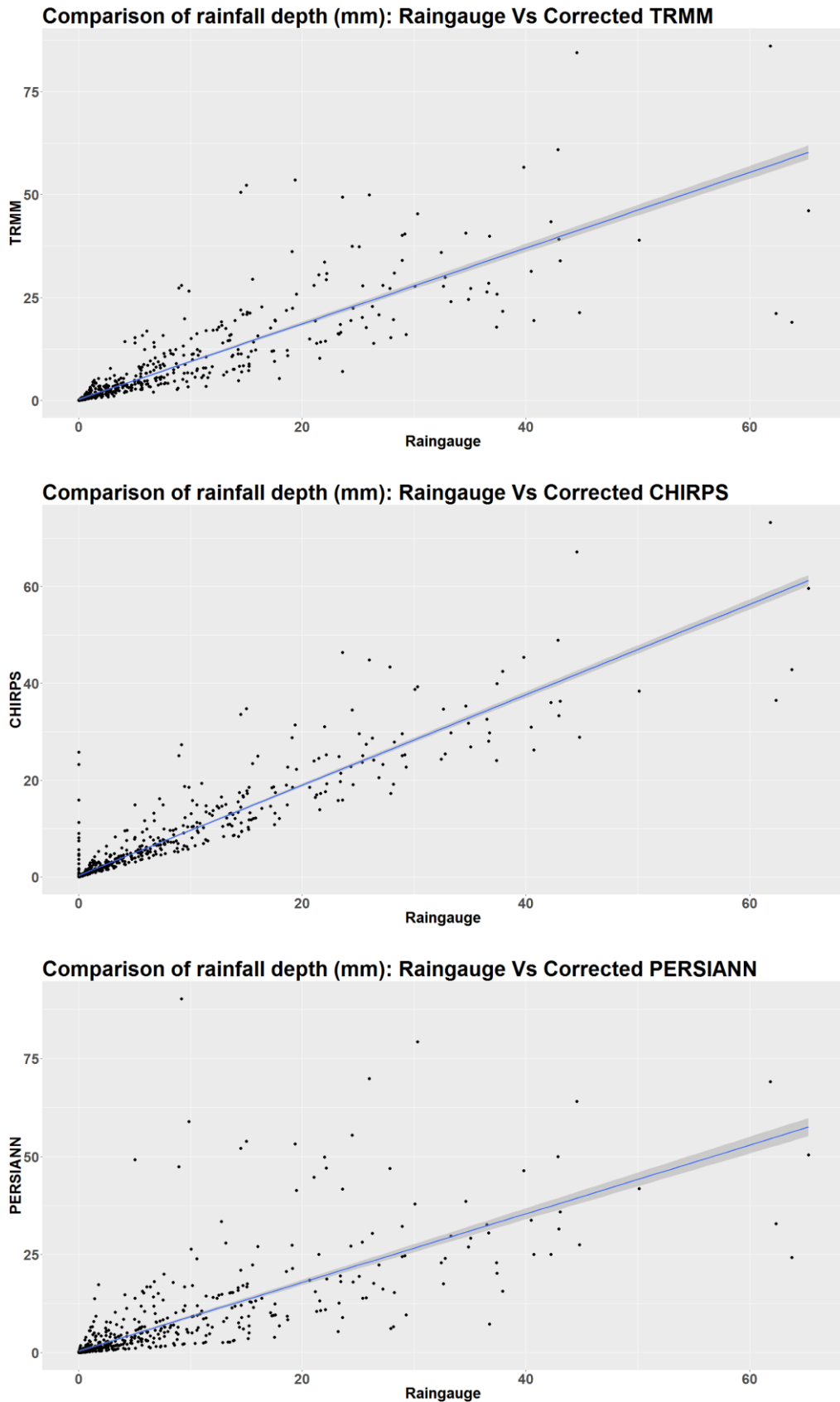


Figure A 4: Scatterplot of bias corrected satellite rainfall estimates Vs rain gauge rainfall (Pearson correlation statistic was improved after bias correction)